Cellular Prion Protein (PrP^C): Identification and Characterization of Novel Interacting Partners

Dissertation

zur Erlangung des Doktorgrades

der Mathematisch-Naturwissenschaftlichen Fakultäten

der Georg-August-Universität zu Göttingen

vorgelegt von

Saima Zafar

aus Lahore, Pakistan

Göttingen, 2010

D7

Referent: Prof. Dr.Uwe Groβ

Korreferent: Prof. Dr. Nils Brose

Tag der mündlichen Prüfung: 17-01-2011

I hereby declare that the PhD thesis entitled "Cellular Prion Protein (PrP^C): Identification and Characterization of Novel Interacting Partners" was written independently and with no other sources and aids than those quoted.

Saima Zafar

Dedicated to **Hazrat Muhammad** (Peace Be Upon Him)

Table of Contents

List of Figures

List of Tables

Abbreviations

^{o}C	Celsius
µl	Micro liter
µm	Micro meter
2-DE	Two-dimensional gel electrophoresis
aa	Amino acid
AD	Alzheimer's disease
Arf1	ADP-ribosylation factor 1
ATP	Adenosine triphosphate
BFA	Brefeldin A
bp	Base pair
BPB	Bromophenol blue
BSA	Bovine serum albumin
BSE	Bovine spongiform encephalopathy
cDNA	Complementary deoxyribonucleic acid
CSF	Cerebrospinal fluid
ddH$_2$O	Double distilled water
DMEM	Dulbecco's Modified Eagle Medium
DMSO	Dimethylsulfoxide
EDTA	Ethylene diamine tetra acetic acid
ELISA	Enzyme-linked immunosorbent assay
ER	Endoplasmic reticulum
ERAD	Endoplasmic reticulum associated degradation
ERGIC	ER–Golgi intermediate compartment
ESI-QTOF-MS	ElectroSpray Ionisation-Time-of-Flight Mass Spectrometry
FCS	Fetal calf serum
For	Forward
H	Hour
HEK-293	Human Embryonic Kidney 293 cell line
HpL3-4	Murine Prnp-deficient Hippocampal neuronal cells
HRP	Horseradish peroxidase
IAA	Iodoacetamide
IEF	Isoelectric focusing

IgG	Immunoglobulin G
IPG	Immobilized pH gradient
kDa	Kilodalton
LB	Luria-Bertani broth
LC/MS-MS	Liquid chromatography and tandem mass spectrometry
LSM	Laser-scanning microscope
min.	Minute
ml	Milliliter
MTS	(3-(4,5-dimethylthiazol-2-yl)-5-(3-carboxymethoxyphenyl)-2-(4-sulfophenyl)-2H-tetrazolium)
MW	Molecular weight
no.	Number
ng	Nano gram
OD	Optical density
PBS	Phosphate buffered saline
PCR	Polymerase chain reaction
PDI	Protein disulphide isomerase
PKC	Protein kinase C
PLD	Phospholipase D
PMS	Phenazine methosulfate
PPIase	Peptidyl prolyl cis-trans isomerase
ppm	Parts per million
PrP^C	Cellular prion protein
PrP^{SC}	Infectious isoform of prion protein
PS	Penicillin Streptomycin
rpm	Revolutions per minute
Rab7a	Ras-related protein Rab-7a
Rev	Reverse
RT	Room temperature
s	second
SDS-PAGE	Sodium Dodecyl Sulphate Polyacrylamide Gel Electrophoresis
siRNA	Small interfering RNA
TBS	Tris buffered saline
TBST	TBS with 0.1% Tween

TE	Tris EDTA
TEMED	N, N, N´, N´-tetramethylethylenediamine
Tris	Tris-(hydroxymethyl)-aminomethane
TSEs	Transmissible spongiform encephalopathies
WB	Western blot

Summary

The cellular prion protein (PrP^C) was highly conserved during the evolution of mammals [Pantera *et al.* 2009; Jiayu *et al.* 2009]. The gene tree deduced from the PrP sequences largely agrees with the species tree, indicating that no major deviations occurred in the evolution of the prion gene in different placental lineages [Teun van Rheede *et al.* 2003]. However, the cellular function of this ubiquitous protein is still not clear. The accumulation of misfolded and aggregated forms of PrP^C (known as PrP^{Sc}) causes transmissible neurodegenerative diseases. Despite increasing knowledge concerning PrP^{Sc}, very little is known about the physiological characteristics of PrP^C and its interaction with other cellular proteins.

The present study was undertaken to identify proteins interacting with PrP^C that could provide new insights into its physiological functions and pathological role. Human PrP^C was expressed in prion protein-deficient murine hippocampus (HpL3-4) neuronal cells. The PrP^C along with its interacting proteins were affinity purified using STrEP-Tactin chromatography, in-gel digested, and then identified by Q-TOF MS/MS analysis. Forty three proteins appeared to interact with PrP^C in this neuronal cell line. Of these, fifteen were already known for their interaction with PrP^C or PrP^{Sc}, while twenty eight new proteins were identified. All 43 (known and new) proteins which were identified as interacting partners were structural constituents of the cytoskeleton. Some are involved in cell growth, some in metabolism, and some in energy pathways. In addition, proteins that are important for cell homeostasis, cell communication, signal transduction, stress response and protein folding were also among the newly identified interacting partners of PrP^C.

Interactions of two novel (newly discovered) interacting partners of the GTPase family (Rab7a and Arf1) which have a suggested role in vesicle trafficking as well as the cytoskeleton associated protein alpha-tubulin 1 were further investigated using confocal laser scanning microscopy and reverse co-immunoprecipitation. Both reverse co-immunoprecipitation and immunofluorescence results confirmed potential interactions of Rab7a, Arf1 and alpha-tubulin 1 with the PrP^C. SiRNA against the Rab7a gene was used to decrease the expression of Rab7a protein ("knockdown"), in PrP^C expressing HpL3-4 and SH-SHY5Y cells. This depleted Rab7a expression led to the enhanced accumulation of PrP^C in Rab9 positive endosomal compartments. The PrP^C which

accumulated within these Rab9 positive late endosomes remained sensitive to proteinase K digestion. Furthermore, Arf1 deactivation by brefeldin A treatment down regulated PrP^C expression and redistributed PrP^C into the cytosol, whereas nocodazole treatment increased PrP^C expression and redistributed PrP^C into the cytosol.

The work described demonstrated for the first time that Rab7a and Arf1 interact with PrP^C and may possibly be involved in the cellular trafficking and distribution of PrP^C into microtubules. These results highlight the pivotal involvement of endosomal compartments in the trafficking and regulation of PrP^C.

1. Introduction

1.1   Prions and prion biology

The term prion (*proteinaceous infectious particle*) was coined by Stanley Prusiner in 1982. Prions are unique infectious agents devoid of nucleic acid which cause a group of fatal neurodegenerative diseases associated with the misfolding of the cellular prion protein (PrP^C). Bovine spongiform encephalopathy (BSE), Scrapie in sheep, and Creutzfeldt–Jakob disease (CJD) in humans are among the most notable prion diseases.

1.1.1 Prion diseases and infectivity

In the past decade, prion diseases or transmissible spongiform encephalopathies (TSE) have received enhanced attention largely because of the potential risk for human infection with BSE or ``mad cow disease.´´ These diseases can affect subjects in many age groups causing a variety of motor or cognitive symptoms. The pathogenesis of prion diseases is attributed to the major conformational changes in the cellular form of prion protein (PrP^C) which result in the diseased form of these proteins (PrP^{Sc}) [Prusiner 1998a]. The BSE are uncommon but invariably fatal [Aguzzi 2000; Knight and Will 2004; Aguzzi and O'Connor 2010].

The first documented prion disease was CJD, characterized by Creutzfeldt in 1920 and Jakob in 1921. Later, studies of kuru among the Fore (http://www.everyculture.com/Oceania/Fore-i-Orientation-i.html) people of Papua-New Guinea indicated that disease transmission relies on a single protease-resistant protein component of the prion [Prusiner 1998a; Prusiner 1998b]. According to the "protein-only" hypothesis, PrP^{Sc} is a potentially infectious agent that uses a self-propagating reaction to convert PrP^C into the disease form. Additionally, transmission of the disease requires the presence of PrP^C [Bueler *et al.* 1993; Brandner *et al.* 1996; Legname *et al.* 2004; Sakudo and Ikuta 2009; Lee *et al.* 2010; Mallik *et al.* 2010].

The clinical symptoms of prion diseases vary in humans. The neuropathology of prion diseases is characterized by extensive neuronal death, accompanied by spongiform vacuolation as well as astro- and microgliosis to extracellular amyloid aggregates. The deposited extracellular amyloid contains the causative agent PrP^{Sc}.

This amyloid accumulation occurs in the majority of prion diseases, but not in all cases. These accumulations lead to progressively severe motor disturbance and dementia resulting in death within a few months to several years after diagnosis. Whereas, in transmissible cases, death can occur years to decades after the initial infection.

1.1.2 The Structure of prion protein

The human form of PrP^C consists of 253 highly conserved amino acids [Goldmann 1993]. The majority of the mature form is attached to the plasma membrane, anchored through the C-terminus glycosyl-phosphatidylinositol (GPI) (Figure 1A). The N-terminal half of the PrP^C polypeptide chain is essential for efficient clathrin-mediated endocytosis. Deletions within this region diminish internalisation of PrP^C and direct translocation of the N-terminus of the polypeptide chain across the membrane and produce ^{Sec}PrP or ^{Ntm}PrP) [Stahl et al. 1987]. In the C-terminus of the PrP, there are two conserved N-linked glycosylation sites for complex oligosaccharide attachment at residues 181 (Asn-Ile-Thr) and 197 (Asn-Phe-Thr) [Caughey et al. 1989; Lawson et al. 2005]. The molecular weight of PrP^C is about 25-35 kDa, indicating the presence of post translational modification including variable glycosylation (non-, mono- and diglycosylated forms). The types of glycans attached to both full-length and truncated PrP appear to be extremely diverse. More than 50 sugar chains have been observed, using both biochemical and mass spectrometry methods [Rudd et al. 1999; Pan et al. 2002], to be differentially distributed in various areas of the central nervous system (CNS) [DeArmond et al. 1999; Beringue et al. 2003]. The C-terminus of PrP contains two cysteine residues (Cys 179 and Cys 214) where post translationally a disulphide bridge is formed [Caughey et al. 1989; Rudd et al. 2002]. The relevance of these modifications is still under investigation.

The N-terminus of PrP^C contains an octapeptide repeat (OR) domain [Roucou and LeBlanc 2005]. This domain is made up of a PQGGGGWGQ peptide sequence followed by four identical repeats of PHGGGWGQ. These last four ORs show similarity to the BH2 domain found in the Bcl-2 family of proteins, suggesting that the protein may play a role in cell survival. In addition, the repeating motif provides a region rich in histidine, which is known to bind copper ions. A domain comprised of highly hydrophobic residues is found between amino acids 110 and 135 of PrP and plays an important role in generating transmembrane proteins [Lopez et al. 1990]. The NMR

spectroscopy deduced tertiary structure of the cellular prion protein (Figure 1B) shows predominantly an α-helical (42%) folded C-terminal domain and a tangled N-terminal flexible domain [Riek *et al.* 1997]. In contrast to the pathological form (PrP^{Sc}), the PrP^C is sensitive to proteinase K (PK) digestion.
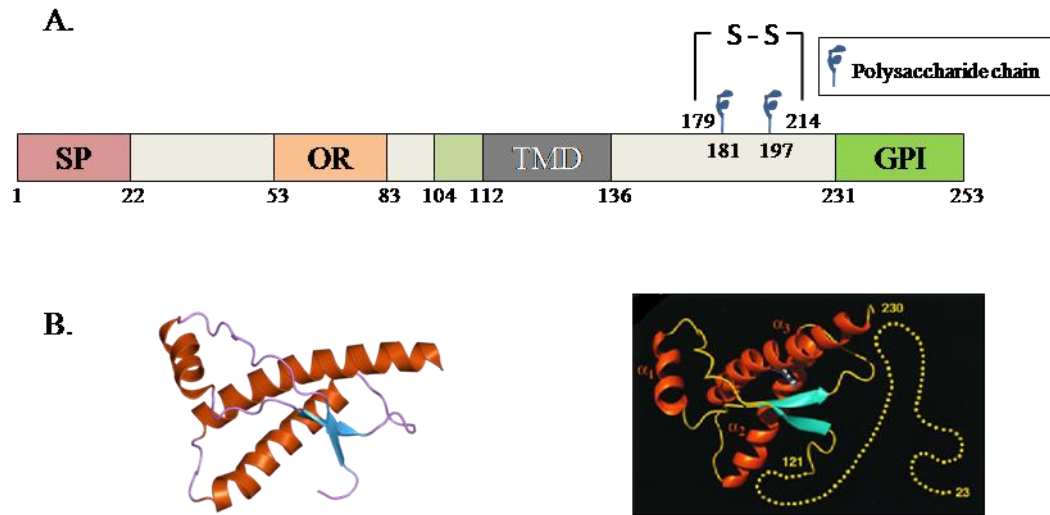
Figure 1 The structural features of the cellular prion protein: (A) The schematic representation of PrP^C structure contains an N-terminal signal peptide (SP) and a glycosyl-phosphatidylinositol (GPI) anchor signal at the C-terminus. In addition, PrP^C has an octapeptide repeat (OR) region, a hydrophobic transmembrane domain (TMD), one disulphide bridge and two N-linked glycosylation sites ( ) (B) Cartoon of the three-dimensional structure of the human PrP^C [Riek *et al.* 1997].

1.1.3 Biosynthesis and internalization of PrP^C

The biosynthesis of PrP^C is similar to that of other membrane and secreted proteins. PrP^C contains a specific N-terminal signal peptide (SP) which translocates it into the endoplasmic reticulum (ER) from where it transits the Golgi on its way to the cell surface [Harris 2003a]. Targeting of the PrP^C to the ER is subject to several post-translational modifications including cleavage of the N-terminal signal peptide, addition of N-linked oligosaccharide chains, formation of a single disulphide bond, and the attachment of GPI anchor at C-teminus [Haraguchi *et al.* 1989; Stahl *et al.* 1987; Turk *et al.* 1988].

Following, glycosylation and the addition of the GPI anchor, PrP^C is transported to the cell surface where it is attached via the GPI anchor [Borchelt *et al.* 1990a] (Figure 2). The majority of PrP^C is found in detergent-resistant raft domains on the cell surface [Gorodinsky and Harris 1995; Naslavsky *et al.* 1997] and constitutively cycles between the plasma membrane and the endocytic compartment [Shyng *et al.* 1993]. Kinetic analysis demonstrates that PrP^C molecules cycle through the cell with a transit time of approximately 60 min [Magalhaes *et al.* 2002]. Shyng *et al.* in 1993 reported that most of the protein is recycled without degradation. Internalization of PrP^C occurs possibly via i) clathrin coated pits [Shyng *et al.* 1995a] and/or ii), caveolae-like membranous domains [Vey *et al.* 1996], or sphingolipid/cholesterol rafts [Shyng *et al.* 1995b].

i) Clathrin-mediated endocytosis is a process by which cells internalize molecules by the inward budding of plasma membrane. It involves the recruitment of clathrin and adaptor proteins, such as AP-2 at phosphoinositides in the membrane [Gaidarov and Keen 1999]. Shyng *et al* in 1994 used hypertonic media to disrupt clathrin lattices and thereby impair endocytosis via clathrin and reported impaired PrP^C internalization, suggesting that PrP^C may not behave like other GPI anchored proteins.

ii) Caveolae is a special type of 50–100 nm in diameter lipid raft which invaginates the plasma membrane. Internalization of proteins through caveolae has been suggested to divert proteins from the endosomal/ lysosomal pathway [Pelkmans *et al.* 2001]. Vey *et al.* in 1996 showed that both PrP^C and PrP^{Sc} proteins localized in these caveolae and may use these caveolae for their internalization.

The prion protein is highly expressed within the nervous system, although its expression changes among differing cell types and among neurons with distinct neuro-chemical phenotypes. Various cellular components of the immune system, in the bone marrow, blood, and peripheral tissues, also express substantial amounts of PrP^C. PrP^C has also been reported in endosomes containing transferrin receptors in adult mouse sensory neurons and N2a neuroblastoma cells [Sunyach *et al.* 2003]. Also in neurons, PrP^C has been demonstrated both in the Golgi and within cytoplasmic organelles resembling endosomes [Laine *et al.* 2001]. Although the majority of PrP^C is expressed on the cell surface [Borchelt *et al.* 1990b; Mironov *et al.* 2003], significant amounts are present within the cytoplasm of a subpopulation of neurons in the cortex, hippocampus and thalamus [Mironov *et al.* 2003]. Some of these cytoplasmic PrP may arise from the

endocytosed cell surface PrP. A few cytosolic PrP are derived from the endoplasmic reticulum associated degradative (ERAD) pathway. Accumulation of PrP in the cytosol of cells treated with proteasomal inhibitors has been reported [Ma and Lindquist 1999], indicating that excess PrP^C is degraded by the proteasome system [Yedidia *et al.* 2001]. According to another hypothesis, PrP can also be translated, after losing its signal peptide [Rane *et al.* 2004], as a cytosolic protein which retains both the N-terminal and C-terminal signal peptides [Drisaldi *et al.* 2003].
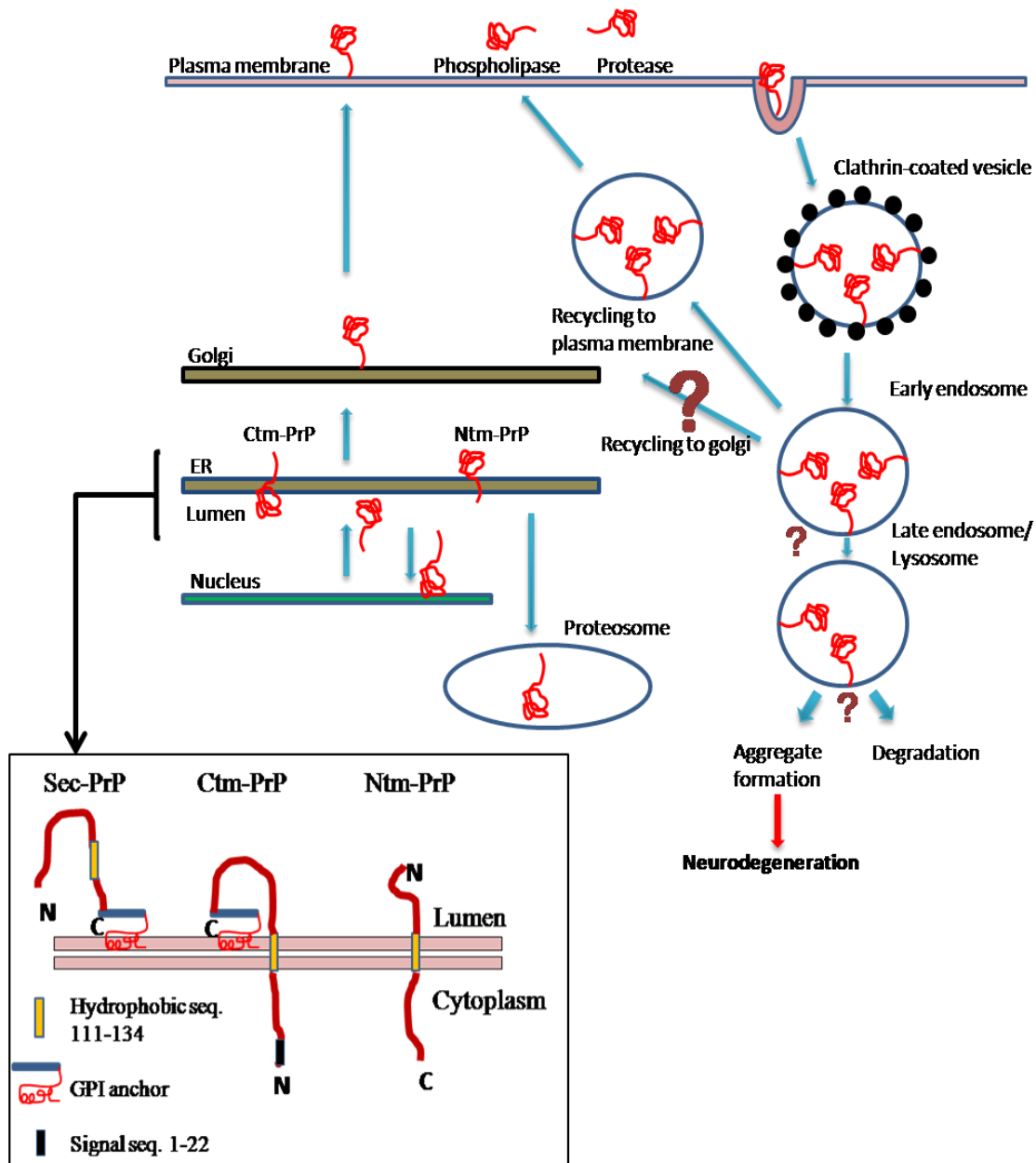
Figure 2 Biosynthesis and cellular trafficking of PrP^C: The PrP^C synthesis, folding, glycosylation and GPI anchor addition all take place in the endoplasmic reticulum (ER). Three different

topological forms of PrP are synthesized in the ER (Ctm-PrP: with the C-terminus in the lumen and the N-terminus in the cytosol, Ntm-PrP: with the N-terminus in the lumen and the C-terminus in the cytosol and Sec-PrP: secretary PrP). Modified PrP^C then translocate to the outer leaflet of the plasma membrane and cycle between the plasma membrane and the endocytic compartments (Zafar *et al.* submitted).

1.1.4 Physiological functions of PrP^C

The exact function of PrP^C is still not clear; however, several putative functions have been reported including e.g. regulatory activity of copper metabolism [Brown *et al.* 1997a; Korte *et al.* 2003; Toni *et al.* 2005; Varela-Nallar *et al.* 2006; Turu *et al.* 2008], antioxidant effects [Brown *et al.* 1997b; Brown *et al.* 2001; Sakudo *et al.* 2005; Anantharam *et al.* 2008], neuronal differentiation [Mouillet-Richard *et al.* 1999; Mouillet-Richard *et al.* 2000; Steele *et al.* 2006; Lima *et al.* 2007; Barenco *et al.* 2009], neuroprotective signaling, and synaptic function [Collinge *et al.* 1994; Re *et al.* 2006].

PrP^C is also found in pre-synaptic nerve terminals, synapses in the brain and neuromuscular junctions [Brown, Clive, and Haswell 2001]. Furthermore, PrP^C may be a part of synaptic vesicle membranes, since the PrP^C interacting protein synapsin I is associated with small synaptic vesicles [Spielhaupter and Schatzl 2001] and PrP^C co-localizes with the pre-synaptic vesicle protein synapthophysin [Fournier *et al.* 1995; Fournier 2008].

PrP^C affects neurotransmitter release via synaptic vesicles as shown for acetylcholine in the neuromuscular junction [Re *et al.* 2006]. This would suggest a role in the recycling of vesicles or a more direct role in synaptic activity. The latter has been suggested by some electrophysiological studies conducted in mice devoid of PrP^C, which demonstrate weakened GABA$_A$-mediated fast inhibition [Collinge *et al.* 1994]. Recombinant PrP induces rapid polarization and development of synapses in embryonic rat hippocampal neurons [Kanaani *et al.* 2005]. *In vivo* accumulation of PrP deposits correlate with abnormal synaptic protein expression in the cerebellum of CJD brains [Ferrer 2002], and Scrapie-infected mice showed a loss of synapses [Jeffrey *et al.* 2000], intrinsic dysfunction of cortical and hippocampal neurons [Jeffrey *et al.* 1996], and altered properties of the membrane and synapses [Johnston *et al.* 1997]. Beyond synaptic function, PrP^C binds copper via histidines in the octarepeat region and could regulate copper concentration in the synaptic region of neurons and decrease oxidative stress in synapses [Herms *et al.* 1999; Kretzschmar *et al.* 2000; Morot-Gaudry-

Talarmain *et al.* 2003]. This anti-oxidative activity of PrP^C has been shown to be the result of copper/zinc-dependent superoxidedismutase activity [Brown *et al.* 1997b; Brown *et al.* 1999; Rachidi *et al.* 2003; Sakudo *et al.* 2005]. The signaling function of PrP^C has been demonstrated by the activation of the non-receptor tyrosine kinase fyn [Kanaani *et al.* 2005; Mouillet-Richard *et al.* 2000; Santuccione *et al.* 2005], which is enriched in brain synaptosomes.

1.2   Cellular trafficking

1.2.1 Vesicular trafficking

Small membrane-bounded vesicles transport proteins from one organelle to another in the secretory and endocytic pathways. These vesicles bud from the membrane of a particular "parent" organelle and fuse with the membrane of a particular "target" (destination) organelle. They are critical for the sorting of proteins newly made in the rough endoplasmic reticulum and of proteins internalized from the cell surface (Figure 2). There are three well characterized transport vesicles – COPI (which transport proteins from the rough ER to the Golgi), COPII (which transport proteins in the retrograde direction between Golgi cisternae and from the *cis*-Golgi back to the rough ER), and clathrin vesicles (which transport proteins from the plasma membrane and the *trans*-Golgi network to the late endosomes). All types of coated vesicles are formed by the polymerization of cytosolic coat proteins, initiated by the recruitment of a small GTP-binding protein, onto a donor (parent) membrane. Then the complexes of coat and adapter proteins in the cytosol bind to the cytosolic domains of membrane cargo and receptor proteins; the latter bring soluble luminal cargo proteins into the budding vesicle. Shortly after vesicle release, the coat protein is shed exposing proteins (SNARE proteins) required for fusion with the target membrane [Kaiser and Ferro-Novick 1998].

1.2.2 RAS superfamily of monomeric GTP-binding proteins

In eukaryotes, a family of GTP-binding proteins (Arf, Rab, Rho and dynamin families) regulates vesicle trafficking from the formation of vesicles on donor membranes to facilitating vesicle docking on target membranes [Bucci *et al.* 2000; Nielsen *et al.* 2008]. The budding of coated vesicles is initiated when molecules of Arf

protein exchange their bound GDP for GTP, a reaction catalyzed by an enzyme in the Golgi membrane. After Arf-GTP binds to Arf receptors on Golgi cisternae, coatomers bind to the cytosolic face of the Golgi cisterna and polymerize into a fibrous coat that induces vesicle budding. Because they can bind to coatomer, certain integral membrane proteins are incorporated into the vesicles. These include a V-SNARE, which functions in targeting vesicles to appropriate acceptor membranes [Weis and Scheller 1998]. Soluble proteins in the lumen are selected for entry into these vesicles by binding to specific membrane receptor proteins. Fatty acyl CoA is essential for the final separation of the transport vesicle from the donor membrane, but how this happens is not known. Finally, hydrolysis of GTP bound to the Arf proteins causes depolymerization of the coat and release of coatomers and ARF-GDP [Rothman 1996].

In the case of Rab-proteins, a cytosolic protein called GDI catalyzes the exchange of GDP which binds to cytosolic Rab, inducing a conformational change in Rab. This enables Rab to bind to a surface protein on a particular transport vesicle. After vesicle fusion, the GTP bound to the Rab protein is hydrolyzed to GDP triggering the release of the Rab protein which can then undergo another cycle of GDP-GTP exchange, binding, and hydrolysis. The rate of vesicle fusion is controlled by the absolute amount of Rab-GTP, which is modulated by unidentified protein regulators [Schimmoller *et al.* 1998; Zerial and McBride 2001]. Several lines of evidence support the involvement of specific Rab proteins as timers of vesicle fusion events. For instance, Rab3 is found predominantly in the donor compartment [Tuvim *et al.* 2001] and Rab5 is localized to *early* endosomes, organelles that form from clathrin-coated vesicles, just after they bud from the plasma membrane during receptor-mediated endocytosis [Morrison *et al.* 2008]. Rab7 is known to be associated with late endosomes and regulates membrane transport leading the transition from early to late endosomes [Feng *et al.* 1995]. Thus, some individual Rab proteins are clearly essential for specific vesicle fusion reactions to occur [Markgraf *et al.* 2007]. However, it is not known whether Rab proteins interact with V-SNARE proteins to determine the specificity of vesicle fusion with target membranes [Lodish 2004].
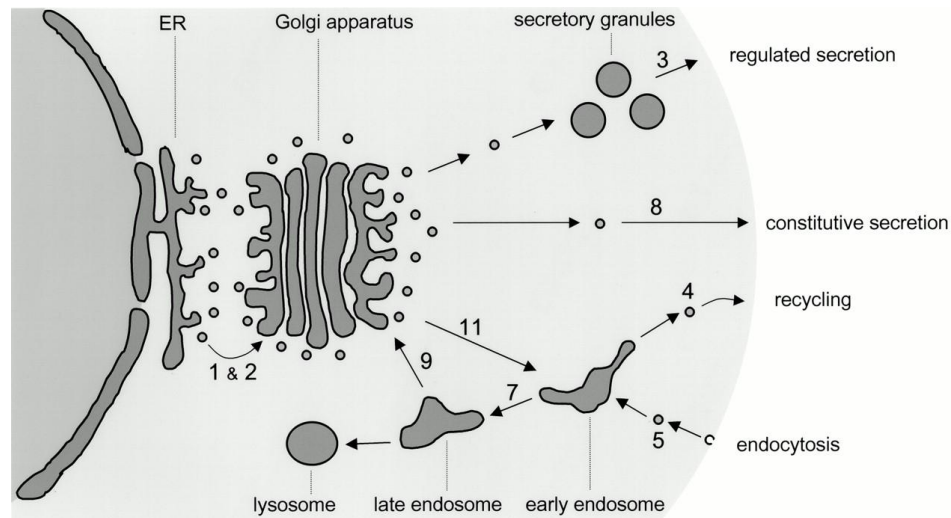
Figure 3 Rab proteins and vesicular trafficking: Individual Rab proteins are associated with distinct intracellular compartments. In some cases, the Rab protein is found predominantly localized on the target compartment (e.g., Rab 5 trafficking from plasma membrane to early endosomes), whereas in other cases it is found predominantly on the donor compartment (e.g., Rab3 in the regulation of exocytosis in secretory granules) [Tuvim et al. 2001].

1.2.3 Microtubules

The cytoskeleton is a network of fibrous elements, consisting primarily of microtubules, actin microfilaments, and intermediate filaments which are found in the cytoplasm of eukaryotic cells. Microtubules are 25 nm in diameter cytoskeletal fibers which are formed by polymerization of α, β-tubulin monomers (which belong to an ancient family of GTPases) and exhibit structural and functional polarity. They are important components of cilia, flagella, the mitotic spindle, and other cellular structures [Lodish 2004].

Membrane vesicles are transported along microtubules in every eukaryotic cell, the best-studied system is the intracellular movement of Golgi vesicles. In cultured fibroblasts, the Golgi complex is concentrated near the microtubule-organizing centre (MTOC). During mitosis or after drug (colcemid) induced depolymerization of microtubules, the Golgi complex breaks into small vesicles that are dispersed throughout the cytosol. When the cytosolic microtubules re-form during interphase or after removal of the colcemid, the Golgi vesicles move along these microtubule tracks towards the MTOC. There these Golgi vesicles re-aggregate to form large membrane complexes [Schmoranzer and Simon 2003]. In addition to the Golgi complex,

microtubules are also associated with the endoplasmic reticulum (ER). Fluorescence microscopy, using anti-tubulin antibodies and $DiOC_6$, a fluorescent dye specific for the ER, reveals an anastomosing network of tubular membranes in the cytosol that colocalizes with microtubules. If microtubules are destroyed by drugs such as nocodazole or colcemid, then the ER loses its network-like organization. After the drug is washed from the cell, tubular fingers of ER grow as new microtubules. This close association between ER and intact microtubules suggests that certain proteins act to bind ER membranes to microtubules [Lodish 2004].

In most familial cases of neurodegenerative disorders, dysfunction of the cytoskeleton changes vesicular biogenesis, vesicle/organelle trafficking, and synaptic signaling [Fletcher and Mullins 2010]. Cytoskeleton disruption is caused by activation of DNA damage followed by a cascade of events including mitochondrial dysfunction and oxidative stress [McMurray 2000]. The endosomes move along with microtubules, and microtubule disruption may produce enormous Rab5 and Rab7 positive endosomes. During clathrin-coated endocytosis the primary endocytic vesicles contain Rab5 and Arf1 domains but they do not contain Rab7. Later Rab7 is recruited to these endosomes and the other early endosome-associated small GTPases are eliminated The Rab7-containing endosomes move along microtubules and fuse with other late endosomes.

1.3   Interactomics

Proteins rarely act alone; rather they interact with other molecules to perform their functions. In most biological systems protein-protein interactions are of critical importance. There are various approaches used to identify these interactions, such as the yeast two-hybrid system, immunoprecipitation, tagged purifications, or affinity purification-mass spectrometry.

1.3.1 PrP[C] – putative interacting partners

The molecules interacting with PrP[C], because of their intrinsic activity, localization in the same cell compartment and within a specific signaling pathway, are a major focus of studies investigating the possible functions of PrP[C]. The first known interacting partners of PrP[C] were Pli45 and Pli110 [Oesch *et al.* 1990]. Pli 45 was identified as glial fibrillary acidic protein (GFAP), an astrocytic marker that accumulates concomitantly with disease-associated PrP[C] during TSEs [DeArmond *et al.* 1992]. The

two-hybrid system of yeast was used to identify anti-apoptotic protein Bcl-2 [Kurschner and Morgan 1995; Kurschner and Morgan 1996]; Heat shock protein 60 [Edenhofer *et al.* 1996]; the 37kDa laminin receptor precursor [Rieger *et al.* 1997]; synapsin Ib; adaptor protein Grb2, and prion interaction protein Pint 1 [Spielhaupter and Schatzl 2001].

PrP^C was also immunoprecipitated with antibodies to the binding proteins calnexin, protein disulphide isomerase, and calreticulin [Capellari *et al.* 1999]. It has also been shown that PrP^C binds with many proteins including laminin [Graner *et al.* 2000]; neural cell adhesion molecules (N-CAMs) [Schmitt-Ulms *et al.* 2001]; 67 kDa laminin receptor [Gauczynski *et al.* 2001]; glycosaminoglycans (GAGS) [Priola and Caughey 1994; Pan *et al.* 2002]; stress inducible protein STI-1 [Zanata *et al.* 2002]; casein kinase 2, dystroglycan, aldolase C, heterogeneous nuclear ribonucleoprotein A2/B1 [Lasmezas 2003]; tubulin [Nieznanski *et al.* 2005]; vitronectin [Hajj *et al.* 2007] and signal protein 14-3-3 beta [Mei *et al.* 2009]. The functional influences of these interacting partners are still largely unknown, but both the biochemical features and the biological functions of PrP^C may change through these interactions.

1.4 Aims of the Study

In the present study experiments were designed to identify interacting partners of PrP^C using an affinity purification strategy. In recent years many groups have tried to identify these interacting proteins; however, the hydrophobic nature and intracellular trafficking of PrP^C pose a challenge. The use of One-STrEP-tag affinity purification was hypothesized to yield better results with less background contaminants due to the high specificity and binding affinity of STrEP-tactin. These studies were designed to provide a more comprehensive set of potential interacting proteins and lead to greater insight into the various cellular events mediated through PrP^C.

The following strategy was adopted to identify and characterize PrP^C interacting proteins:

1. Transient PrP^C expression in neuronal cell models.
2. Purification and identification of interacting partners of PrP^C.
3. Characterization of GTPase related (Rab7a and Arf1) and alpha-tubulin 1 interacting proteins involved in PrP^C trafficking and internalization.

2. Materials

2.1 Antibodies

Antibodies used for immunoblotting (IB), immunoprecipitation (IP) and immunofluorescence (IF) are listed in Table 1

Table 1 List of antibodies and their application in present study

Primary Antibody	Origin	Dilution IB/IP	Dilution IF	Company/ Cat. No.
3F4 PrP	mouse IgG2a	1:1000	1:200	Chemicon/MAB1562
6H4 PrP	mouse IgG1	1:500	-	Prionics/01-010
α-Tubulin	rabbit IgG	1:1000/1:100	1:50	Cell Signaling/2125
Actin (cytoplasmic 1)	mouse IgG1	1:1000	1:200	Sigma/A5441
Annexin A2	mouse IgG	1:5000	-	BD Transduction/610069
Annexin A5	mouse IgG	1:5000	-	abcam/ab14196
Arf1	mouse IgG1	1:500/1:500	1:500	Affinity BioReagents/ MA3-060
Cofilin-1	rabbit IgG	1:1500	1:200	Sigma/C8736
Peroxiredoxin-1	rabbit IgG	1:1000	-	abcam/ab15571
Rab7(D95F2)	rabbit IgG	1:1000/1:100	1:50	Cell Signaling/9367
Rab9(D52G8)	rabbit IgG	-	1:50	Cell Signaling/5118
SAF 70 PrP	mouse IgG2b	1:1500	-	SPIbio/A03206
STrEP MAB-Classic	mouse IgG1	1:1000	1:100	IBA/ 2-1507-001
Tropomyosin (alpha-4 chain)	rabbit	1:1500	-	Chemicon/Ab5449
Vimentin	mouse IgG2a	1:5000	-	Dako/M7020

Secondary antibody	Origin	Dilution IB	Dilution IF	Company/ Cat. No.
α-mouse-HRP	rabbit	1:5000	-	IBA/2-1591-001
α-mouse-HRP	goat	1: 15000	-	Bio-Rad/170-6516
α-rabbit-HRP	goat	1:5000	-	Bio-Rad/170-6515
α-mouse-Cy3	goat	-	1:200	Dianova/115-165-146
α-mouse-A488	goat	-	1:200	Invitrogen/522263
α-rabbit-A488	goat	-	1:200	Molecular Probes/A11070

2.2 Antibiotics, enzymes and standards

Table 2 List of antibiotics, enzymes and standards

	Company/ Cat. No.
Antibiotics	
Ampicillin	Calbiochem/171254
Geniticin	Invitrogen/10131019
Kanamycin	Invitrogen/11815-024
Enzymes	
Rstriction Endonuclease Xba I	Boehringer / 674 257
Restriction enzymes (Others)	New England Biolabs/ Germany
Standards (DNA & protein)	
Mass Ruler DNA ladder mix 10kDa	Fermentas/SM0403S
DNA ladder low range	Fermentas/SM0383S
λDNA/HindIII fragments	GibcoBRL/10382-018
C-Terminus One-STrEP-tag Protein Ladder	IBA/ 2-1011-100
Precision Plus Protein Standard	Bio-Rad/ 161-0374

2.3 Bacterial strain and culture media

Table 3 List of bacterial strain and culture media

	Company/ Cat. No.
Bacterial strains (E.coli) DH5α/Top10	Invitrogen-18258-012/C4040-10
LB-medium	Applichem/A0954,9010
LB-agar	Applichem/A0927,9010
Agarose	Biozym/840004
Low melting agarose	Biozym/840101

2.4 Chemicals

All chemicals used in this study were obtained from Amersham (Freiburg, Germany), Sigma and Fluka (Deisenhofen, Germany), Merck (Haar, Germany), Applichem (Darmstadt, Germany), Serva (Heidelberg, Germany), Roth (Karlsruhe, Germany) and BioRad (München, Germany), if not stated otherwise in the text.

2.5 Eukaryotic cells and culture media

Prnp-deficient (Prnp$^{-/-}$) Murine hippocampal neuronal cells (HpL3-4): HpL3-4 cells were kindly provided by Prof. Takashi Onodera, Department of Molecular Immunology, School of Agricultural and Life Sciences, University of Tokyo, Japan. The cells were cultured in Dulbecco's modified Eagle's medium (DMEM) (Sigma-Aldrich Chemie, Germany), supplemented with 10% fetal bovine serum (FBS) (Biochrom AG, Germany), and 1% penicillin/Streotomycin (PS) (Biochrom AG, Germany) at 37°C, supplied with 5% CO_2 and 95% humidity.

SH-SY5Y (Stably expressing PrP^C) cells: SH-SY5Y cells were obtained from Prof. Walter Schulz-Schaeffer, Department of Neuropathology, University medical center (UMG), Goettingen, Germany. The cells were cultured in DMEM, supplemented with 10% FBS, 1% PS, Geniticin 200µg/ml, at 37 °C, supplied with 5% CO_2 and 95% humidity.

Human embryonic kidney (HEK) 293 cells: HEK-293 cells were purchased from the American Type Culture Collection (ATCC). The cells were cultured in DMEM, supplemented with 10% FBS, and 1% PS, at 37°C, supplied with 5% CO_2 and 95% humidity.

2.6 Instruments and other materials

Table 4 List of the instruments used in this study

Appliance	Model or Description	Manufacture
Bio-safety Cabinet	Hera safe KS	Heraeus/ Osterode, Germany
Centrifuges	5415C	Eppendorf/Hamburg,Germany
	Rotina 35R	Hettich/ Tuttlingen, Germany
	Mikro 200	Hettich/ Tuttlingen, Germany
	Minifuge T	Heraeus /Hanau, Germany
	Optima TL 100	Beckman**/** Krefeld, Germany
Chamber slide	Lab-Tek™ II Chamber Slide, 154534	nunc/ New York, USA
Culture dishes	60 mm, 351016	Becton Dickinson /NJ, USA
Electro blotting apparatus,	Mini Trans-Blot®,	Bio-Rad /Munich, Germany
Electrophoresis apparatus,	Mini-Protean® III,	Bio-Rad /Munich, Germany
Electroporation cuvette	1mm, 748 011	Biozym/ Oldendorf, Germany
Freeze drier	Alpha 1-4 LD	SciQuip Ltd/ Shropshire, UK
Gene Pulser Xcell Electroporation Systems	165-2660	Bio-Rad/ California, USA
Heated magnetic stirrer	iKAMAG RCT	IKA-Labortechnik/ Staufen, Germany
Ice machine	-	Ziegra /Isernhagen, Germany
Incubator	IFE 400	Memmert/ Schwabach, Germany
IPG strips	163-2002**,** 7 cm, pH 3–10	Bio-Rad/ Munchen, Germany
Microscope	Zeiss LSM 510 Meta	Carl Zeiss/ Goettingen, Germany
Microwave oven	ER-6320 PW	Brother International/ Bad Vilbel, Germany
Power supply	Power Pac 300	Bio-Rad /Munich, Germany
PROTEAN IEF cell	165-4001	Bio-Rad/ Munchen, Germany
Safe-Lock tubes	0.2, 0.5, 1.5 and 2ml	Eppendorf /Hamburg, Germany
Semi-Dry transfer Cell	Transblot SD	Bio-Rad/ Munchen, Germany

Serological pipettes	2, 5, 10, 25ml	Sarstedt /Germany
plastic tubes	15 and 50ml	
pH meter	pH 526	WTW/ Weilheim, Germany
Shakers	CERTOMAT R	Sartorius/ Goettingen, Germany
Spectrophotometers	EL808	Bioteck instruments/Winooski-vermont, USA
	DU 7500	Beckman/ Krefeld, Germany
Sterile filter Nalgene	0.2µm	Sartorius/ Goettingen, Germany
Sterile filter pipette tips	-	Biozym /Oldendorf, Germany
Syringes BD Discardit	2, 5, 20ml	Becton Dickinson /NJ, USA
Thermal Cycler	TGradient	Biometra/ Goettingen, Germany
Thermomixer	5436	Eppendorf/ Hamburg, German
UV-transilluminator	200x 200mm	Bachofer/ Reutlingen, Germany
Vacuum drier	UNIVAPO 150H	UNIEQUIP/ Martinsried, Germany
Vortexer	Genie 2™	Bender and Hobein /Zurich, Switzerland
Water bath	1003	GFL/ Burgwedel, Germany
X-ray films	HyperfilmTM	Amersham Biosciences /Freiburg, Germany

2.7 Kits

All the listed kits were used according to the manufacturer's instructions.

Table 5 list of the kits used in this study

Name	Company/ Cat. No.	Application
Caspase-3 activity assay kit	Promega/G7220	Apoptotic activity assay
C-terminus One-STrEP-tag AP detection kit	IBA/2-1503-000	C-Terminus One-STrEP-tagged protein detection

22

C-terminus One-STrEP-tag Starter kit	IBA/2-1101-000	Purification of C-Terminus One-STrEP-tag protein
EndoFree Plasmid Maxi Kit	Qiagen/12362	Plasmid DNA preparation
QIAfilter Plasmid Midi Kit	Qiagen/12243	Plasmid DNA preparation
Qiaprep Spin Miniprep Kit	Qiagen/27106	Plasmid DNA preparation
QIAquick gel extraction Kit	Qiagen/28704	DNA gel extraction
QIAquick PCR purification Kit	Qiagen/28106	DNA fragment purification
StarGate Transfer / combinatorial Cloning kit	IBA/5-1603-020	Cloning of C-Terminus One-STrEP-tag plasmids

2.8   Oligonucleotids

The oligonucleotides used in this study are listed in Table 6

Table 6 List of oligonucleotides

Oligo	Sequence (5'-3')	Accession/Cat. No.
Prnp-For	AATGGCGAACCTTGGCTGCTGGAT	DQ408531
Prnp-Rev	TCCCACTATCAGGAAGATGAGGAA	DQ408531
Prnp-M129v-For	CACATGGCTGATGCTGCAGCAG	DQ408531
Prnp-M129v-Rev	GTGTACCGACTACGACGTCGTC	DQ408531
Prnp-H169y-For	CCATGGATGAGCACAGCAACCAG	DQ408531
Prnp-H169y-Rev	GGTACCTACTCGTGTCGTTGGTC	DQ408531
Pesg-sequencing-Primer-For	GAGAACCCACTGCTTACTGGC	IBA/5-0000-121
Pesg-sequencing-Primer-Rev	TAGAAGGCACAGTCGAGG	IBA/5-0000-122
siRNA Duplex		
siRNA-Rab7a	CUGCUGCGUUCUCCUAUUU	Operon
siRNA Negative control	-	EUROGENTES/SR-CL000-005

Note: Colour highlights the combinatorial sites for combinatorial cloning (see section 3.2.2).

2.9 Plasmids

pENTRY- IBA1 (Lot. No. 4095-) and pESG-IBA103 (Cat. No. 5-4503-000) plasmids were provided by IBA, Goettingen. The construct maps for these vectors are provided in the Appendix.

2.10 Software

The following is a list of scientific software used in the study.

Table 7 List of scientific software

Program	Use	References
Decodon Delta2D	2-DE gel analysis	DECODON GmbH, Greifswald Germany
Graphpad Prism 5	Statistical analysis	GraphPad Software, Inc. California, USA
ImageJ 1.43u	Densitomatric analysis	National institutes of Health, USA
ImageJ 1.43u WCIF	Colocalization analysis	National institutes of Health, USA
KC4 V3.4	Absorbance reader	Bioteck instruments, USA
LabImage 2.7.1	Densitomatric analysis	Kapelan GmbH, Halle, Germany
Protein-Lynx-Global-Server v 2.1	LS MS/MS data analyzer	Micromass, Manchester, U.K
Zeiss LSM 4.2.0.121	Immunofluorescence	MicroImaging GmbH, Goettingen, Germany

2.11 Stock solutions

Blocking solution for WB: 5% Milk Powder in TBS-T

Cell lysis buffer I: 50 mM Tris-HCl pH 8.0, 0.5% CHAPS, 1mM EDTA, 1% triton x100

Cell lysis buffer II: 7 M urea, 2 M thiourea, 4% CHAPS, 2% ampholytes, 1% DTT and a protease inhibitor mixture

Electrophoresis buffer (SDS-running buffer): 192 mM glycine, 0.1% SDS, 25 mM Tris-HCl pH 8.3

Elution buffer (C-terminus One-STrEP-tag purification): 100 mM Tris-HCl pH 8.0, 150mM NaCl, 1mM EDTA, 1% triton x100

Equilibration buffer I: 6 M urea, 2% SDS, 30% glycerin, 0.375 M Tris pH 8.8, 2% (w/v) DTT

Equlibration buffer II: 6 M urea, 2% SDS, 30% glycerin, 0.375 M Tris pH 8.8, 2.5% (w/v) IAA, BPB in traces

Laemmli Buffer (6x): 125 mM tris-Cl, 4% SDS, 20% glycerol, 2% mercatoethanol, pH 6.8

Rehydration buffer: 8 M urea, 2.5 M thiourea, 4% CHAPS, 66 mM DTT and 0.5% ampholytes

Silver staining solutions:

    Developing solution: 6% Na_2CO_3, 0.0185% formaldehyde, 16 µM $Na_2S_2O_3$ in ddH_2O

    Fixation solution: 50% methanol, 12% acetic acid in ddH_2O

    Sensitizing solution: 0.8 mM $Na_2S_2O_3$ in ddH_2O

    Silver nitrate solution: $AgNO_3$ 0.2% and 0.026% formaldehyde in ddH_2O

TBE: 42 mM Boric Acid, 10 mM EDTA, 50 mM Tris-HCl pH 8.0

TBS-T: TBS and 0.1% of Tween-20

TE: 0.01 M Tris-HCl, pH 7.4, 1 mM EDTA pH 8.0

Transblot buffer for Nitrocellulose membrane: 192 mM glycine, 20% methanol, 25 mM Tris-HCl pH 8.3

Transblot buffer for PVDF membrane (semi dry): 192 mM Glycine, 10% methanol, 25 mM Tris-HCl pH 8.3

3. Methods

3.1 Microbiological methods

3.1.1. Culturing and storage of *E. coli*

The *E. coli* strains were cultured for about 12-16 H in LB-medium at 37ºC on an orbital shaker at 180-250 rpm until approximately 0.6 OD_{600}. For long-term storage bacterial strains were mixed with glycerol (9:1) and stored at -80ºC.

3.1.2. Preparation of electrocompetent *E. coli* cells

One liter of LB medium was inoculated with 10 ml of fresh overnight culture of *E.coli* (DH5α strain). The culture was incubated for about 12-16 H in LB-medium at 37ºC on an orbital shaker at 180-250 rpm until the OD_{600} reached to approximately 0.5-0.8. The culture was cooled on ice for 1 H and centrifuged at 5,000 x g for 10 min. at 4ºC. The pellet was resuspended in 10 ml ice-cold ddH_2O and centrifuged at 5,000 x g for 15 min. at 4ºC. The resuspension and centrifugation step was repeated as before. The pellet was then resuspended in 5 ml ice-cold ddH_2O. After centrifugation at 5,000 x g for 15 min. at 4ºC, the bacterial pellet was resuspended in 30 ml ice-cold ddH_2O with a final concentration of 10% glycerol. Following the last centrifugation step (5,000 x g for 15 min. at 4ºC), the pellet was then resuspended in ice-cold ddH_2O followed by slow addition of glycerol to a final concentration of 10%. This cell suspension was dispensed in 0.5 ml aliquots which were first subjected to shock freezing in liquid N_2 before storage at -80°C. Cells were kept on ice during the entire procedure.

3.1.3. Transformation of electrocompetent *E. coli* with plasmid DNA

An aliquot of competent cells was first allowed to thaw on ice. About 5 ng DNA ligation product was added to 50 µl of competent cells and incubated for 5 min. The mixture was then subjected to electroporation pulse using Bio-Rad Gene Pulser II (Bio-Rad, München, Germany). Electroporation was carried out at 1.8 kV with capacitance of 25 µF and pulse-controller-resistance of 200 Ω. Immediately after the pulse, 900 µl of pre-warmed LB medium was added to the cuvette. After resuspension cells were incubated for 40 min. at 37ºC with shaking (180 rpm). The transformed cells were then

plated on pre-warmed LB agar supplemented with 100 µg/ml ampicillin and 50 µg/ml X-Gal, or 50 µg/ml Kanamycin and then incubated at 37ºC for 12-16 H.

3.1.4 Extraction of plasmid DNA

Plasmid DNA was extracted using the QIAPrep Spin Miniprep Kit (QIAGEN, Hilden, Germany). A single colony of *E. coli* was inoculated into 5 ml LB medium supplemented with ampicillin to a final concentration of 100 µg/ml and then incubated for 16 H at 37°C with shaking (180 rpm). The cells were harvested by centrifugation at 5,000 x g for 10 min. at 4°C. The remaining steps were performed according the manufacturer's instructions.

3.2 Molecular biology methods

3.2.1 Extraction of genomic DNA

A total of 500 µl fresh anticoagulated/EDTA whole human blood was supplemented with RNase A (100 mg/ml) to obtain RNA-free genomic DNA. The blood cells were then lysed in 1 ml of lysis buffer, briefly mixed by vortexing, and then incubated for 10 min. at 56ºC followed by the addition of 200 µl of 100% ethanol and brief vortexing. The mixture was then carefully applied to a QIAamp spin column and centrifuged for one minute at approximately 11,000 x g in a table-top microcentrifuge. The bound DNA was washed with 500 µl of washing buffer and the column was centrifuged for one minute. An additional washing step was carried out by applying 500 µl of washing buffer to the QIAamp spin column which was then centrifuged for 3 min. at maximum speed (13,000 x g). Any residual contaminants were removed by another 1 min. centrifugation step. Finally, the QIAamp spin column was loaded with 200 µl of elution buffer, incubated for 5 min. at RT and centrifuged at approximately 11,000 x g for an additional minute. Small- and large-scale plasmid extractions were performed using the QIAGEN Mini and Maxi kits respectively according to the manufacturer's instructions.

Ethanol DNA precipitation was carried out in order to improve the purity of the eluted DNA. Two volumes of ice-cold 100% ethanol and one tenth volume of 3 M sodium acetate buffer (pH 5.0 - 5.3) were added to one volume of eluted DNA. The solution was briefly vortexed and left on dry ice for 2-5 min. The supernatant was

quickly discarded after centrifugation (11,000 x g) in a microcentrifuge for 30 min. at 4ºC. Then 200 µl of ice-cold 70% ethanol was added to the precipitate. Following another centrifugation step at maximum speed (11,000 x g) for 10 min at 4ºC, the supernatant was discarded and any residual ethanol was carefully removed without disturbing the pellet. The pellet was then air-dried for 2-3 min. and subsequently resuspended in TE buffer (pH 8.0). The solution was briefly mixed by vortexing, shortly centrifuged (13,000 x g) and stored at 4ºC for further analysis.

3.2.2 Combinatorial cloning procedures

All the procedures were performed according to the instructions provided in the StarGate Transfer/combinatorial Cloning kit-IBA with a slight modification, briefly described (below);

3.2.2.1 Primer design

The 5′- phosphorylated primers for combinatorial cloning (see section 2.8) were equipped with combinatorial sites at the 5′- and 3′- ends with the initial hybridization region having a melting temperature of 60-63ºC. The 3′- end of the primers was designed to be phosphorothioate protected with a proof reading DNA polymerase. The 5′- ends of the standard forward primers were formed by an additional -AATG- quadruplet to generate the upstream combinatorial site. The 3′- ends of the standard reverse primers were formed by an additional –TCCC- quadruplet to generate the downstream combinatorial site.

3.2.2.2 Amplification of *PRNP*

The amplification of *PRNP* was carried out in a total volume of 50 µl containing 2 mM $MgSO_4$, 10x ThermoPol Reaction buffer (New England Biolabs), 20 mM dNTPs (New England Biolabs), 25 pmol of each oligonucleotide primer, 1 U DNA polymerase (2,000 U/ml) (New England Biolabs), 100 ng of the template DNA and ddH_2O. Thirty-five cycles were done with initial denaturation at 95ºC for 120 s, denaturation at 95ºC for 30 s, annealing at 60ºC for 45 s and extension at 72ºC for 60 s.

3.2.2.3 Donor vector generation

The pENTRY-IBA1 entry vector was mixed with 4 nM of water diluted PCR product and Star Solution E (1 µl), then incubated for 1 H at 22°C. An aliquot of 10 µl from the reaction mixture was incubated for 30 min. on ice with competent cells. The

mixture was mixed gently and incubated for 5 min. at 37°C and subsequently on ice for 2-5 min. Then the mixture was supplemented with 900 µl LB medium (without antibiotics) and incubated at 37°C with shaking for 45 min. The mixture was then plated on pre warmed LB Agar containing 50mg/L kanamycin and incubated at 37°C for 12-16 H.

3.2.2.4 Mammalian expression vector generation

The supplied lyophilized , liquid acceptor vector pESG-IBA103 was diluted with generated donor vector solution to make the final concentration 1 ng/µl. Star solution A1, A2, A3 (1 µl each) were added and incubated with the StarMixll at 30°C for 1 H. The generated vectors were then transformed in competent cells previously thawed on ice. The mixture was mixed gently and incubated on ice for 30 min, then incubated at 37°C for 5 min., and finally put on ice for 2 min. The mixture was then supplemented with 90 µl LB medium (without antibiotics), plated on LB Agar containing 100mg/L ampicillin and 50 mg/L X-Gal, and finally incubated at 37°C for 12-16 H. The generated vectors were then extracted as mentioned previously in section 3.1.4.

3.2.2.5 Restriction digestion of vector DNA

For cloning and analytical confirmation of the resultant clones, DNA was digested using *Xba1/Hindlll* restriction enzymes (FERMENTAS, St.Leon-Rot, Germany, New England Biolabs, Frankfurt, Germany). Generally 5-10 µg of plasmid DNA was digested for 1-2 H in a total volume of 20 µl at 37ºC using appropriate endonucleases in corresponding buffers. Three white colonies were selected and DNA mini preparation was performed (see section 3.1.4).

3.2.3 Site directed mutagenesis

Site directed mutagenesis was used to generate mutations (base substitutions) from double-stranded plasmid without the need for subcloning. The cDNA (0.5 pmole) was added to a PCR cocktail containing, 2 mM $MgSO_4$ buffer, 0.2 mM of each dNTP, 25 pmol of each oligonucleotide primer, 2.5 U *Taq/Pfu* DNA polymerase mix and 5% DMSO. Twenty-five cycles were performed with initial denaturation at 95ºC for 120 s, denaturation at 95ºC for 30 s, annealing at 60ºC for 30 s and extension at 72ºC for 60 s with a final extension of one cycle at 72ºC for 120 s. The parental template DNA and the linear, mutagenesis-primer incorporating newly synthesized DNA were treated with *DpnI*

(15 U) and *DpnI* buffer 5µl/50µl. The *DpnI* enzyme is specific for methylated and hemi-methylated DNA and therefore digests the parental DNA template but does not digest the mutant synthesized DNA. As most *E.coli* strains produce methylated DNA, they are not resistant to *Dpn I* digestion. This reaction was incubated at 37°C for 2 H. Undigested DNA was then purified by the PCR purification kit according to the manufacturer's instructions. The purified mutated DNA was then transformed into competent cells (see 3.1.3).

3.2.4 DNA agarose gel electrophoresis

Agarose was melted in TBE buffer and 0.3 µg/ml ethidium bromide solution was added after being cooled to RT. The agarose was then poured into the agarose gel chamber. DNA samples were mixed with DNA loading buffer and ddH$_2$O up to a final volume of 12.5 µl for loading of the gel. Gels were run in 1 x TBE buffer at 80-100 V for 1-2 H, depending on the size of the examined DNA fragment or on the degree of the band separation required. The DNA bands were then visualized by UV light at 302 nm using a Gel Documentation 2000™ UVtransilluminator (Bio-Rad) and the Quantity One software (version 4.2.1). The estimation of DNA was done by visual comparison of the band intensity with that of a standard marker.

3.2.5 Purification of DNA from agarose gels

The PCR products were purified using QIAquick gel extraction Kits. The DNA fragments (bands) were excised from the agarose gels. The remaining steps were done exactly as described in the manufacturers instructions provided. The concentration of DNA in the final solution was measured at the Biophotometer (Eppendorf) at 260 nm.

3.3 Cell biology methods

3.3.1 Cryopreservation and thawing of eukaryotic cells

For long-term storage, cells were frozen in the presence of dimethylsulphoxide (DMSO). The 60-90% confluent cells were centrifuged at 400 x g for 5 minutes at 4°C. The cells were then resuspended in ice-cold medium containing 70% DMEM, 20% FBS and 10% DMSO and finally aliquoted into 1ml cryogenic storage vials. The storage vials

were incubated at -20°C for 5 H and then 12-16 H at -80°C before they were finally stored in cryogenic vials suspended in liquid nitrogen.

To re-freeze the cryo-preserved cells, the cryogenic stored vials with cells were quickly thawed in a water bath at 37°C. Subsequently, the cells were directly mixed with complete culture media (see section 2.5) and centrifuged at 400 x g for 5 min. in order to remove the cryopreservative (DMSO). The cells were then resuspended in the complete culture media and seeded in tissue culture flasks.

3.3.2 Cultivation of eukaryotic cells

All cell lines were cultured in their respective media (see section 2.5) and underwent between 5 and 25 passages. The cells were diluted 1:4 every 3-5 days after reaching approximately 70% confluency. The cell medium was removed and 3-5 ml of pre-warmed (37°C) 0.05% trypsin/0.02% EDTA solution was added to the culture, incubated for 2-5 min. until the cells detached from the flask at 37°C. Cell culture medium (10 ml) was then added to stop the trypsin activity. The detached cells were carefully transferred to a Falcon tube and were spun down at 4°C for 5 minute at 400 x g. After removing the supernatant the cell pellet was resuspended in 10 ml fresh media and seeded in four flasks (75 cm^2). In the case of neuronal SH-SY5Y (PrP^C Stable expressed) cells, Geniticin 200µg/ml containing media in 75 cm^2 flasks was used for selection.

3.3.3 Liposome-mediated transient transfection

Transfection assays were performed using Lipofectamine 2000 (Invitrogen) following the supplier's recommendations. The cells were seeded in 6-well plates at a cell density of 2-5 x 10^5 per well and maintained for 24 H in the medium containing 10% FBS. Prior to transfection cells were washed with Opti-MEM® I and subsequently transfected with 5 µg of DNA/well in Opti-MEM® I. After an incubation period of 24 H the transfection medium was replaced with DMEM supplemented complete medium. Cells were collected from confluent cultures after 48 H of transfection.

3.3.4 Small interference RNAi treatment

The cells were cultured (see section 3.3.2) for 24 H in complete DMEM medium prior to transient transfection (see section 3.3.3). The C-Terminus One-STrEP-tag PrP^C (5 µg) was co-transfected with siRNA (100 nM) (see section 2.8) in HpL3-4 cells. In SH-

SY5Y siRNAs with 100 nM duplexes were transfected using Lipofectamine 2000 (Invitrogen, Carlsbad, CA, USA) according to the manufacturer's instructions. The cells were also simultaneously transfected with non-targeting siRNA duplex (control siRNA Duplex Negative Control: Eurogentec). After 48 H of transfection the cells were lysed (see section 3.3.7) for expression analysis and immunofluorescence (see section 3.3.6) for localization studies.

3.3.5 Immunocytochemical and quantification analysis

Cells were plated on chambered slides (Lab-Tek™ II; Thermo Fisher Scientific (Nunc GmbH & Co. KG), Langenselbold Site) and transfected with the C-terminus One-STrEP-tag PrP^C for 24, 36, and 48 H. Cells were subsequently washed in a phosphate-buffered saline (PBS) and were fixed for 15 min. with 100% ethanol. After fixation cells were permeabilised with 0.2% Triton X-100 in 1xPBS, followed by a 20 min. blocking step using 0.2% casein-solution containing Tween 20. Co-localization of PrP^C with interacting proteins was detected by applying the primary antibodies [anti-PrP 3F4 (1:200), rabbit anti-Rab7a (1:50), rabbit anti-Rab9 (1:50), mouse anti-Arf (1:500), and mouse anti-Tubulin alpha (1:100)] for 12-14 H at 4°C. The primary antibodies were detected by incubating the slides for 60 min with secondary antibodies [Alexa 488 conjugated anti-rabbit (1:200), Alexa 488 conjugated anti-mouse (1:200) or Cy3-labeled anti-mouse secondary antibody (1:200)]. Incubation with Hoechst 33342 or with TO-PRO-3 iodide for 10 min was performed to visualize nuclei. Finally, cover slips were placed on glass slides and mounted with Fluoromount (DAKO, Hamburg, Germany). After secondary antibody incubation all the steps were carried out in a dark humid chamber. The slides were kept dry in dark at 4°C until further microscopic evaluation.

Confocal laser scanning microscopy was carried out using a LSM 510 laser-scanning microscope (Zeiss, Göttingen, Germany; 488 nm Argon, 543 and 633 nm Helium-Neon excitation wavelengths) according to the manufacturer's instructions for the localization of PrP^C and other interacting proteins, using a 63x/1.25 oil immersion lens. Individual images were analyzed separately for colocalization using LSM 5 (Zeiss) or ImageJ (WCIF plugin) software. For two-color analysis, stacks of images with a total thickness of approximately 30μm were acquired, using a dynamic range of 12 bits per pixel. Colocalization expressed as a correlation coefficient indicates the strength and direction of the linear relationship between two fluorescence channels. Pearson's linear

correlation coefficient (r_P) was used in this study to calculate fluorescence channel correlations:

$$r_p = \sum_i (x_i - x_{aver}) \cdot (y_i - y_{aver}) / \left(\sum_i (x_i - x_{aver})^2 \cdot (y_i - y_{aver})^2 \right)^{1/2}$$

Where x_i= intensity of voxel I in image (x_i=0 if x_i is outside threshold of detection)

y_i= intensity of voxel I in image (y_i=0 if y_i is outside threshold of detection)

x_{aver} and y_{aver} represent averages of the x and y channel intensities.

The value of r_P is between -1 and 1, where 0 indicates no correlation, and -1 indicates negative correlation. Values>0 indicate a positive correlation.

Colocalization in the context of fluorescence microscopy is defined as the signal detection of two separated fluorescence channels at the same pixel. Threshold settings were generated automatically from regions of interest. Colocalization coefficients were calculated according to published methodology [Manders *et al.* 1993] in which

$$\text{Colocalization coefficient } (M_x) = \sum_i x_{i,coloc} / \sum_i x_i$$

and

$$\text{Colocalization coefficient } (M_y) = \sum_i y_{i,coloc} / \sum_i y_i$$

Where $x_{i,coloc}=x_i$ if y_i is within the intensity range defined by region of interest

$x_{i,coloc}=0$ if y_i is outside the intensity range and

$y_{i,coloc}=y_i$ if x_i is within the intensity range defined by region of interest

$y_{i,coloc}=0$ if x_i is outside the intensity range.

Values of colocalization coefficients range between 0 and 1. A value of 0 indicates that none of the signal within thresholds in that channel exists as co-localized with the other channel. A value of 1 indicates that the entire signal within thresholds in that channel exists as colocalized with the other channel. Two perfectly colocalized images will generate a scatter plot where the points fall in a line at 45° to either axis.

3.3.6 Cell lysis and protein extraction

Total cell lysate was prepared from 70% confluent HpL3-4, HEK-293 and SH-SY5Y cells. For C-Terminus One-STrEP-tag purification, HpL3-4 cells after 48 H of transient transfection were washed with ice cold 1xPBS, scraped and centrifuged at 4°C for 5 min at 400 x g. The pellet was resuspended in ice cold 1x PBS and centrifuged at 4°C for 5 min at 400 x g. The washed cells were then lysed in lysis buffer I (50 mM Tris-HCl, pH8, 1% Triton X-100, 0.5% CHAPS, 1mM DTT, Roche protease and phosphatase inhibitor cocktail). Cell lysates were homogenized with an ultra sonicator on ice (5 strokes) and were then ultra-centrifuged for 15 min. with 543,000 x g at 4°C. Protein concentration was estimated (see section 3.3.8) and either underwent further C-Terminus One-STrEP-tag purification or was stored at -20°C.

3.3.7 Determination of protein concentration

The protein concentration of cell lysate was determined by the Bradford assay (Bio-Rad). Working solution was prepared by diluting a dye reagent (Bio-Rad) with dH$_2$0 1:5 followed by filtration through Whatmann filter paper. BSA protein standards were prepared in dH$_2$0 with a concentration range between 0.0-1.0 mg/ml. Protein samples of unknown concentration were diluted 1:5, 1:10 and 1:20. Protein standards or diluted samples of unknown concentrations (20 µl) were mixed with 1ml of Bradford working solution and incubated for 10 min. at RT. The absorbance of the samples was measured at 595 nm. The calculation of the protein concentration was done using Microsoft Office 2007 Excel software.

3.3.8 One-STrEP-tag purification

Total cell lysate was first prepared (see section 3.3.7). The STrEP-Tactin superflow beads were equilibrated by 3x washing with buffer containing 100mM Tris-HCl, pH8, 1% Triton X-100, 1mM DTT, 150 mM NaCl, Roche protease and phosphatase inhibitor cocktail. The total amount of protein isolated was estimated and then the beads were diluted with wash buffer containing 100mM Tris-HCl, pH8, 1% Triton X-100, 1mM DTT, Protease and Phosphatase inhibitors to make the final concentration of CHAPS 0.1%. The equilibrated STrEP-Tactin superflow beads were incubated with 4 mg total protein for 1 H at 4°C on a rocking platform. Following the centrifugation at 15,000 rpm for 2 min. at 4°C supernatant was removed and STrEP-Tactin superflow beads with attached STrEP-tag protein were washed 4x with wash buffer and then STrEP-tagged protein

complex was eluted with 2.5 mM Desthiobiotin. The eluted proteins were precipitated with methanol/chloroform [Wessel and Flugge 1984].

3.3.9 Immunoprecipitation

Cell lysis was performed as described previously (section 3.3.5). The insoluble cell debris was removed by centrifugation at 543,000xg for 10 min. at 4°C. Immunoprecipitation was performed using Dynabeads protein G (1.5 mg beads/3 mg total protein) according to the manufacturer's instructions. Samples of total cytoplasmic cell extracts or immunoprecipitated proteins (corresponding to 2x10^{6}cells/lane) were subjected to 12.5% SDS-PAGE and transferred to polyvinylidene difluoride membranes (Millipore). Immunoblotting was performed as described in section 3.3.12.

3.3.10 SDS-PAGE

Two-phase gels were used for stacking and separating the proteins of interest according to their molecular weight (4% stacking gel and 12.5% resolving gel). Molecular weight markers were run in parallel in order to determine the size of the loaded proteins. Equal amounts of protein samples and 2x sample buffer (see section 2.9) were mixed, heated for 10 min. at 95ºC and loaded onto the gel. SDS-PAGE was run at 4ºC. A voltage of 20 mA was applied for 15 min. to allow samples to enter the gel and stack without smearing and then increased to 40mA until bromphenol blue reached the bottom of resolving gel.

3.3.11 Immunoblot analysis

Cells were lysed (50mM Tris-HCl, pH8, 1% Triton X-100, 0.5% CHAPS, 1mM DTT), and lysates were cleared off from cellular debris (1 minute, 1000 x g, 4°C). Cell lysates were supplemented with Roche protease and phosphatase inhibitor and were separated on 12.5% SDS-PAGE (see section 3.3.11). Expression of proteins was analyzed by western blot using anti-PrP 6H4 monoclonal antibody (1:1000), anti-PrP SAF70 monoclonal antibody (1:5000), anti-Rab7a mAb (1:1000), anti-Arf1 mAb (1:1000) and anti-Tubulin alpha (1:5000) for 12-14 H at 4°C. Membranes were then rinsed in 1x TBS-T and incubated with the corresponding horseradish peroxidase-conjugated secondary antibody (diluted 1:2000/1:5000) for 1 H at RT. Immunoreactivity was detected after immersion of the membranes into enhanced chemiluminescence (ECL) solution and exposure to ECL-Hyperfilm (Amersham Biosciences, Buckinghamshire,

U.K.). Densitometric values for each band intensity were determined using lab image 2.7.1 data analyzer software.

3.3.12 Two-dimensional gel electrophoresis

First dimension electrophoresis

Proteins were separated in the first dimension by isoelectric focusing (IEF), which separates proteins by their isoelectric point (pI). Seven centimeter pre-cast immobilized pH gradient (IPG) strips (ReadyStrip IPG, Bio Rad) with a linear pH range between 3-10 were used. The amount of protein loaded on each IPG strip varied with the staining method and the length of the strip. The protein load for Coomassie staining was 200 µg whereas for silver staining it was 40 µg. The cell lysates were prepared as described in Section 3.3.7. The total volume of sample applied per IPG strip was 130-135 µl for each 7 cm IPG strip.

Rehydration of IPG strips was carried out in the re-swelling cassette (Bio-Rad). The sample (130-135 µl) containing a certain amount of protein was carefully applied onto the cassette track for strip rehydration. The protective film was removed from the IPG strips and placed (gel side down) onto the cassette without air bubbles. Following 1 H incubation at RT the IPG strips were overlaid with mineral oil (Bio-Rad) to avoid evaporation during an overnight passive rehydration (without any electric field). The focusing of the proteins on IPG strip was initiated at 200 V for 2 H, followed by ramping at 500 V for 2 H, and final focusing at 4000 V for 5 H until a total of 20000 Vh was achieved.

Prior to the second dimension electrophoresis an equilibration step was applied to the proteins separated by IEF in order to reduce disulfide bonds and to alkylate the resultant sulfhydryl groups of the cysteine residues. The IPG strips were incubated on a horizontal shaker with equilibration buffer I for 25 min. followed by incubation in equlibration buffer II for a further 25 min.

Second dimension electrophoresis by SDS-PAGE

Equilibrated strips were placed on top of vertical 12% SDS polyacrylamide gels and overlaid with 1% (w/v) agarose in SDS running buffer. The gels were loaded with the suitable protein markers and run at 100 V for 2 H in Mini Protean II TM gel chamber

at 4ºC. At the end of second dimension electrophoresis gels were removed from the glass plates and either Coomassie stained; silver stained and western blotted to PVDF membranes.

Visualization and imaging of the gels

Coomassie staining was carried out using Roti-Blue staining solution (Roth) mixed with ethanol and water in 40:20:40 ratios. The gels were then briefly destained using ethanol/acetic acid/water (20:5:75) after 12-14 H of incubation and stored in 5% acetic acid in ddH$_2$O. Sensitivity of detection by Coomassie staining requires approximately 40 ng of protein per spot for detection and allows visualization of the broadest spectrum of proteins. The gels were silver stained using the protocol described by Blum and co-workers (1987).

3.3.13 Protein/peptide sequence identification by LC/MS-MS

3.3.13.1 In-gel digestion and preparation of proteins and proteolytic fragments

In-gel digestion was carried out according to the previously described protocol [Asif *et al.* 2007;Asif and Yevzlin 2009]. Specific bands were excised from the silver-stained 1-DE gel into 1−2 mm^2 slices, destained with 15 mM potassium ferricyanide/50 mM sodium thiosulfate (Aldrich/Sigma-Aldrich, Steinheim, Germany) and then equilibrated with 50 mM ammonium bicarbonate/50% acetonitrile (ACN) (Sigma-Aldrich) until destained. Samples were dried for 15 min. using the SpeedVac SVC100 (Savant Instruments, Farmingdale, NY) vacuum concentrator. The dried slices were rehydrated with 10 mM dithiothreitol /100 mM ammonium bicarbonate and incubated at 56°C for 45 min. The slices were then incubated with 55 mM iodoacetamide/ 100 mM ammonium bicarbonate at room temperature for 30 min in the dark and followed by washing with 100 mM ammonium bicarbonate and made 1:1 solution with ACN and incubated for 15 min. Samples were dried for 15 min. and rehydrated on ice with 10−20 μL of trypsin digestion (0.1 μg/μl) solution (Promega, Madison, WI) for 45 min. followed by an overnight incubation at 37°C in digestion solution without trypsin. The peptides were first extracted with 0.1% trifluoracetic acid (TFA) for 30 min. in a sonicating water bath Transsonic 310/H (Elma, Pforzheim, Germany) followed by extraction with 30% ACN in 0.1% TFA and 60% ACN in 0.1% TFA. The eluate was collected in Eppendorf tubes

and dried with the SpeedVac. The extracted peptides were dissolved in 0.1% formic acid (FA) for ESI-QTOF-MS/MS.

3.3.13.2 Identification of protein/peptide sequence analysis

One microliter of tryptic digested peptide solution was introduced using a CapLC auto sampler (Waters) onto a µ-precolumn cartridge C18 pepMap (300 µm × 5 mm; 5 µm partical size) and further separated through a C18 pepMap100 nano Series (75 µm ×15 cm; 3 µm partical size) analytical column (LC Packings). The mobile phase consisted of solution A (0.1% FA in 5% ACN) and solution B (0.1% FA in 95% ACN). The single sample run time was set for 60 min. The chromatographically separated peptides were then analyzed on a Q-TOF Ultima Global (Micromass, Manchester, U.K.) mass spectrometer equipped with a nanoflow ESI Z-spray source in positive ion mode. Data acquisition was performed using MassLynx (v 4.0) software on a Windows NT PC and data were further processed on Protein-Lynx-Global-Server (v 2.1), (Micromass, Manchester, U.K.). Processed data were searched against MSDB and Swiss-Prot databases through the Mascot search engine using a peptide mass tolerance of 0.5 Da and fragment mass tolerance of 0.5 Da. The search criteria were set to a maximum of one missed cleavage allowed by trypsin and protein modifications set to methionine oxidation and carbamidomethylcysteine when appropriate.

3.3.14 Enzyme-linked immunosorbent assay (ELISA)

For ELISA analysis the BetaPrion® BSE EIA Test Kit (Leipzig, Germany) was used and all procedures were performed according to the supplier's recommendations. Briefly, equal amounts of protein (50 µg) from cell lysates of control and *PRNP*-transfected cells were added to a microtitre plate coated with a monoclonal anti-PrP antibody and incubated for 60 min. at 37ºC. Recombinant human PrP^C (Roboscreen, Leipzig, Germany) was used as a standard. After washing the plate three times a monoclonal, peroxidase-labeled, anti-PrP antibody was added followed by 60 min. incubation at 4ºC. Following five more washes a microtitre plate was incubated for 15 min. with a developing solution containing hydrogen peroxide and tetramethylbenzidine. Afterwards the reaction was stopped, extinction measured (at 450/620 nm) and PrP^C concentration (ng/ml) was determined. Means and standard deviations were calculated from three independent sets of experiments. Significant differences in PrP^C levels were

determined using unpaired Student's *t*-test ($p<0.05$). Each sample was run in duplicate in a blinded fashion.

3.4 Biochemical methods

3.4.1 Cell viability assays

The adherent cells were grown to 60-70% confluency and then detached from flasks using 1x Trypsin-EDTA. The cells were spun down at 4ºC for 5 min. at 400 x g and resuspended in culture media. Cells were then dispensed into 24-well plates (Nunc, Roskilde, Denmark) at a final concentration of $1x10^5$ cells/well and incubated for 12 H at 37°C . The cells were then transfected (see section 3.3.3) with C terminus One-STrEP-tag PrP^C plasmids for variable times (24 H, 36H and 48 H). The culture media was then removed and replaced prior to MTS [3-(4, 5-dimthylthiazol-2-yl)-5-(3-carboymethoxyphenyl)-2-(4-sulfophenyl)-2Htetrazolium, inner salt] treatment. The effect of PrP^C presence on cell viability was measured using the MTS cell proliferation assay, which measures the reduction of MTS tetrazolium salt to formazan by metabolically active cells [Cory *et al.* 1991]. The cells were then treated with a 1:20 ratio of MTS reagent (Promega Co. Madison, WI, USA) 2mg/ml with 05% Glucose and PMS 0.92mg/ml with 0.5% Glucose. Cells were incubated for 1 H at 37°C for color development, and the absorbance values were read at 490 nm using a Multiscan plate reader (Labsystems, Virginia, USA) and Accent software 2.6. Background absorbance from controls was subtracted from sample wells after the final absorbance was obtained.

Trypan blue exclusion was also used to check for cell viability. In subsequent experiments viability was determined by counting the number of cells in 10 fields (20x objective) selected at random on coverslips containing either transfected or un-transfected (control) cells.

The Nuclear Area Factor (NAF) for transfected and non-transfected cells was ere determined by fluorescent staining of the nucleus using DAPI, followed by digital microscopy. The measurement of the nuclear area and nuclear circularity was done using Image J analysis software [Daniel and DeCoster 2004].

3.4.2 Caspase-3 activity assay

The Caspase-3-activity assay allows quantitative measurement of change in caspase-3 (DEVDase) protease activity, which is an early regulatory event in the apoptotic cell death process. The assay was performed using Caspase-3 activity assay kits according to the manufacturer's recommendations. Briefly, untreated conrol, empty vector transfected and C-terminus One-STrEP-tag PrP^C transfected cells were lysed in the cell lysis buffer for 15 min. at 4 °C followed by centrifugation at 10000 x g. Protein concentration was estimated in the supernatants and the total cell lysate (50 µg) was then incubated with 50 µM caspase-3 specific substrate DEVD-pNA for 4-5 H at 37 °C. The caspase-3 inhibitor Z-vad-FMK (20 mM) was used as a control. Caspase-3 mediated release of pNA was measured by absorbance at 405 nm. Background absorbance from the control (untreated cells) was subtracted from the the final absorbance obtained for the samples.

3.4.3 Brefeledin A treatment

Brefeldin A (BFA), a metabolite of the fungus *Eupenicillium brefeldianum*, specifically and reversibly blocks protein transport from the endoplasmic reticulum (ER) to the Golgi apparatus in many cell-types and species. The cells were treated with 1 µg/ml and 10 µg/ml of BFA after 24-48 H of transient transfection at different time points in HpL3-4 cells and same treatment was applied to the SH-SY5Y stable PrP^C cells. After BFA treatment the cells were lysed (see section 3.3.7) for expression analysis and immunomounted (see section 3.3.6) for localization analysis.

3.4.4 Microtubule disruption treatment

The microtubules were disrupted as preiously described [Vonderheit and Helenius2005]. Briefly, cells were cultivated (see section 3.3.2) and treated with 5 µM nocodazole for 30 min., 3 H, and 24 H at 37ºC after transient (section 3.3.3) transfection in HpL3-4 cells and SH-SY5Y stable PrP^C cells. After nocodazole treatment the cells were lysed (see section 3.3.7) for expression analysis or immunomounted (see section 3.3.6) for localization analysis.

3.4.5 Protease K degradation assay

The total cell lysates (siRNA treated and non-treated) were incubated for 60 min. with shaking at 37°C in the presence of PK (50 µg/ml). The digestion was stopped by

adding electrophoresis sample buffer and the protease-resistant PrP was examined by western blotting.

3.5 Statistical analysis

All results in this study were obtained from at least four independent sets of experiments and were expressed as mean ± S.D using descriptive statistics. Densitometric analysis of 1-DE gels were performed using ImageJ 1.43u software.

3.6 Safety measures

All operations with genetically modified organisms and plasmid DNA were performed in accordance with the Gentechnikgesetz of 1990 and the rules described by the Gentechnik-Sicherheitsverordnung of 1990. Ethidium bromide, formaldehyde, acrylamide and other chemicals deleterious for the environment, when used in the course of the work, were carefully managed and disposed of properly in accordance with institutional guidelines. All waste was disposed of according to institutional instructions.

4. Results

Proteins interact with each other to perform their biological functions. Therefore, it is crucial to identify the different partners with which PrP^C might be associated in the cell in order to uncover its physiological role. In recent years, many groups have tried to identify the proteins which functionally interact with PrP^C. However, the complex trafficking and internalization pattern of PrP^C restricts ligand purification.

In this study, a neuronal cell model expressing C-terminus One-STrEP-tag PrP^C was established to identify the interacting proteins of PrP^C. The novel interacting proteins of PrP^C identified, with suggested roles in trafficking and internalization, were further characterized using different molecular biological techniques.

4.1 Generation and expression of C-terminus One-STrEP-tag-PrP^C

Mammalian expression vector encoding C-terminus One-STrEP-tag PrP^C was established with combinatorial cloning. The PRNP gene was first equipped with essential recombination sequences for the transfer of PRNP from pENTRY-IBA (donor vector) to the acceptor vector. The generated acceptor vector (pESG-103-PRNP) was checked by restriction digestion analysis, which showed the 830bp fragment of PRNP-C-Terminus One-STrEP-tag (Figure 4).

To test the C-terminus One-STrEP-tag system, HpL3-4 cells lacking endogenous PrP^C were transiently transfected with the vector containing C-terminus One-STrEP-tag PrP^C (PrP$^{+/+}$ or PrP^C) or control vector without the PrP^C construct (PrP$^{-/-}$). Immunoblotting with PrP^C and One-STrEP-tag antibody confirmed its expression in transfected cells (Figure 5A-C). The PrP^C expression/localization was further confirmed using anti-One-STrEP-tag antibody which showed complete overlapping with PrP^C (Figure 6).
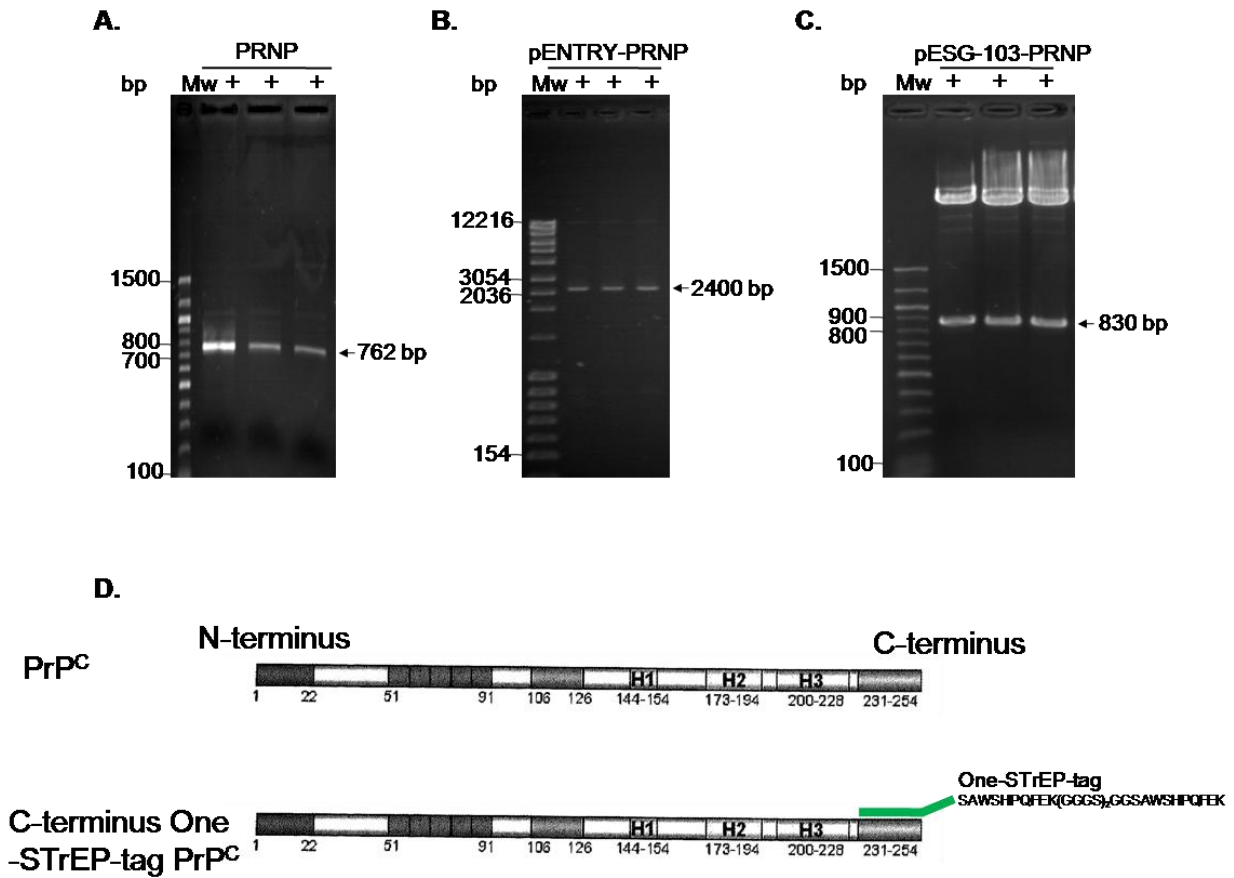
Figure 4 C-terminus One-STrEP-tag PrP^C plasmid: (A) Amplification of the PRNP gene (molecular weight 762 bp) through genomic DNA extracted from whole human blood. (B) Donor vector (pENTRY-PRNP, molecular weight 2400 bp) generated with combinatorial cloning. (C) Restriction digestion of pESG-103-PRNP with XbaI and Hind III enzymes showed an 830 bp PRNP-C-terminus One-STrEP-tag fragment (D) Schematic representation of PrP^C attached with One-STrEP-tag at its C-terminus.

A.

B.

C.
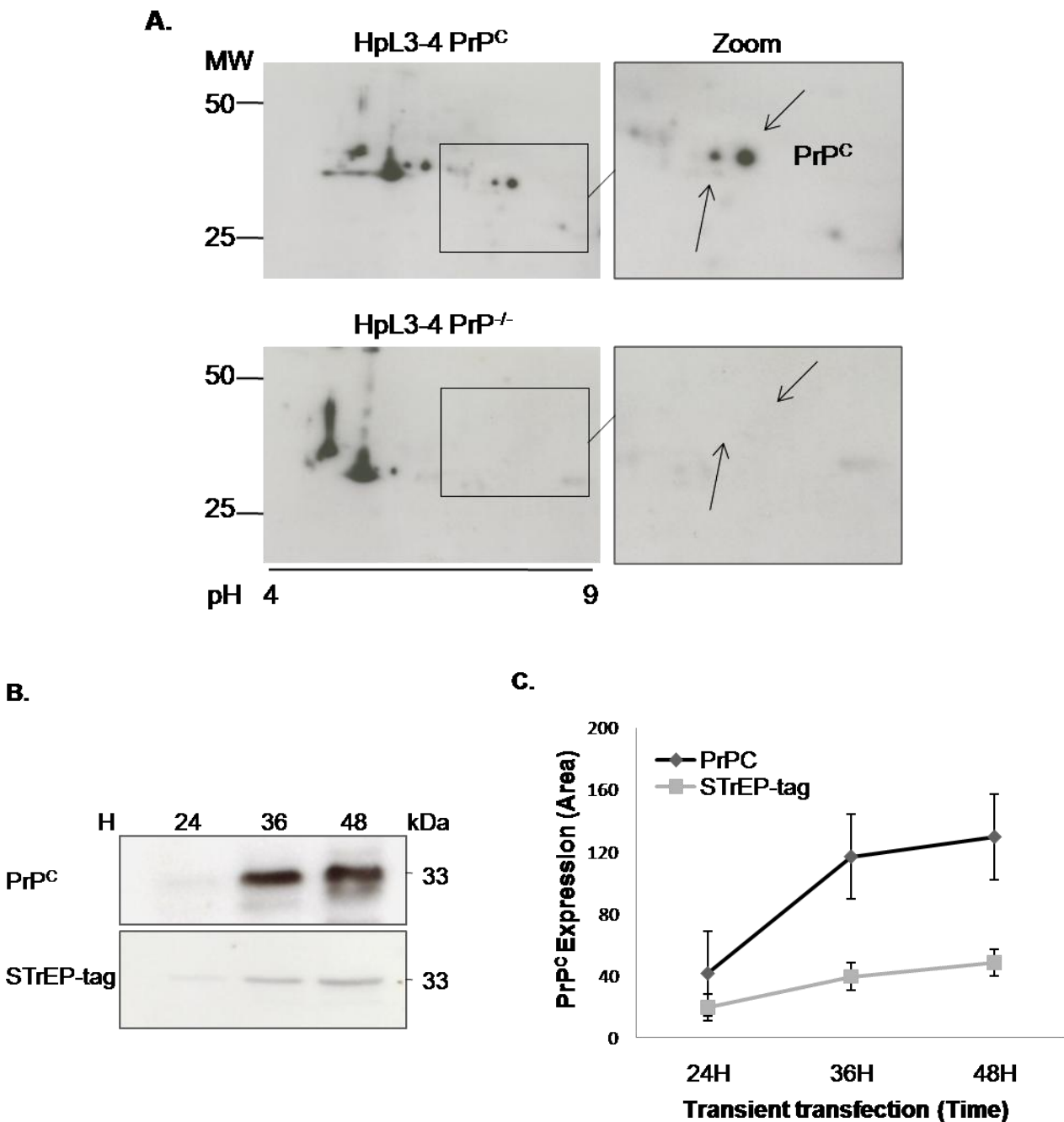
Figure 5 PrP^C expression in HpL3-4 cells after transient transfection: (A) C-terminus One-STrEP tagged PrP^C (HpL3-4 PrP^C) and control vector without PrP^C construct (HpL3-4 PrP$^{-/-}$), transiently expressed for 48 H in HpL3-4 cell line. Linear 7cm IPG strips (pH 3-10) were used and loaded with 80 µg of total cell lysate and were analyzed by 2-DE immunoblotting using 6H4 PrP^C specific antibody (B) PrP^C expression after 24, 36 and 48 H of C-terminus One-STrEP-tag PrP^C transient transfection (B) Densitometric analysis of time dependent PrP^C expression after transient transfection. n=4.
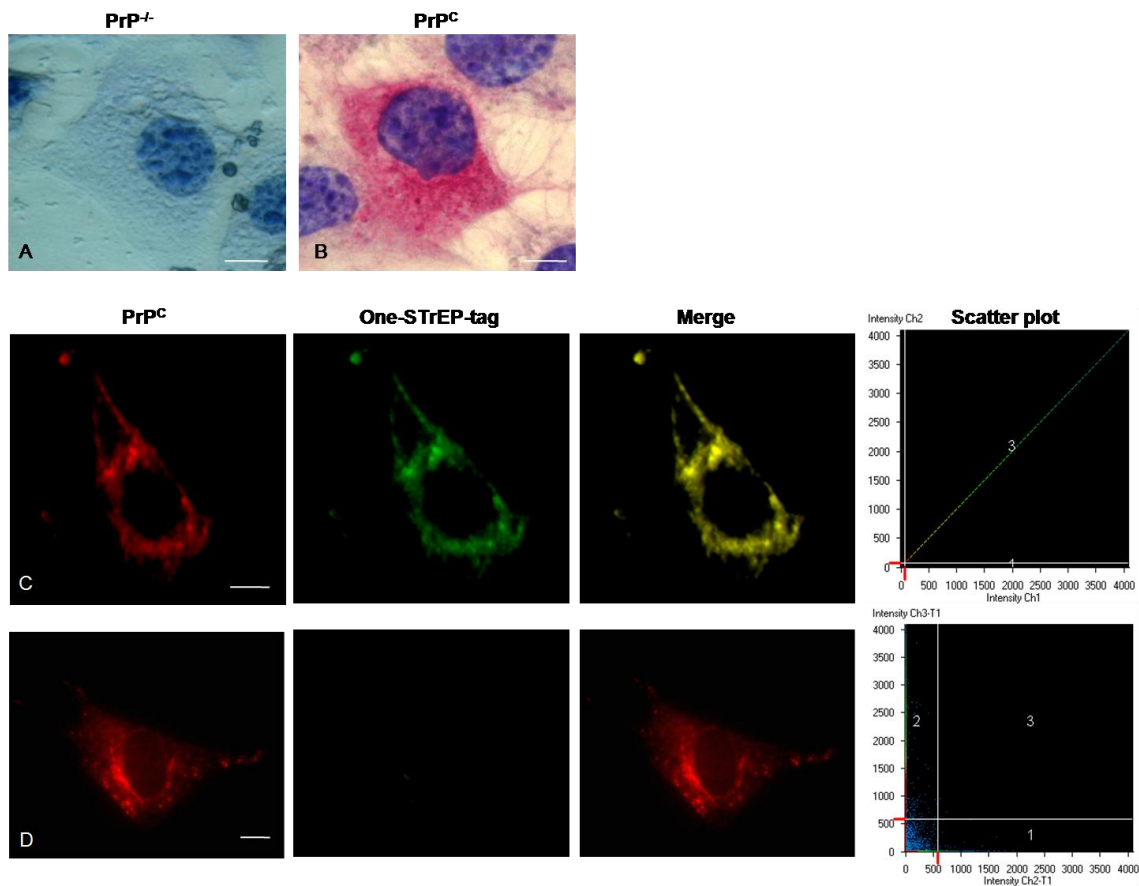
Figure 6 PrP^C localization in HpL3-4 cells after transient transfection: C-terminus One-STrEP tagged PrP^C and control PrP^C transiently expressed for 48 H in HpL3-4 cell line. Cells were fixed, made permeable with Triton-X-100. (A and B) Immunohistochemistry of PrP^C expression labeled with 6H4 anti- PrP^C antibody. Immunofluorescent staining of One-STrEP tagged PrP^C(C) and control PrP^C (D) with 6H4 anti- PrP^C antibody and STrEP mAb classic anti- One-STrEP tag antibody followed detection by Cy3 (red)- and Alexa488 (green)- conjugated secondary antibodies. (Scale bar: 10 μm). Typical scatter plot of the individual pixels from paired images. The region 3 demonstrated the overlapping region, regions 2 and 1 corresponding to *green* and *red pixels*, respectively, with no color mixing. Overlapping was quantified with the LSM 510 3 software (Carl Zeiss, Germany).

4.2 PrP^C expression and cell viability

4.2.1 PrP^C expression and cell viability in HpL3-4 and SH-SY5Y cells

To check the influence of PrP^C expression on cell viability, C-terminus One-STrEP-tagged PrP^C was transiently transfected for 24, 36 and 48 H in HpL3-4 cells (Figure 5). The mitochondrial respiratory activity of non-apoptotic cells was determined

by MTS assay. Cell viability of HpL3-4 PrP^C was not significantly different as compared to PrP$^{-/-}$ after 24 H and 36 H of transient transfection. However, the cell viability was slightly but significantly increased after 48 H of transient expression (Figure 7). On the other hand, the stably expressing PrP^C SH-SY5Y cells showed significant decreased viability as compared to control pCIneo cells (Figure 8).
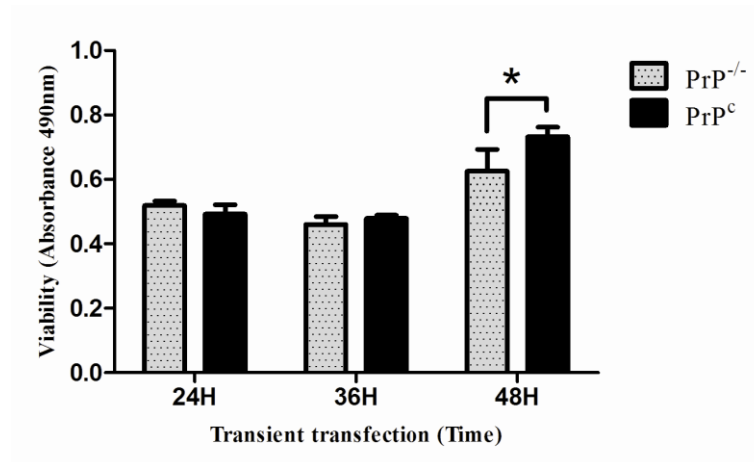
Figure 7 Viability of transient PrP^C expressing HpL3-4 cells: Cells were transiently transfected with PrP$^{-/-}$ and PrP^C and cell viability was measured by MTS assay after 24, 36 and 48 H of expression. The viability values are shown as absorbance at 490nm. Data points are the means ± SEM of values from four different experiments. The significance was performed by student's t-test (*P< 0.05).
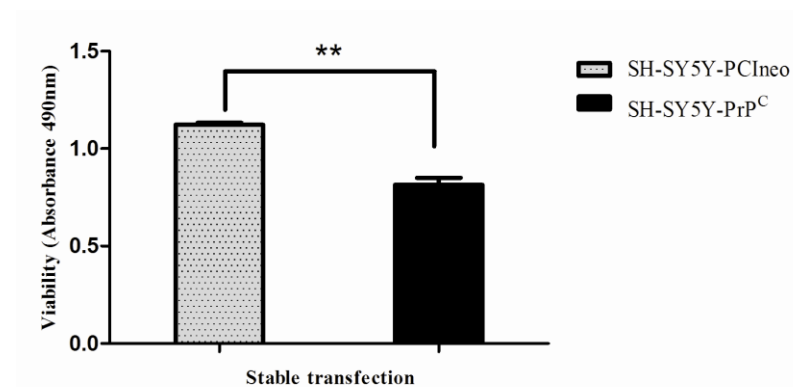
Figure 8 Viability of stable PrP^C expressing SH-SY5Y cells: SH-SY5Y cells stably expressing pCIneo (control) and PrP^C (0.5 x 10^6 cells/ml) and the viability of the cells were measured by MTS assay at 490 nm by spectrophotometry. The viability values are shown as absorbance at 490nm.

Data points are the means ± SEM of values from four different experiments. The significance was performed by student's t-test (**P< 0.01).

4.2.3 Caspase-3 activity in PrP^C expressing cells

To test the cytotoxic nature of PrP^C, an apoptotic marker enzyme caspase-3 activity was measured in transient and stable PrP^C expressing cells. Caspase-3 activity was analyzed in cell lysates incubated with pNA-conjugated caspase-3 specific substrate DEVD. Free cleaved pNA was detected by fluorescence measurement. Relative Caspase-3 activity was analyzed in SH-SY5Y cells stably expressing pCineo (control) and PrP^C and also in transient expressing PrP^C HpL3-4 cells. The Caspase-3 activity was significantly increased in pCineo control and in HpL3-4 PrP$^{-/-}$ cells after staurosporine treatment. The cells expressing transient and stable PrP^C showed no significant (ns) regulation of caspase-3 enzyme activity and demonstrated the anti-apoptotic nature of PrP^C after staurosporine treatment (Figure 9).
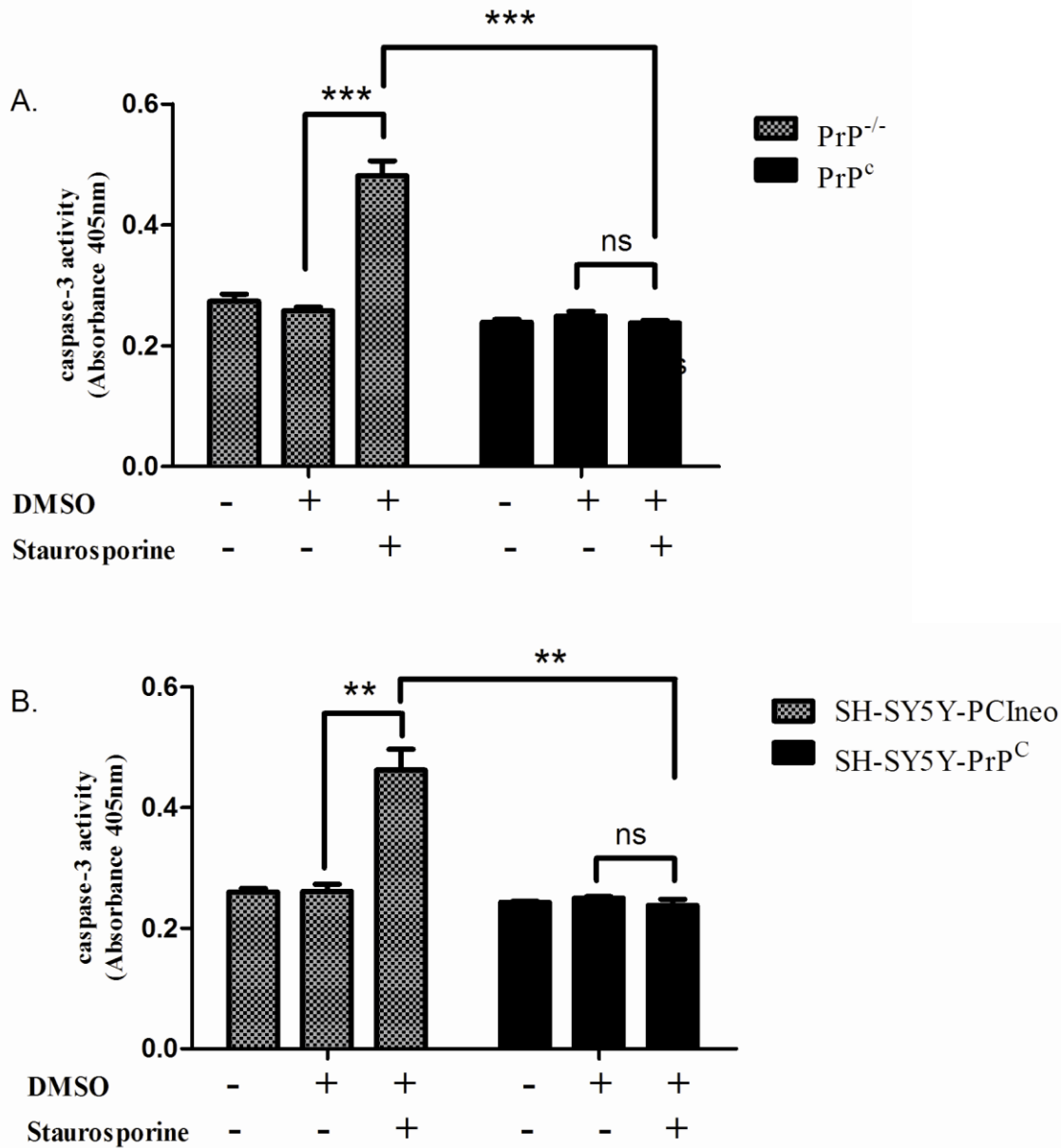
Figure 9 Caspase-3 activity in HpL3-4 and SH-SY5Y cells: Total cell lysates were isolated from HpL3-4 cells (transiently expressing PrP^C) and SH-SY5Y cells (expressing stable PCIneo (empty vector) and PrP^C). Caspase-3 activity was detected by fluorescence measurement of the cleaved pNA from the substrate peptide DEVD-pNA. Densitometric analysis (A) HpL3-4 cells (B) SH-SY5Y cells. Data points are the means ± SD of values from four different experiments. The significance was tested by student's t-test (**P < 0.01, ***P< 0.001) and ns=non significant.

4.3 Purification and identification of PrP^C interacting proteins

C-terminus One-STrEP-tag affinity chromatography and reverse co-immunoprecipitation methods were employed in this study to purify the interacting proteins under physiological conditions.

4.3.1 C-terminus One-STrEP-tag PrP^C affinity purification of PrP^C complex

HpL3-4 cells lacking endogenous PrP^C were transiently transfected with the vector containing C-terminus One-STrEP-tag PrP^C (PrP$^{+/+}$) or control vector without PrP^C construct (PrP$^{-/-}$). The efficiency of C-terminus One-STrEP-tag PrP^C protein recovery through the STrEP-Tactin column was optimized by using buffers designed to not disrupt physiological binding of the protein during its elution and purification. The total cell lysate (TCL) was prepared and then incubated (4 mg) with pre-equilibrated STrEP-Tactin superflow beads to purify PrP^C along with its interacting proteins from the total cell lysates. The eluates from STrEP-Tactin superflow beads were precipitated with methanol/chloroform and then resuspended in Laemmli buffer, 1-DE separated, electro-transferred to a PVDF membrane and detected with 6H4 PrP^C as well as One-STrEP-tag antibodies (Figure 10A and B). Following 6H4 PrP^C and One-STrEP-tag specific western blots, the remaining eluate was 1-DE separated and silver nitrate stained (Figure 10C). Whole lanes from PrP$^{+/+}$ and PrP$^{-/-}$ transfected eluates were excised, in-gel digested and proteins were identified by Q-TOF MS/MS analysis. All the proteins identified in the PrP$^{-/-}$ lane bands were considered background contaminants and subtracted from the list of proteins identified from PrP$^{+/+}$ transfected eluates. Both known and novel PrP^C interacting partners were among the proteins identified in this study (Table 8).
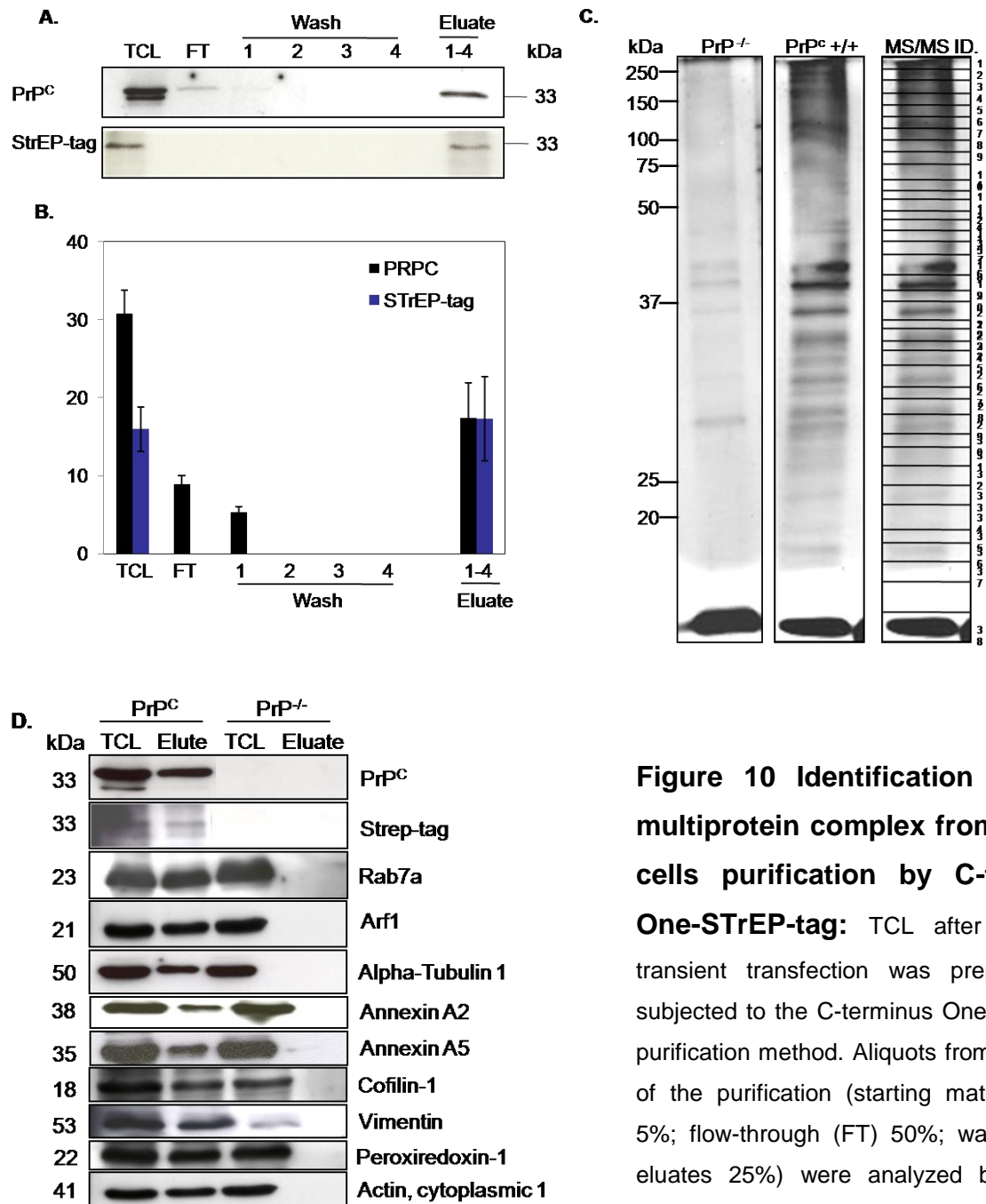
Figure 10 Identification of PrP^C multiprotein complex from HpL3-4 cells purification by C-terminus One-STrEP-tag: TCL after 48 H of transient transfection was prepared and subjected to the C-terminus One-STrEP-tag purification method. Aliquots from each step of the purification (starting material (TCL) 5%; flow-through (FT) 50%; washes 50%; eluates 25%) were analyzed by immuno blotting using (A) 6H4 and One-STrEP-tag specific antibodies (B) Densitometric analysis from immuno blotts n=4 (±SD). (C) Silver-stain 1-DE, proteins identified by MS/MS analysis are listed in Table 8 (D) Confirmatory immuno blotting using 3F4, One-STrEP-tag, and other interacting proteins specific antibodies.

Fifteen out of the forty-three identified proteins have already been described as interacting partners of PrP^C in previous studies (Table 8). Three of them (tubulin alpha-1A, tubulin beta-5 chain, elongation factor 1-alpha-1), are also known for their interaction with PrP^{SC}. However, five other proteins (actin, cofilin-1, Glyceraldehyde 3-

50

phosphate dehydrogenase (GAPDH), D-3-phosphoglycerate dehydrogenase and heat shock protein 90-alpha) from our identified proteins were identified in these experiments as interacting partners for PrP^{Sc} but not for PrP^{C}. Collectively, 23% of the interacting partners of PrP^{C} identified in this study are associated with cytoskeleton-cell growth/maintenance, 23% cell communication and signal transduction, 14% metabolism: energy pathways, 14% protein metabolism, 14% oxioreductase: stress response and 5% protein folding proteins. The remaining 7% proteins fall into other three functional groups (Figure 11). A selection of identified proteins was further validated by immunoblotting using the protein specific antibodies from purified One-STrEP-tag eluate. PrP^{C} and Strep-tag signal was detected in TCL and One-STrEP-tag elute from PrP$^{+/+}$ or PrP^{C}. Rab7a, Arf1, alpha tubulin 1, annexin A2, annexin A5, actin cytoplasmic 1, cofilin-1, vimentin, and peroxiredoxin-1 was only detected in PrP^{C} One-STrEP-tag elute. No signal was detected in the control purified elutes (Figure 10D), confirming the specificity of the purification process.

Table 8 PrP^C interacting proteins: Interacting proteins were identified after C-terminus One-STrEP-tag purification and Q-TOF MS/MS analysis. The biological functions are assigned according to the ExPASy protein database (http://expasy.org/) and the Human Protein Reference Database [Keshava Prasad *et al.* 2009]. B. No = Band No. listed in Figure 4C, Acc. No.= Swissprot Accession No., PrP^C ligand = previously identified as a PrP^C interacting partner, PrP^{Sc} ligand= previously identified as a PrP^{Sc} interacting partner. The detailed list of list of interacting proteins with score, peptide match, sequence coverage and sequences can be found in appendix B.

B. No	Acc. No.	Protein Description	PrP^C Ligand	PrP^{Sc} Ligand	Mass (kDa)	Function (ExPASy)/ References
		Cytoskeleton: Cell growth /maintenance				
14	P60710	Actin, cytoplasmic 1	Novel	Known [Morel *et al.* 2008]	41.7	Highly conserved, involved in cell motility
21	P07356	Annexin A2	Known [Morel *et al.* 2008]	-	38.6	Calcium-regulated membrane-binding protein
14	Q8BFZ3	Beta-actin-like protein 2	Novel	-	41.9	Cell motility
35	P18760	Cofilin-1	Novel	Known [Giorgi *et al.* 2009]	18.5	Controls reversible actin polymerization, depolymerization and is major component of intranuclear and cytoplasmic actin rods
9	P26041	Moesin	Novel	-	67.7	Probably involved in connection of major cytoskeletal structures to the plasma membrane
3	Q8VDD5	Myosin-9	Novel	-	226.2	Cytokinesis, cell shape, secretion and capping
33	Q9WVA4	Transgelin-2	Novel	-	22.3	Muscle organ development
12	P68369	Tubulin alpha-1A	Known	Known [Nieznanski *et al.* 2005]	50.1	Major constituent of microtubules
13	P99024	Tubulin beta-5 chain	Known	Known	49.6	Major constituent of microtubules
12	P20152	Vimentin	Novel	-	53.6	Class-III intermediate filaments, found in various non-epithelial cells
		Cell communication : Signal transduction				
27	P62259	14-3-3 protein epsilon	Known [Satoh *et al.* 2005]	-	29.1	Adapter protein in signaling pathway
27	P63101	14-3-3 protein zeta/delta	Known	-	27.7	Adapter protein in signaling pathway
24	P14206	Laminin receptor 1	Known [Gauczynski *et al.* 2001]	-	32.8	Receptor for laminin, cell adhesion, cell fate determination and tissue morphogenesis, acts as a receptor for pathogenic prion protein, viruses, and bacteria

15	P63038	60 kDa heat shock protein	Known [Edenhofer *et al.* 1996]	-	60.9	Facilitates the correct folding of imported proteins, prevents misfolding and promotes the refolding under stress conditions in the mitochondrial matrix
34	P84078	ADP-ribosylation factor 1	Novel	-	20.6	Involved in protein trafficking among different compartments
21	P10107	Annexin A1	Novel	-	38.7	Calcium/phospholipid-binding protein, promotes membrane fusion and is involved in exocytosis This protein regulates phospholipase A2 activity
22	P48036	Annexin A5	Novel	-	35.9	Anticoagulant protein, indirect inhibitor of the thromboplastin-specific complex, which is involved in the blood coagulation cascade
11	Q60864	Stress-induced-phosphoprotein 1	Known [Zanata *et al.* 2002]	-	62.5	Mediates the association of the molecular chaperones HSC70 and HSP90
32	P51150	Ras-related protein Rab-7a	Novel	-	23.4	Involved in late endocytic transport
8	Q8N3E9	Phosphatidylinositol-4,5-bisphosphate phosphodiesterase delta-3 (PLC)	Novel	-	89.2	Hydrolyzes phosphatidylinositol 4,5-bisphosphate (PIP2) to generate 2 second messenger molecules diacylglycerol (DAG) and inositol 1,4,5-trisphosphate (IP3). DAG mediates the activation of protein kinase C (PKC), while IP3 releases Ca^{2+} from intracellular stores. May participate in cytokinesis by hydrolyzing PIP2 at the cleavage furrow.
Metabolism: Energy pathways						
16	P17182	Alpha-enolase	Novel	-	47.1	Multifunctional enzyme, role in glycolysis, growth control, hypoxia tolerance, allergic responses, serves as a receptor and activator of plasminogen on the cell surface of leukocytes and neurons, stimulates immunoglobulin production
16	P05202	Aspartate aminotransferase, mitochondrial	Novel	-	47.3	Amino acid metabolism, facilitates cellular uptake of long-chain free fatty acids
17	P05064	Fructose-bisphosphate aldolase A	Novel	-	39.3	Glycolysis
18	P16858	GAPDH	Novel	Known [Giorgi *et al.* 2009]	35.7	Glycolysis
26	O09131	Glutathione S-transferase omega-1	Novel	-	27.4	Exhibits glutathione-dependent thiol transferase and dehydroascorbate reductase activities

33	P35700	Peroxiredoxin-1	Novel	-	22.1	Involved in redox regulation, eliminating peroxides generated during metabolism, participates in the signaling cascades of growth factors and tumor necrosis factor-alpha, and regulates GDPD5 function
Protein metabolism						
6	P58252	Elongation factor 2	Novel	-	95.2	GTP-dependent translocation of the nascent protein chain from the A-site to the P-site of the ribosome
10	P63017	Heat shock cognate 71 kDa protein	Novel	-	70.8	Chaperone
12	P09103	Protein disulfide-isomerase	Novel	-	57.1	Catalyzes the formation, breakage and rearrangement of disulfide bonds
12	P27773	Protein disulfide-isomerase A3	Novel	-	56.6	Catalyzes the rearrangement of -S-S-bonds in proteins
16	P19324	Serpin H1 (47 kDa heat shock protein)	Novel	-	46.5	Binds specifically to collagen, involved as a chaperone in the biosynthetic pathway of collagen
10	P38647	Stress-70 protein, mitochondrial	Novel	-	73.4	Implicated in the control of cell proliferation and cellular aging, also act as a chaperone
Regulation of nucleic acid metabolism						
18	Q9EQU5	Protein SET	Novel	-	33.3	Involved in apoptosis, transcription, nucleosome assembly and histone binding
Protein folding						
33	Q99LP6	GrpE protein homolog 1, mitochondrial	Novel	-	24.4	Essential component of the PAM complex, control the nucleotide-dependent binding of mitochondrial HSP70 to substrate proteins
36	P17742	Peptidyl-prolyl cis-trans isomerase A	Novel	-	17.9	Accelerates the folding of proteins, catalyzes the cis-trans isomerization of proline imidic peptide bonds in oligopeptides
Cell cycle						
14	P10126	Elongation factor 1-alpha 1	Novel	Novel	50	Promotes the GTP-dependent binding of aminoacyl-tRNA to the A-site of ribosomes during protein biosynthesis
Lipopolysaccharide binding; ATP binding						
10	P20029	78 kDa glucose-regulated protein (Bip)	Known [Jin *et al.* 2000]	-	72.3	Role in facilitating the assembly of multimeric protein complexes inside the ER
Oxidoreductase, Stress response						
13	Q61753	D-3-phosphoglycerate	Novel	Known	56.5	Amino-acid biosynthesis, serine

		dehydrogenase		[Jin *et al.* 2000]		biosynthesis
9	P07901	Heat shock protein HSP 90-alpha	Novel	Known [Jin *et al.* 2000]	84.7	Molecular chaperone with ATPase activity
9	P11499	Heat shock protein HSP 90-beta	Novel	-	83.2	Molecular chaperone with ATPase activity
20	P06151	L-lactate dehydrogenase A chain	Known [Cooper *et al.* 2010]	-	36,4	Role in glycolysis
20	P08249	Malate dehydrogenase, mitochondrial	Novel	-	35.5	Role in glycolysis, oxidation reduction
31	P17751	Triosephosphate isomerase	Novel	-	26.6	Glycolysis, fatty acid biosynthesis, gluconeogenesis, lipid synthesis
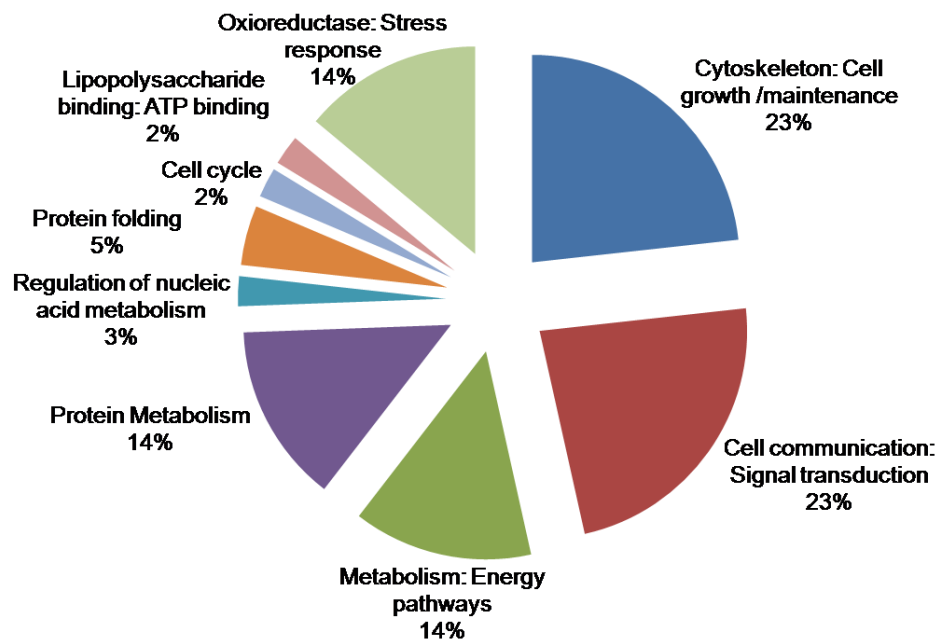
Figure 11 The functional categorization of identified interacting partners of PrP^C:

Interacting proteins identified by C-Terminus One-STrEP-tag purification were identified by Q-TOF MSMS analysis. The biological functions are assigned as in ExPASy protein database (http://expasy.org/) and Human Protein Reference Database [Keshava Prasad *et al.* 2009].

4.2.2 Binding of C-terminus One-STrEP-tag PrP^C by interacting partners

In order to further confirm the observations from the One-STrEP-tag purification system, TCL prepared from transiently PrP^C transfected neuronal HpL3-4 cells and control PrP$^{-/-}$ transfected were reverse co-immunoprecipitated with Rab7a, Arf1 and PrP^C specific antibodies using G-protein coupled magnetic beads Eluates from this reverse co-immunoprecipitation revealed a significant PrP^C signal at 27kDa to 37kDa (Figure 12A). Figure 12B-D showed the reverse co-immunoprecipitation results with PrP^C, Rab7a, Arf1 and alpha-tubulin1 antibodies, providing additional evidence for their interaction.
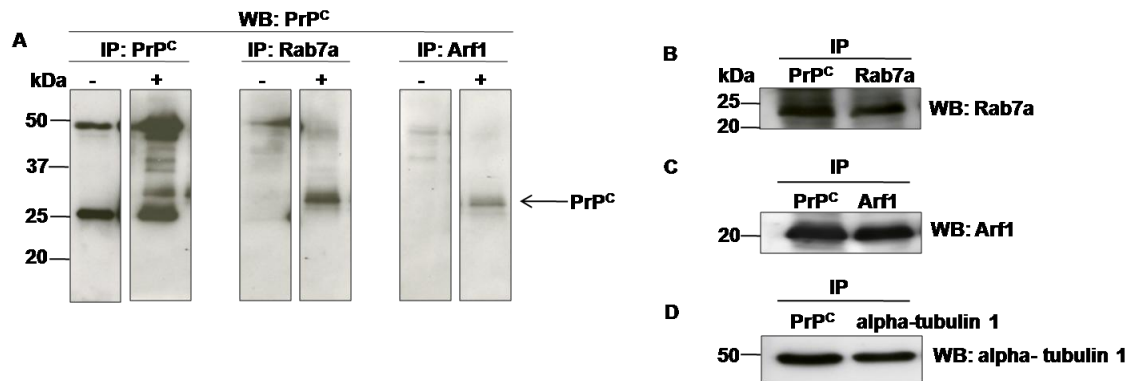
Figure 12 PrP^C interacts with Rab7a, Arf1 and alpha-tubulin 1: (A) TCL were co-immunoprecipitated (IP) with 3F4 PrP^C (Lane1 PrP$^{-/-}$ transfected and lane 2 PrP$^{+/+}$ transfected), Rab7a (lane 3 PrP$^{-/-}$ transfected and lane 4 PrP$^{+/+}$ transfected) and Arf1 (Lane 5 PrP$^{-/-}$ transfected and lane 6 PrP$^{+/+}$ transfected) and immunoblotted with Saf70 PrP^C antibody. (B) IP with 3F4 PrP^C (Lane1), Rab7a (lane 2) and immunoblotted with Rab7a antibody, (C) IP with 3F4 PrP^C (Lane1), Arf1 (lane 2) and immunoblotted with Arf1 antibody, (D) IP with 3F4 PrP^C (Lane1), alpha-tubulin 1 (lane 2) and immunoblotted with alpha-tubulin 1 antibody.

4.3 Characterization of interacting partners

4.3.1 Rab7a and PrP^C

One-STrEP-tag purification and co-immunoprecipitation assays provided evidence that Rab7a might be an interacting partner of PrP^C. To further check the potential interaction and influence of Rab7a on PrP^C localization and expression, PrP^C was transiently expressed in HpL3-4 PrP^C knockout. In addition, SH-SY5Y cells stably expressing PrP^C were examined. PrP^C showed colocalization with Rab7a in the cytosolic area. In order to quantify the extent of colocalization, Imagej (WCIF plugin) software was used (Figure 13). Colocalization in fluorescence imaging characterizes the overlap extent between two different fluorescent labels with different emission wavelengths. The detection of fluorescence signals from two differently labeled proteins within the same voxel (three-dimensional pixel) determines that these proteins are located in the same area or very near to each other. Two perfectly colocalized fluorescence signals, each displayed on separate x and y axes, will generate a scatter plot wherein the points fall in a line at 45° to either axis. In the situation of non-colocalized molecules, the resulting scatter plot reveals each color along its own axis, with no overlap at 45°. Quantification of co-localization of Rab7a and PrP^C, using the distribution of fluorescence intensities in the scatter plots showed a partial colocalization between Rab7a and PrP^C (Figure 13).

Pearson's correlation coefficient rp (-1≤ rp ≤1) was used to measure the relatedness of two fluorescence channels, where values of 0 indicate no relatedness, whereas values >0 indicate a relatedness between the two fluorescence channels. On the basis of positive correlation coefficients for all analyzed pairs of fluorescence channels, further calculations were permissible for colocalization coefficients, M1 and M2, which express the contribution of each fluorescence channel to the pixels of interest. Values of colocalization coefficients range between 0 and 1. A value of 0 indicates that none of the signal within thresholds in that channel colocalizes with the other channel. A value of 1 indicates that the entire signal within thresholds in that channel colocalizes with the other channel. Results of Pearson's correlation coefficient of colocalization demonstrated a partial colocalization between Rab7a and PrP^C (Table 9).

PrP^C distribution was then evaluated after depleting Rab7a expression using the siRNA duplex. Approximately 70-75% Rab7a expression depletion was achieved in transiently and stably PrP^C expressed HpL3-4 and SH-SY5Y cells, respectively (Figure 13A). The immunoflurescence results demonstrated that a significant fraction of PrP^C accumulated as a punctuated form and that the localization pattern of PrP^C staining is dramatically altered in Rab7a depleted HpL3-4 cells (Figure 13D) as compared to cells treated similarly but without siRNA (control) (Figure 13C). Immunoblot analysis showed a significant (*P< 0.05) increase of PrP^C levels in HpL3-4 cells after Rab7a knockdown in comparison to similar knockdown in PrP$^{-/-}$ control cells (Figure 14A and B). These Rab7a siRNA knockdown results were confirmed in SH-SY5Y stably PrP^C expressing cells (Figure 14C). The increase in the PrP^C expression was confirmed in SH-SY5Y PCIneo endogenously and SH-SY5Y stable PrP^C expressing cells (*P< 0.05; Figure 14A, C). Subsequent immunoblots showed the influence of Rab7a knockdown on the expression of Arf1 in cells with and without Rab7a knockdown. The Arf1 was markedly decreased by Rab7a siRNA knockdown in HpL3-4 PrP^C cells (Figure 14A-B) as well as in SH-SY5Y PrP^C stable cells (Figure 14A and C).
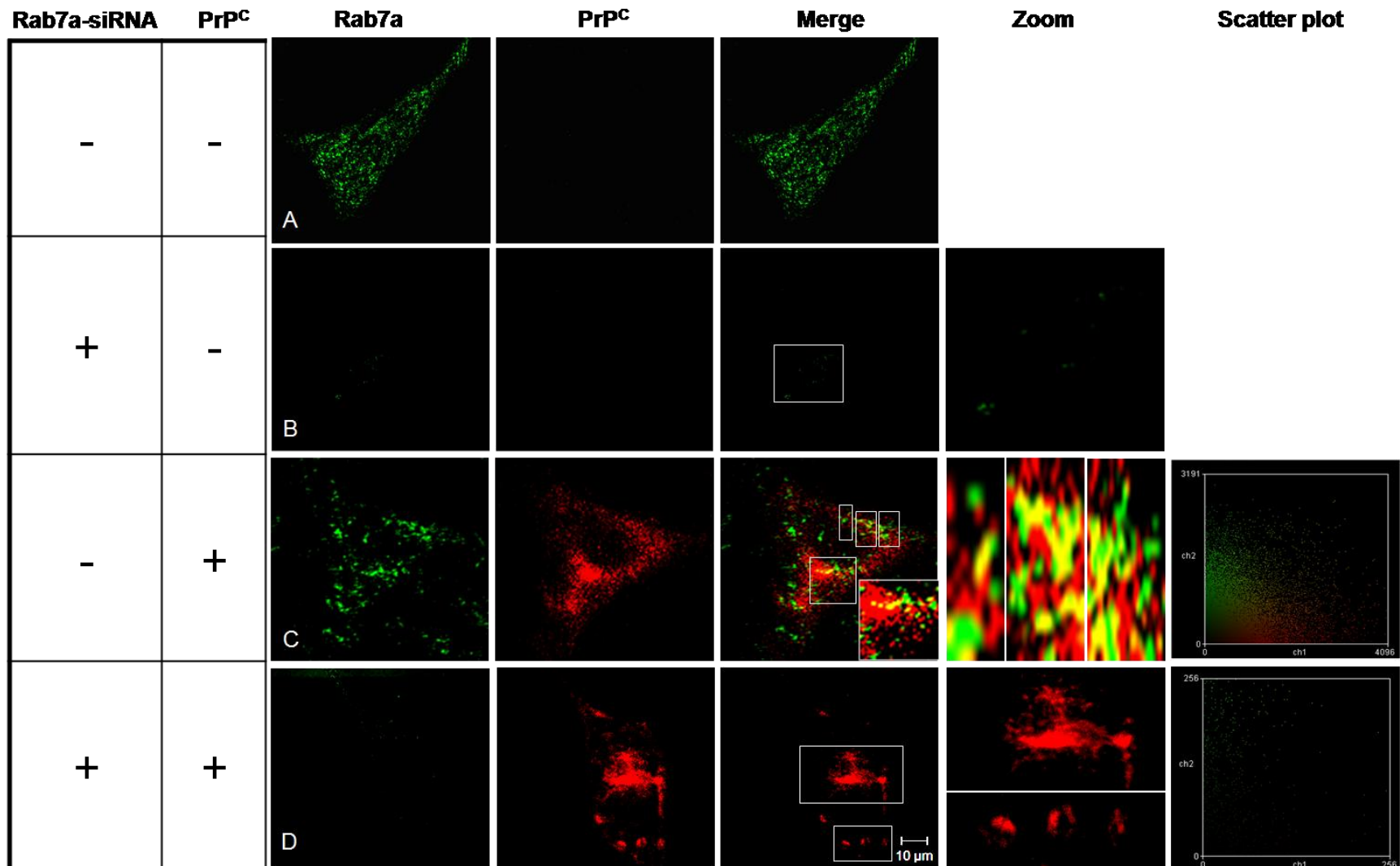
Figure 13 Effect of Rab7a depletion on PrP^C localization: HpL3-4 PrP^C knockout cells were treated with siRNA duplex (100 nM) to target Rab7a and PrP^C. 48 H after transfection, PrP^C and Rab7a expression was analyzed by using 3F4 anti-PrP^C (red) and anti-Rab7a

(green), antibodies. (A) HpL3-4 PrP^C knockout cells transfected with non targeting siRNA (negative control) and PrP$^{-/-}$, (B) HpL3-4 PrP^C knockout cells transfected with Rab7a siRNA and PrP$^{+/+}$. PrP^C and Rab7a distribution was analyzed by using 3F4 PrP^C (red) and anti-Rab7a (green) antibodies. At least 25 cells were observed per condition per experiment for an equal exposure time. The scatter plots of the individual pixels from paired images. The threshold levels of red on x-axis and green signals on y-axis determined the overlapping yellow region (midle). Quantification of colocalization was determined by Zeiss LSM 510 (version 3.2) and Imagej (WCIF plugin) softwares.

Table 9 Rab7a partially colocalizes with PrP^C: Pearson's correlation coefficient r_p (-1≤ r_p ≤1) demonstrated partial colocalization in HpL3-4 PrP^C knockout cells transfected with non targeting siRNA and PrP^C. Colocalization coefficients, *M1* and *M2* ranged between 0 and 1, showed partial colocalized pixels of interest with in each channel.

Rab-siRNA	PrP^C	rp	Coloc. Coefficient PrP^C (*M1*)	Coloc. Coefficient Rab7a (*M2*)
-	+	0.121	0.592	0.239
+	+	-0.068	0.006	0.339
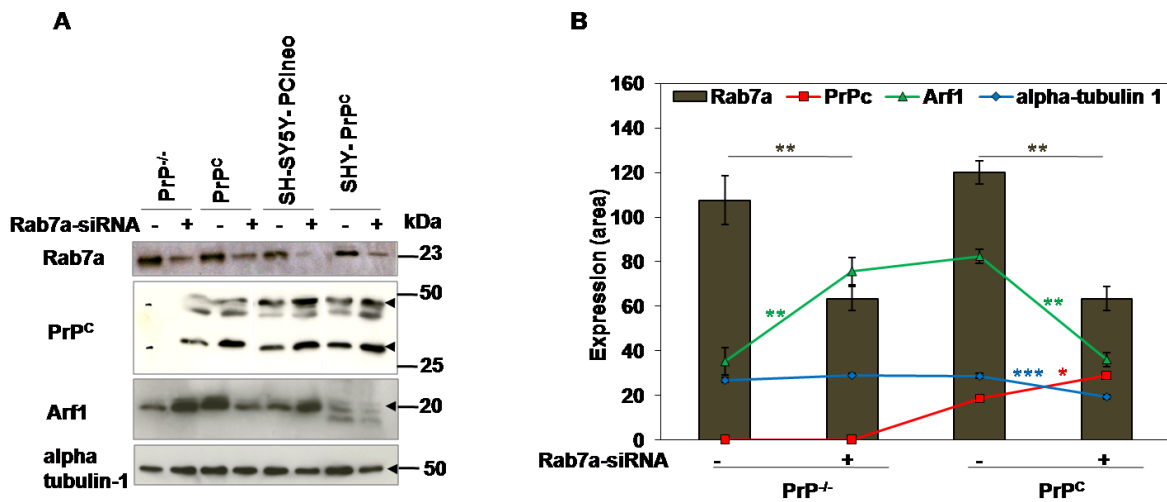
Figure 14 Effect of Rab7a depletion on PrP^C, Arf1 and alpha-tubulin 1 expression: HpL3-4 PrP^C knock out with transient PrP^C expressing and SH-SY5Y stable PrP^C expressing cells were transfected with siRNA duplex (100 nM) to target Rab7a. (A) PrP^C, Arf1, alpha-tubulin 1 and Rab7a expression was analyzed after 48 H of transfection by immnoblotting using specific Saf70 PrP^C, Arf1, alpha-tubulin1 and Rab7a antibodies. (B, C) Densitometry analysis from four independent (±SD) immnoblotting experiments and the significance was calculated by student's t-test (*P < 0.05, **P < 0.01, ***P < 0.001).
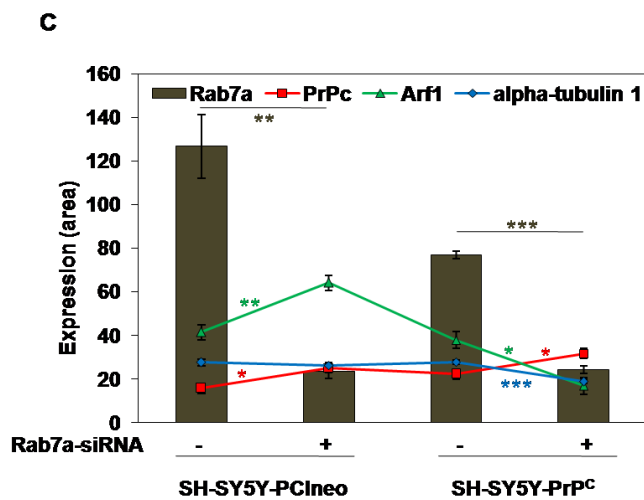
To determine the subcellular localization of PrP^C in these siRNA knock down of Rab7a HpL3-4 cells, an immunofluorescence experiment with co-staining of PrP^C and Rab9 (late endosomal marker [Russell *et al*. 2006] was performed. Interestingly accumulated PrP^C higly co-localized with Rab9 positive compartments (Figure 15). Figure 15 showed respective scatter plots generated from representative images. Rab9 (green) and PrP^C (red) was largely overlapping, as indicated in the scatter plot at 45° (Figure 15B) as compared to control HpL3-4 PrP^C knockout cells transfected with non

targeting siRNA and PrP^C. Calculations of Pearson's correlation coefficient of colocalization demonstrate that colocalization between PrP^C and Rab9 increased after Rab7a-siRNA treatment (Table 10).
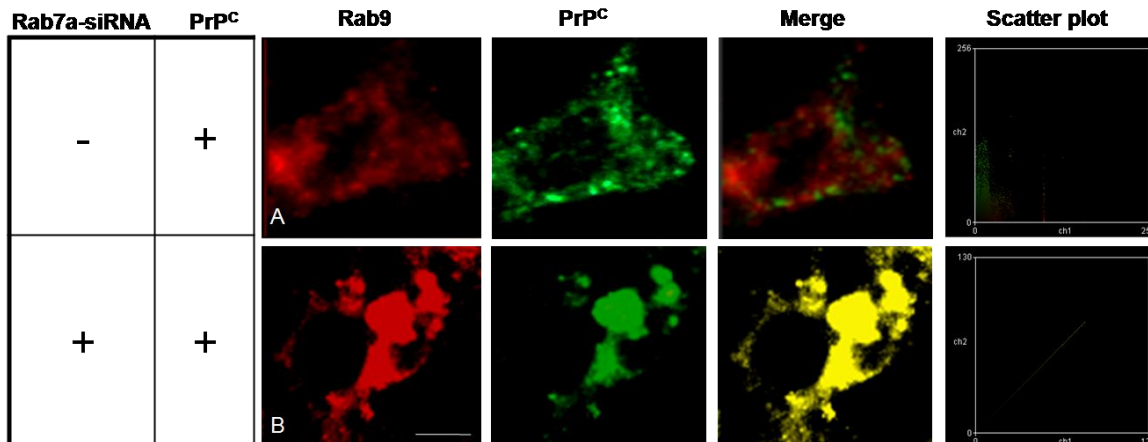
Figure 15 Effect of Rab7a depletion on PrP^C localization: HpL3-4 PrP^C knockout cells transiently transfected (48H) with PrP^C and treated with siRNA (100 nM) to target Rab7a. PrP^C and late endosomal marker Rab9 expression were analyzed using 3F4 anti-PrP^C (red) and anti-Rab9 (green), antibodies. (A) HpL3-4 PrP^C knockout cells transfected with non targeting siRNA and PrP^C (B) HpL3-4 PrP^C knockout cells co-transfected with PrP^C and Rab7a siRNA. At least 25 cells were observed per condition per experiment for an equal exposure time (Scale bar: 10 μm). The scatter plots of the individual pixels are from paired images. The threshold levels of red on x-axis and green signals on y-axis determined the overlapping yellow region. Quantification of colocalization was determined by Imagej (WCIF plugin) software.

Table 10 Rab9 colocalizes with PrP^C in Rab7a depleted HpL3-4 cells: Pearson's correlation coefficient r_p ($-1 \leq r_p \leq 1$) demonstrated high colocalization between Rab9 and PrP^C in HpL3-4 PrP^C knockout cells transfected with Rab7a-siRNA and PrP^C. Colocalization coefficients, *M1* and *M2* ranged between 0 and 1, showed high colocalized pixels of interest within each channel.

Rab7a-siRNA	PrP^C	rp	Coloc. Coefficient PrP^C (M1)	Coloc. Coefficient Rab9 (M2)
-	+	0.306	0.679	0.793
+	+	0.779	0.970	1.000

In order to see if transiently expressed PrP^C has similar characteristics to the proteinase K (PK) resistant PrP^{Sc} form, the total cellular lysate of HpL3-4 cells containing transiently transfected PrP^C and treated with Rab7a-siRNA, were digested with PK (10 µg/ml) and analyzed by western blot using Saf70 antibody. The results demonstrated that the accumulated PrP^C does not acquire the PK resistant form, at least not within the 48 H tested (Figure 16).
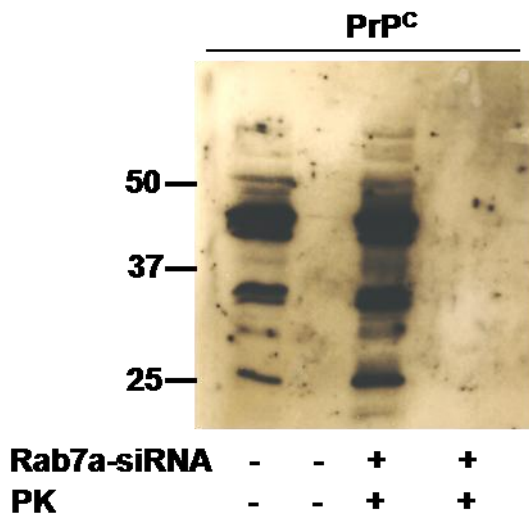
Figure 16 Figure 16 PK-digestion of PrP^C under Rab7a knockdown HpL3-4 cells: HpL3-4 PrP^C knockout cells were transfected with PrP^C and siRNA to target Rab7a protein. SiRNAs (100 nM) were co-transfected with C-terminus One-STrEP-tag PrP^C into cultured HpL3-4 PrP^C knockout cells. The TCL was treated with 10 µg/ml PK and PrP^C was analyzed by immunoblot using Saf70 antibody.

4.3.2 Arf1 and PrP^C

One-STrEP-tag purification and co-immunoprecipitation assays also identified Arf1 as a novel potential interacting partner of PrP^C. Arf1 is an activator of phospholipase D and plays an important role in vesicular trafficking. To demonstrate the effects of Arf1 on PrP^C expression and localization, HpL3-4 PrP^C transfected and SH-SY5Y PrP^C stably expressing cells were treated with different concentrations of Brefeldin A (BFA). BFA is an inhibitor of intracellular protein transport and is commonly used to demonstrate the role of Arf1 in the morphology of the Golgi apparatus and recruitment of coat proteins to the Golgi [Volpicelli-Daley *et al.* 2005]. Immunofluorescence data showed significant changes in PrP^C localization as compared to untreated cells (Figure 17). Quantification of the co-localization of Arf1 and PrP^C by using the distribution of fluorescence intensities in the scatter plots demonstrated a

partial colocalization between Arf1 and PrP^C (Figure 17). Pearson's correlation coefficient rp (-1≤ rp ≤1) also demonstrated partial colocalization between Arf1 and PrP^C (Table 11). The long term exposure to BFA (24 H of 1µg/ml BFA) showed the accumulation of PrP^C and drastically altered localization (Figure 17D) as compared to the control cells (Figure 17B). In contrast; however, after 1.5 H of 1µg/ml BFA treatment cells showed dispersed co-localization of PrP^C with Arf1 (Figure 17C and E). The extent of colocalization decreased after BFA treatment as compared to the control, untreated cells (Table 11).

The immunoblot analysis showed that the Arf1 expression was significantly decreased after BFA treatment in HpL3-4 cells transiently transfected with PrP^C (Figure 18A-B) as well as in SH-SY5Y PrP^C stably expressing cells (Figure 18A-C). Immunoblotting experiments showed a significant decrease of PrP^C concentrations in BFA treated cells (*$P< 0.05$, **$P< 0.01$, ***$P< 0.001$) in comparison to control cells (Figure 18A-C).
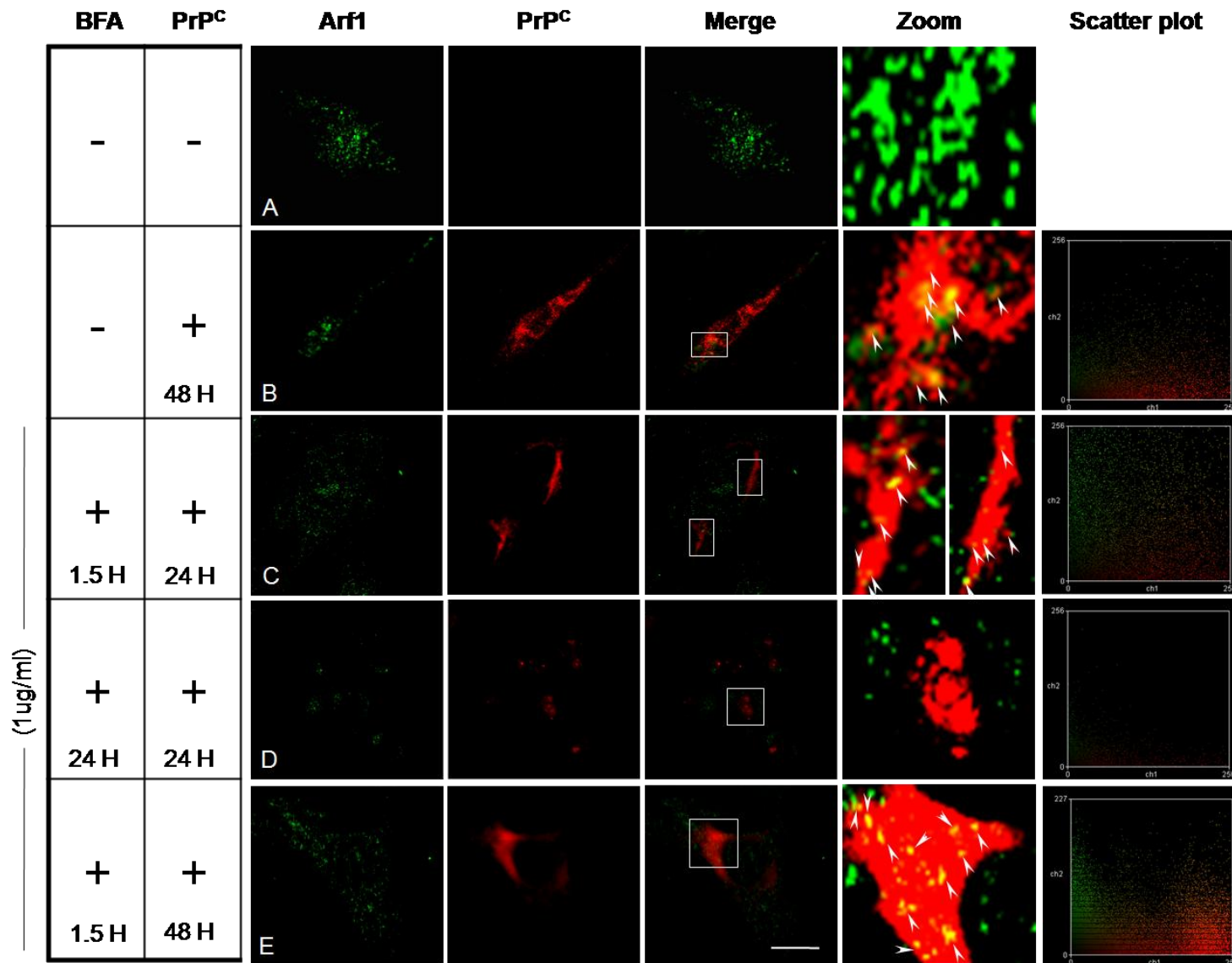
Figure 17 Effect of BFA on Arf1 and PrP^C localization: HpL3-4 PrP^C knockout cells were transiently transfected with PrP^{+/+} or PrP^{-/-} and treated with BFA (1μg/ml) for different time intervals (A) untreated HpL3-4 PrP^{-/-} transfected cells (B) untreated HpL3-4 PrP^C transfected cells, (C) 1.5 H of BFA treatment after 24 H of PrP^C transient transfection (D) 24 H of BFA treatment after 24 H of PrP^C transient transfection, (E) 1.5 H of BFA treatment after 48 H of PrP^C transient transfection. PrP^C and Arf1 distribution was analyzed by using 3F4 anti-PrP^C (red) and anti-Arf1 (green) antibodies. At least 25 cells were observed per condition per experiment for an equal exposure time (Scale bar: 10 μm). The scatter plots of the individual pixels from paired images were generated by Imagej (WCIF plugin) software.

Table 11 Arf1 partially colocalizes with PrP^C: Pearson's correlation coefficient r_p (-1≤ r_p≤ 1) demonstrated partial colocalization (0.142) between Afr1 and PrP^C in HpL3-4 PrP^C knockout cells transfected with PrP^C and without BFA treatment. 1.5 H and 24 H of BFA treatment showed less colocalization as compared to control untreated cells. Colocalization coefficients, *M1* and *M2* ranged between 0 and 1, showing partial colocalized pixels of interest within each channel.

BFA (1ug/ml)	PrP^C	rP	Coloc. Coefficient PrP^C (*M1*)	Coloc. Coefficient Afr1 (*M2*)
-	+	0.142	0.359	0.662
+ 1.5 H	+	0.028	0.242	0.224
+ 24 H	+	-0.003	0.359	0.140
+ 1.5 H	+	0.048	0.472	0.412

A

B

C
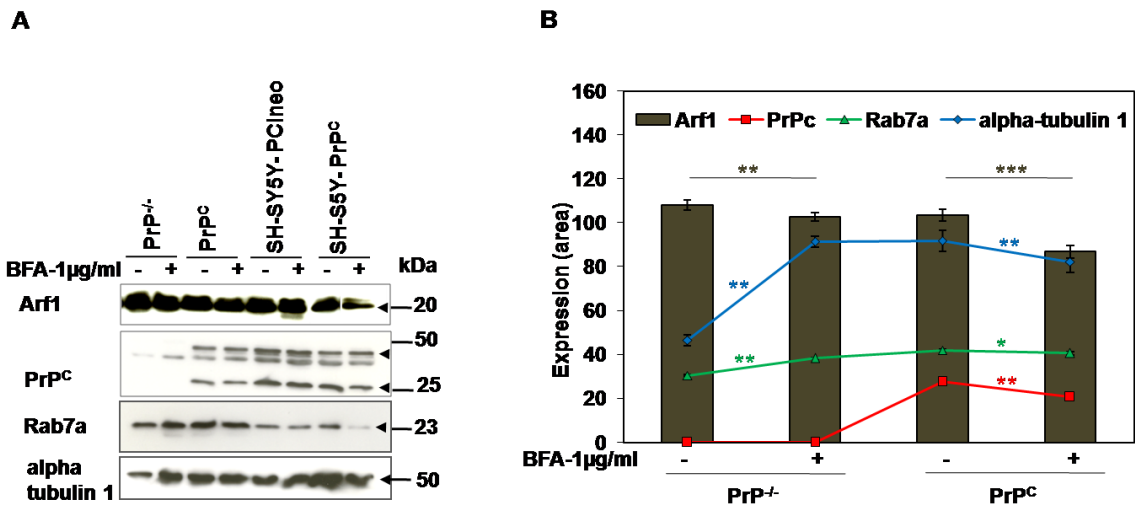
Figure 18 Effect of BFA treatment on PrP^C, Rab7a, Arf1 and alpha-tubulin 1 expression: HpL3-4 PrP^C knockout with 48 H of transient PrP^C expressing and SH-SY5Y stable PrP^C expressing cells were treated with 1µg/ml BFA for 1.5 H. (A) PrP^C, Rab7a, Arf1 and alpha-tubulin 1 expression was analyzed by immnoblotting using specific Saf70 PrP^C, Rab7a, Arf1 and alpha-tubulin1 antibodies. (B, C) Densitometry analysis from four independent (±SD) immnoblotting experiments where the significance was calculated by student's t-test (*P < 0.05, **P < 0.01, ***P < 0.001).
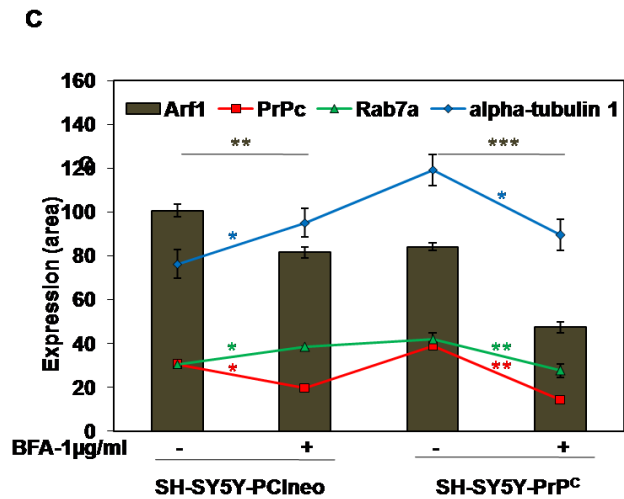
4.3.3 Rab7a/Arf1 interdependent role

To search for the molecular link between Rab7a and Arf1 during sorting, candidate Rab7a was depleted by siRNA interference, and the resulting phenotypes were examined. The expression of Arf1 was markedly decreased by Rab7a knockdown in HpL3-4 PrP^C cells and also in the control SH-SY5Y PrP^C stable cell line (Figure 14A-C). Rab7a activity was then monitored during BFA treatment. No significant influence was observed on Rab7a expression by BFA treatment (Figure 18A-C).

4.3.4 Microtubule fate in PrP^C, Rab7a and Arf1 internalization

PrP[C] binds directly to tubulin and this interaction leads to the inhibition of microtubule formation [Nieznanski *et al.* 2005; Nieznanski 2009] which is a necessary component of vesicle transportation for endosome movement [Nielsen *et al.* 1999; Nielsen *et al.* 2001; Bananis *et al.* 2000; Bananis *et al.* 2004; Matteoni and Kreis 1987]. When cells were treated for 3 H with nocodazole, a microtubule polymerization interfering agent, an altered localization pattern of PrP[C] was observed; more towards the cytosolic region of the cell (Figure 19B). The quantification of the co-localization of alpha-tubulin 1 and PrP[C] after treatment for 3 H with nocodazole, using the distribution of fluorescence intensities in the scatter plots, demonstrated no significant colocalization between alpha-tubulin 1 and PrP[C] (Figure 19B), as compared to the control, untreated cells (Figure. 19A). Pearson's correlation coefficients of colocalization shown in Table 12 also demonstrated that alpha-tubulin 1 and PrP[C] after 3 H of treatment with nocodazole showed less colocalization. But interestingly after longer exposure to nocodazole (24 H), PrP[C] and alpha-tubulin 1 were still sharing the same compartments (Figure 19C) which showed that the effects of nocodazole on the organization of microtubules were reversible [Polioudaki *et al.* 2009]. Pearson's correlations also showed partial colocalization (Table 12).

The TCL from HpL3-4 and SH-SY5Y treated cells were then used to verify PrP[C] and alpha-tubulin 1 expression. Total expression of alpha-tubulin 1 was not changed significantly after the treatment but the PrP[C] expression was upregulated significantly (*$P < 0.05$, **$P < 0.01$, ***$P < 0.001$) after microtubule-disruption (Figure 20A-C). The Arf1 and Rab7a protein levels were significantly (*$P < 0.05$, **$P < 0.01$, ***$P < 0.001$) decreased by microtubule disruption.
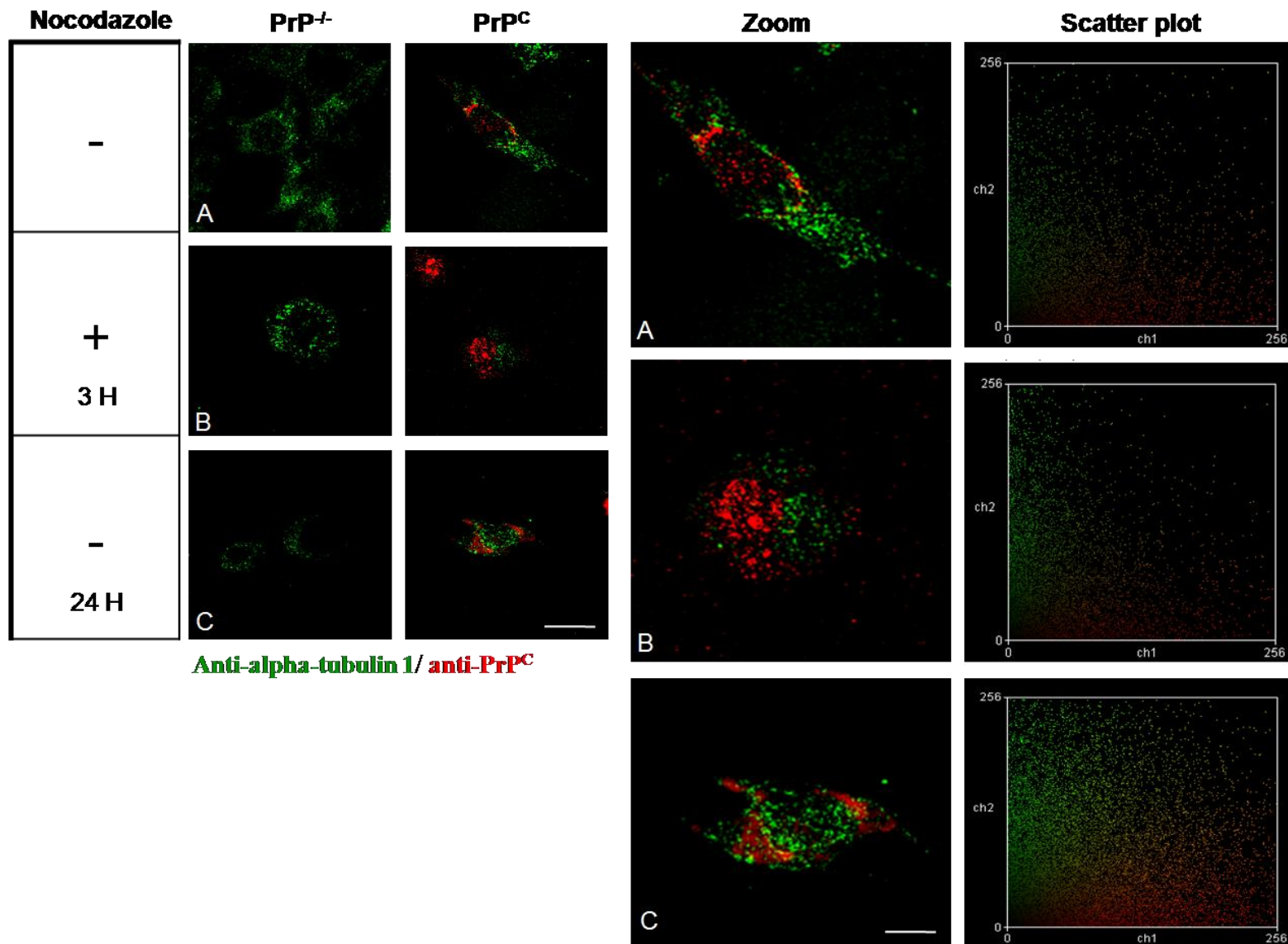
Figure 19 Effect of nocodazole on alpha-tubulin 1 and PrP^C localization: HpL3-4 PrP^C knockout cells were transfected with PrP^{+/+} or PrP^{-/-} and treated with norcodazole (1µmol) for different time intervals (A) untreated cells (B) 3H of nocodazole treatment after 24H of PrP^C transfection (D) 24H of nocodazole treatment after 24H of PrP^C transfection. PrP^C and alpha-tubulin 1 distribution were analyzed using 3F4

anti-PrP^C (red) and anti-alpha-tubulin 1 (green) antibodies. At least 25 cells were observed per condition per experiment for an equal exposure time (Scale bar: 10 µm). The scatter plots of the individual pixels from paired images were generated by Imagej (WCIF plugin) software.

Table 12 Alpha-tubulin 1 partially colocalizes with PrP^C: Pearson's correlation coefficient r_p (-1≤ r_p≤ 1) demonstrated partial colocalization (0.049) between alpha-tubulin 1 and PrP^C in HpL3-4 PrP^C knockout cells transfected with PrP^C but without nocodazole treatment. 3 H and 24 H of nocodazole treatment showed less colocalization as compared to control, untreated cells. Colocalization coefficients, *M1* and *M2* ranged between 0 and 1, showing partial colocalized pixels of interest within each channel.

Nocodazole (1umol)	PrP^C	rp	Coloc. Coefficient PrP^C (*M1*)	Coloc. Coefficient alpha-tubulin 1 (*M2*)
-	+	0.049	0.584	0.426
+ 3 H	+	-0.068	0.298	0.213
+ 24 H	+	0.006	0.554	0.533

A

B

C
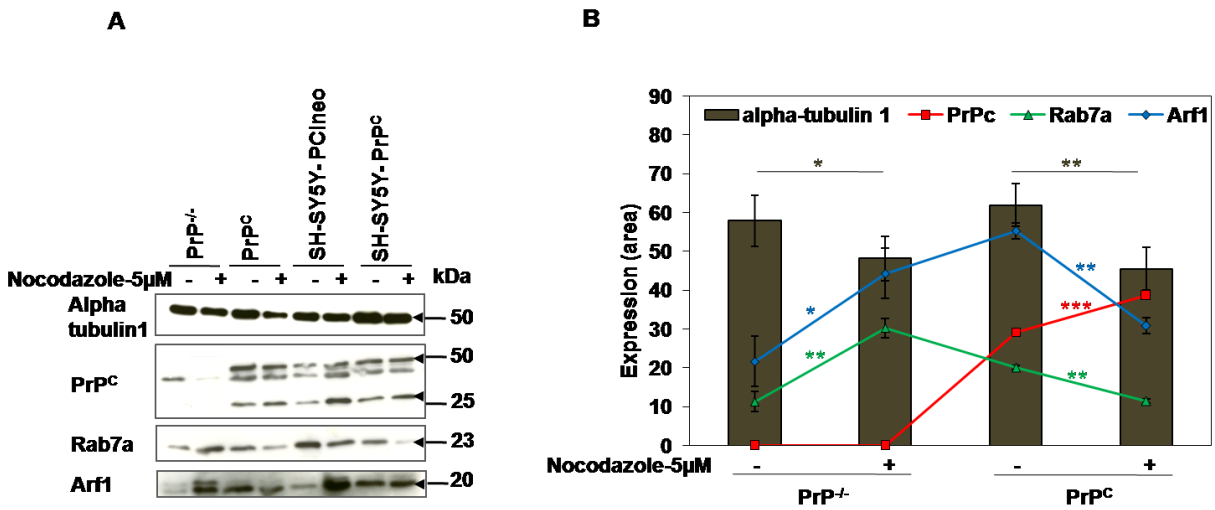
Figure 20 Effect of nocodazole on PrP^C, Rab7a, Arf1 and alpha tubulin 1 expression: HpL3-4 PrP^C knockout with 24 H of transient PrP^C expressing and SH-SY5Y stable PrP^C expressing cells were treated with 5 μmol of nocodazole for 24 H (A) PrP^C, Rab7a, Arf1 and alpha-tubulin 1 expression was analyzed by immnoblotting using specific Saf70 PrP^C, Rab7a, Arf1 and alpha-tubulin1 antibodies. (B, C) Densitometry analysis from four independent (±SD) immnoblotting experiments and the significance was calculated by student's t-test (*P < 0.05, **P < 0.01, ***P < 0.001).
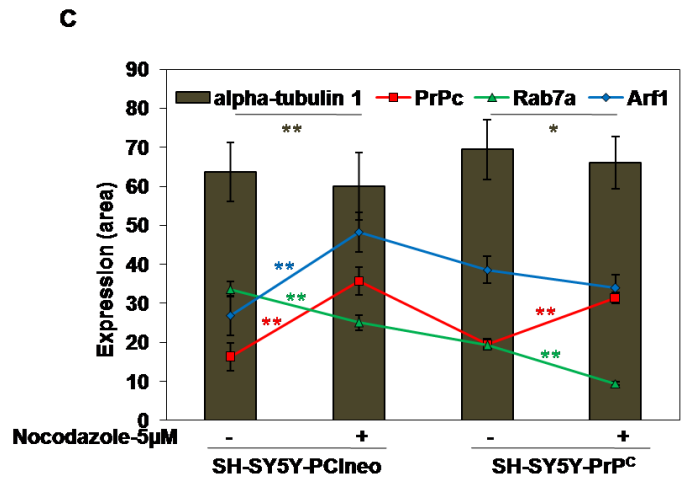
5. Discussion

In the last few years, several new PrP^C interacting proteins have been reported, indicating a growing interest in understanding the physiological function of PrP^C. Towards this goal, protein sequencing techniques have greatly facilitated the identification of proteins and their complexes. Although the sensitivity of mass spectrometry methods is currently sufficient to identify proteins, the isolation of protein complexes still poses serious challenges. Protein complexes need to be isolated from a densely populated cellular environment, in which the complex of interest may represent only a small fraction of the total protein population. Thus, successful purification requires a method that is stringent enough to differentiate the complex of interest from all other proteins in the mixture. On the other hand, the isolation method must also be gentle enough not to compromise the integrity of the complex. A method enabling identification of protein complexes by employing one-step purification would present several advantages. Therefore, the use of a single-step purification system known as the STrEP-tag method was explored for the isolation of interacting proteins from mammalian cells. This protein purification system has previously been shown to allow the rapid, single-step purification of recombinant proteins from bacterial or mammalian cellular lysates [Junttila *et al.* 2005]. One-STrEP-tag purification enhances the specificity of protein purification; the elution of the STrEP-tag fusion protein is achieved by the addition of desthiobiotin, a reversibly binding derivative of biotin, which binds to the biotin binding pocket on STrEP-Tactin in competition with the STrEP-tag [Junttila *et al.* 2005]. The short peptide tag, enabling fast and simple one-step purification, coupled with competitive elution, under physiological conditions, are unique characteristics of the STrEP-tag system that make it an ideal candidate method for isolating PrP^C interacting partners from mammalian cells.

In order to evaluate the usefulness of the STrEP-tag method for purifying protein interacting partners, mammalian expression vectors encoding PrP^C fused to the One-STrEP-tag at its C-terminus were first generated. The specificity of these interactions was ensured by comparative purification using control vector without the PrP^C construct (PrP$^{-/-}$). Besides reporting a number of novel PrP^C interacting proteins, several already identified protein partners were identified using these techniques (essentially providing a positive control). Some of the previously described PrP^C-interacting proteins are

summarized in recent reviews [Linden *et al.* 2008; Caughey and Baron 2006]. The novel, previously undescribed interacting proteins identified in the present study include cytoskeleton proteins and proteins that are important for the cell homeostasis, cell communication, signal transduction, stress response, as well as protein folding and trafficking (Table 1).

5.1 Interacting partners of PrP^C

Cytoskeleton associated proteins [*actin, cytoplasmic 1, beta-actin-like protein 2, annexin A2, alpha-tubulin 1 and tubulin beta-5, cofilin-1, moesin, myosin-9 and vimentin*]: Actin, cytoplasmic 1, and beta-actin-like protein 2 proteins are involved in cell motility, cell adhesion and reorganization of the actin cytoskeleton. PrP also plays an important role in cell adhesion [Malaga-Trillo *et al.* 2009]. Annexin A2 is known to contribute to the regulation of actin cytoskeleton dynamics in epithelial cell junctions [Benaud *et al.* 2004]. Tubulin is the major constituent of microtubules and a known interacting partner of PrP^C [Nieznanski *et al.* 2005]. Tubulin was identified in our study as two novel isoforms, alpha-tubulin 1 and tubulin beta-5 chain. Cofilin-1 also co-purified in our study although cofilin has been shown to be associated with the disease form of prion protein PrP^{Sc} and to also be involved in abnormal formation of rods in the brain of Alzheimer disease patients [Giorgi *et al.* 2009]. Moesin, myosin-9 and vimentin have well defined roles in the maintenance of cytoskeleton assembly [Kosako *et al.* 1999]. These cytoskeleton associated interacting proteins are associated with PrP^C during intracellular sorting and transportation [Nieznanski *et al.* 2005].

Proteins involved in cell communication and signal transduction [*14-3-3, Laminin receptor 1, stress-induced-phosphoprotein 1, Rab7a, Arf1, annexin A1, A5 and phosphatidylinositol-4,5-bisphosphate phosphodiesterase delta-3*]: 14-3-3 is a biomarker for Creutzfeldt-jacob disease (CJD) [Hsich *et al.* 1996] and is also known to be an interacting partner of PrP^C in association with heat shock protein 60 (Hsp60) [Satoh, Onoue, Arima, and Yamamura2005]. Laminin receptor 1 or 37/67 kDa laminin receptor (identified previously as an interacting partner using the yeast two hybrid system) functions as a cell surface receptor for laminin. It plays a significant role in cell adhesion and in the consequent activation of signaling transduction [Linden *et al.* 2008]. Stress-induced-phosphoprotein 1 is a known interacting partner of PrP^C with a suggested role in neuroprotection [Zanata *et al.* 2002]. Ras-related protein Rab7a, ADP-

ribosylation factor 1, annexin A1, A5 and phosphatidylinositol-4, 5-bisphosphate phosphodiesterase delta-3 (PLC) which were identified as novel interacting partners have a suggested role in cell communication.

Protein metabolism and energy pathways [*heat shock cognate 71 kDa protein, 47 kDa heat shock protein, stress-70 protein, glyceraldehyde 3-phosphate dehydrogenase, aspartate aminotransferase, fructose-bisphosphate aldolase A, glutathione S-transferase omega-1, peroxiredoxin-1*]*:* the molecular machinery required for protein metabolism is provided by a variety of molecular chaperones that include both heat shock proteins and glucose-regulated proteins [Henle *et al.* 1998]. Heat shock cognate 71 kDa protein, 47 kDa heat shock protein and stress-70 protein (GRP75) were identified as PrP[C] interacting partners with possible chaperone activity. Protein disulfide isomerase which is over expressed in the brains of sporadic Creutzfeldt-Jakob disease (sCJD) patients but not other other neurodegenerative disorders (i.e. Down syndrome and Alzheimer's disease) may simply reflect a cellular defense response against the altered prion protein [Yoo *et al.* 2002]. Glyceraldehyde 3-phosphate dehydrogenase (GAPDH) is a known interacting partner of PrP27-30 fibrils in transmissible spongiform encephalopathies (TSEs) [Giorgi *et al.* 2009]. Alpha enolase, a glycolytic enzyme is upregulated in PrP[C] over expressing cells in response to metabolic alterations [Ramljak *et al.* 2008]. Aspartate aminotransferase plays a key role in amino acid metabolism and is important for metabolite exchange between mitochondria and the cytosol. It facilitates cellular uptake of long-chain free fatty acids. It is being utilized as a CSF biomarker showing central nervous system degeneration [Satoh *et al.* 2007]. Fructose-bisphosphate aldolase A is upregulated in Scrapie-infected mice and its mRNA is increased in Scrapie infection [Jang *et al.* 2008]. Furthermore glutathione S-transferase omega-1 is a well known detoxification enzyme that plays an important role in prostaglandin and steroid hormone synthesis [Oakley 2005]. It is involved in protection against oxidative stress and its isoform, glutathione S-transferase P, is reported to be up-regulated with PrP[C] overexpression [Ramljak *et al.* 2008]. Lastly, peroxiredoxin-1, which was identified as novel interacting protein, functions to protect the ribosomal machinery against damage from oxidative stress [Sideri *et al.* 2010].

Protein folding and nucleic acid metabolism [*GrpE homolog 1 protein, peptidyl-prolyl cis-trans isomerase, protein SET*]: GrpE homolog 1 protein is an essential

component for the correct folding of proteins in the cell under physiological and stress conditions. It can serve as a central cellular tool for the recovery of native proteins from stress-induced aggregates. It can actively remove disease-causing toxic aggregates, such as polyglutamine-rich proteins, amyloid plaques, and prions [Ben-Zvi and Goloubinoff 2001]. Peptidyl-prolyl cis-trans isomerase also accelerates the folding of proteins and is involved in the protection of neurons against oxidative stress [Spisni *et al.* 2009]. Protein SET (Phosphatase 2A inhibitor, I2PP2A), an endogenous PP2A inhibitor, is a multitasking protein, involved in apoptosis; transcription; nucleosome assembly and histone binding [Liu *et al.* 2010].

Cell cycle and lipopolysaccharide; ATP binding proteins [*elongation factor 1-alpha, binding immunoglobulin protein (BiP)*]: Elongation factor 1-alpha, a regulator of cytoskeleton rearrangements, is upregulated in PrP^C overexpressing HEK-293 cells [Ramljak *et al.* 2008]. BiP binds to a mutant prion protein for an abnormally prolonged period of time and mediates mutant prion protein degradation by the proteasomal pathway. The folding of PrP is chaperoned by BiP and BiP plays a role in maintaining quality control in PrP maturation pathways [Jin *et al.* 2000].

Oxidoreductase, stress response proteins [*heat shock protein (HSP) 90-alpha and beta, Lactate dehydrogenase, malate dehydrogenase, triosephate isomerase*]: HSP 90-alpha and beta were up-regulated in the overexpressed PrP^C conditions [Ramljak *et al.* 2008]. Lactate dehydrogenase is a known interacting partner of PrP^C [Watts *et al.* 2009] and lactate dehydrogenase activity in the CSF is increased significantly in patients with Creutzfeldt-Jakob disease [Schmidt *et al.* 2004].

5.2   PrP^C and GTPases

The Rab- and Arf- GTPases play a critical role in regulating the vesicle trafficking in both exo- and endocytic pathways [Bucci *et al.* 2000]. The importance of small GTPases in membrane trafficking is indicated by their conservation throughout eukaryotes [Nielsen *et al.* 2001; Nielsen *et al.* 2008]. Our STrEP-tag affinity purification, immunofluorescence, and reverse co-immunoprecipitation results demonstrated that Rab7a (an isoform of Rab- GTPase) and Arf1 (an isoform of Arf-GTPase) are potential interacting partners of PrP^C. Since the transport routes that determine PrP^C endocytosis and PrP^{SC} conversion remain elusive, this study identified an important possible Rab7a and Arf1 interaction in PrP^C internalization and accumulation.

5.2.1 PrP^C and Rab7a

Rab7a, an important regulator of vesicular transport, is located in specific intracellular compartments (early to late endosomes) and has been shown to be involved in both the sorting and formation of transport vesicles [Vonderheit and Helenius 2005]. Rab7 is not essential for the delivery of early endosome cargo to the late endosome but plays a role in biogenesis of multivesicular bodies and their fusion to the lysosome [Vanlandingham and Ceresa 2009]. Herein, new evidence is provided for Rab7a and Arf1 dependent mechanisms in regulating PrP^C trafficking in this hippocampus neuronal cell line. Intriguingly, Rab7a depletion using the siRNA knockdown system significantly increased PrP^C accumulation in the cytosolic region. The localization pattern also changed to a punctuated form in contrast to the control cells. The data suggests an impairment of PrP^C trafficking from early to late endosomes after knockdown of Rab7a. The immunoblot analysis in both cell lines tested (HpL3-4 transiently PrP^C transfected and SH-SY5Y stable PrP^C expressed cells) after Rab7a knockdown confirmed the increased PrP^C expression. This PrP^C accumulation may be attributed to the impaired biogenesis of lysosomes, which has been strongly suggested as a secondary function of Rab7a [Vanlandingham and Ceresa 2009]. Furthermore, it was demonstrated that Rab7a depletion results in PrP^C accumulation and redistribution within Rab9 positive compartments. Rab9 GTPase resides in a late endosomes. The results with respect to Rab9 and prion protein showed that Rab9 overexpression in prion-infected cultured cells reduced cellular PrP^{Sc} content [Gilch *et al.* 2009].

The neuropathology of most prion diseases has been accompanied by widespread deposits of amyloidal aggregates containing the misfolded prion protein (PrP^{Sc}) [Clarke *et al.* 2001]. This aggregate formation has often been used as a parameter for neuronal toxicity, with characteristic resistance to proteinase K digestion [McKinley *et al.* 1983]. However, no proteinase K resistant PrP^C was found after 48 H in siRNA transfected transiently PrP^C expressed cells (Figure 16). These data suggest that impaired Rab7a machinery leads to accumulation of PrP^C but not the formation of the resistant form of PrP^C.
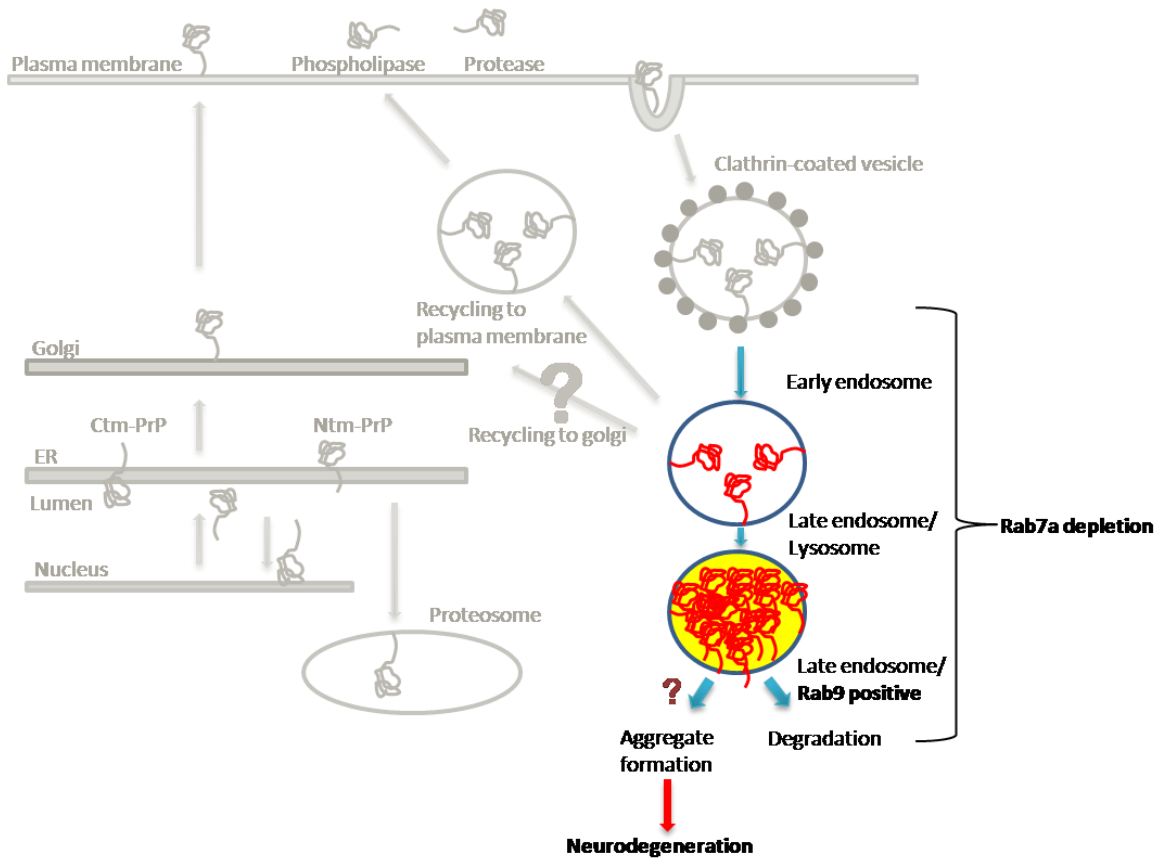
Figure 21 Influence of Rab7a depletion on PrP^C expression and localization: The unique Rab7a interacting effect on PrP^C expression and localization is highlighted with colors. The highlighted (colored) part shows the alteration of trafficking by the depletion of Rab7a expression which leads to the accumulation of PrP^C in the Rab9 positive late endosome compartments.

5.2.2 PrP^C and Arf1

Arfs regulate constitutive membrane trafficking and localize to early/*cis*-Golgi and ER–Golgi intermediate compartments. They play an important role in vesicular trafficking as an activator of phospholipase D (PLD), an enzyme involved in the regulation of secretion, endocytosis and receptor signaling [Brown *et al.* 1993; Fensome-Green and Cockcroft 2006]. Arfs activate PLD [Brown *et al.* 1993; Fensome-Green and Cockcroft 2006; Cockcroft *et al.* 1994] and phosphatidylinositol 4-phosphate 5-kinase (PIP5K) [Honda *et al.* 1999] to generate phosphatidic acid and phosphotidylinositol 4, 5-bisphosphate (PIP2) which are crucial for membrane curvature

and membrane protein recruitment [Donaldson 2005; Donaldson 2009]. PLD directly interacts with kinases such as protein kinase C (PKC) and has been shown to be involved in PrP (106-126) internalization [Paruch *et al.* 2006; Brandenburg *et al.* 2009]. Rab7a depletion was observed to increase PrP^C accumulation in early to late endosomal compartments and to significantly decrease Arf1 expression. A likely explanation would be that Rab7a knockdown may also disturb the Arf1-trans Golgi recycling complex, indicative of a possible link between Rab7a and Arf1 in PrP^C trafficking.

Arfs dependent vesicle formation requires GEP (guanine nucleotide-exchange protein, an activator of Arf1) catalyzed cycling between inactive, Arf-GDP (largely cytosolic), and GTP-bound active (membrane associated) forms [Puxeddu *et al.* 2009]. The effect of the Arf1 interaction on PrP^C localization and expression was studied by inhibiting GEP with BFA. BFA treatment resulted in a marked decline of PrP^C expression. Using co-immunofluorescence techniques, it is demonstrated that BFA-Arf1 deactivation alters the sub-cellular localization and expression of PrP^C. Based on the model of Arf1 function in intra-Golgi trafficking, it is proposed propose that Arf1-GTP stimulates retrograde transport of PrP^C molecules within the trans-Golgi compartment toward the ER and also to the plasma membrane. The functional disruption of Arf1; however, did not influence Rab7a expression in either HpL3-4 transiently PrP^C transfected or SH-SY5Y stable PrP^C expressing cells.

5.3 PrP^C and alpha- tubulin 1

The microtubular cellular structures play a central role in intracellular transport, metabolism, and cell division. Microtubule networks are used as tracks for intracellular protein trafficking. Tubulin is a major component of microtubules and is known to interact with PrP^C [Dong *et al.* 2008; Nieznanski *et al.* 2005]. An interaction of alpha-tubulin 1 with PrP^C was identified. Nocodazole treatment disrupts the microtubular network and affects the intracellular distribution of PrP^C [Hachiya *et al.* 2004a; Hachiya *et al.* 2004b]. The role of nocodazole disruption of microtubules on PrP^C intracellular distribution was examined. Increased PrP^C expression was found in the cytosolic region after nocodazole treatment of PrP^C expressing cells. Moreover, disruption of microtubules also led to the down regulation of Rab7a and Arf1 expression. Decreased Arf1 can be attributed to the Golgi membranes' kinesin-dependent dispersal following

microtubule disruption with nocodazole [Hehnly *et al.* 2010]. The active transport of Rab7-containing endosomes is mediated by microtubules which fuse with other late endosomes [Vonderheit and Helenius 2005]. Disruption of microtubules could influence Rab7a expression.

Based on these results, it is interesting to speculate that PrP^C can be recycled back to the plasma membrane with a Rab7a dependent pathway and that the impaired Rab7a machinery leads to accumulation of PrP^C but not to the formation of the resistant form of PrP^C. It remains to be determined whether this Rab7a dependent PrP^C accumulation in the Rab9 positive endosomal compartments is crucial for the conversion of PrP^C to PrP^{Sc}. The results also suggest that Arf1-GTP stimulates retrograde transport of PrP^C molecules within the trans-Golgi compartment toward the ER and also to the plasma membrane. The functional disruption of Arf1; however, did not influence Rab7a expression. Moreover, disruption of microtubules also led to the down regulation of Rab7a and Arf1 expression.

In conclusion, these studies identified a large number of both known and previously unknown PrP^C interacting proteins. It remains to be demonstrated whether direct interactions take place or not as well as exactly what the actual interaction sites of these proteins have with PrP^C. However, these results further highlight the pivotal role of endosomal compartments in PrP^C trafficking and could help to explain the physiological role of PrP^C and their associations with these interacting proteins.

6. Appendix A

- **pENTRY-IBA1-Cloning site**
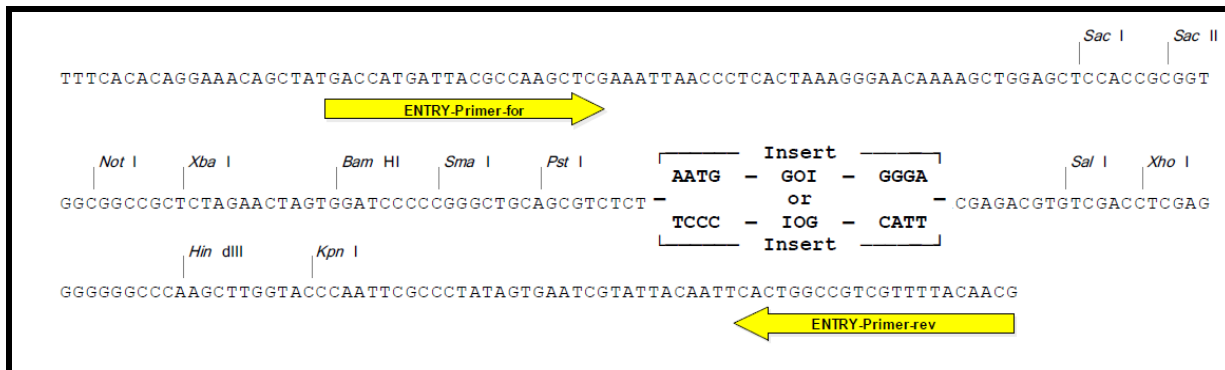
GOI= Gene of interest
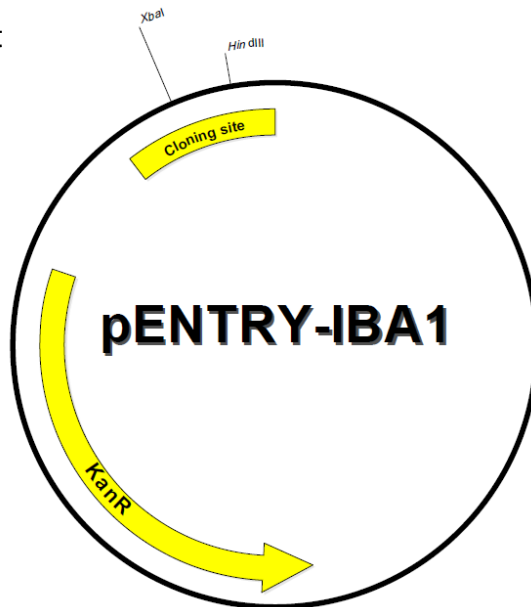
Features	from bp	to bp	Sequencing primer
Kanamycin resistance gene	1143	1937	ENTRY-Primer-for
forward primer binding site	2182	2203	5'– GACCATGATTACGCCAAGCTCG –3'
reverse primer binding site	2370*	2392*	
			ENTRY-Primer-rev
			5'– CGTTGTAAAACGACGGCCAGTG –3'
total vector length		2392*	
* plus length of inserted gene			

- **pESG-IBA103-Cloning site**

GAGAACCCACTGCTTACTGGCTTATCGAAATTAATACGACTCACTATAGGGTCTAGACCCACAATG — GOI — GGGAGCGCTTGG

ESG-Primer-for

One-STrEP-tag

Xba I

M — POI

G S A W
1 2 3 4

M
1

Bst BI

AGCCACCCGCAGTTCGAAAAAGGTGGAGGTTCTGGCGGTGGATCGGGAGGTTCAGCGTGGAGCCACCCGCAGTTCGAGAAATAAGGGAGC

One-STrEP-tag

S H P Q F E K G G G S G G G S G G S A W S H P Q F E K .
5 6 7 8 9 10 11 12 13 14 15 16 17 18 19 20 21 22 23 24 25 26 27 28 29 30 31 32

Hin dIII   Not I   Bgl II

CACCCGCAAGCTTGCGGCCGCAGATCTAGCTTAAGTTTAAACCGCTGATCAGCCTCGACTGTGCCTTCTA

ESG-Primer-rev

GOI= Gene of interest

pESG-IBA

Features	from bp	to bp	Sequencing primer		
f1 origin	259	687	ESG-Primer-for (Cat. No. 5-0000-121)		
SV40 ori	692	1035			
Neomycin resistance gene	1097	1891	5' – GAGAACCCACTGCTTACTGGC –3'		
ColEI ori	2637	3222			
Ampicillin resistance gene	3393	4253	ESG-Primer-rev (Cat. No. 5-0000-122)		
CMV promoter	4621	5208			
forward primer binding site	5221	5241	5' – TAGAAGGCACAGTCGAGG –3'		
One-STrEP-tag	5287*	5379*			
reverse primer binding site	5441*	5458*			
polyA signal sequence	1	213			
total vector length		5458*			
* plus length of inserted gene					

Appendix B

Peptides sequence of identified proteins.

B.No	Acc. No.	Protein Description	Mass (kDa)	MS/MS Score	Peptide matched	pI	Sequence Coverage %	MS/MS analysis
								Cytoskeleton: Cell growth /maintenance
14	P60710	Actin, cytoplasmic 1	41.7	508	18	5.29	36	**Start - End Observed Mr(expt) Mr(calc) Delta Miss Sequence** 19 - 28 488.7444 975.4742 975.4410 0.0332 0 K.AGFAGDDAPR.A 29 - 39 400.2466 1197.7180 1197.6982 0.0197 0 R.AVFPSIVGRPR.H 51 - 61 599.7853 1197.5560 1197.5150 0.0411 0 K.DSYVGDEAQSK.R 51 - 61 599.7866 1197.5586 1197.5150 0.0437 0 K.DSYVGDEAQSK.R 51 - 62 452.2235 1353.6487 1353.6161 0.0326 1 K.DSYVGDEAQSKR.G 51 - 62 677.8400 1353.6654 1353.6161 0.0494 1 K.DSYVGDEAQSKR.G 85 - 95 505.9297 1514.7673 1514.7419 0.0254 0 K.IWHHTFYNELR.V 96 - 113 652.0298 1953.0676 1953.0571 0.0105 0 R.VAPEEHPVLLTEAPLNPK.A 184 - 191 499.7590 997.5034 997.4790 0.0244 0 R.DLTDYLMK.I 197 - 206 566.7804 1131.5462 1131.5197 0.0266 0 R.GYSFTTTAER.E 239 - 254 895.9766 1789.9386 1789.8846 0.0540 0 K.SYELPDGQVITIGNER.F 239 - 254 895.9796 1789.9446 1789.8846 0.0600 0 K.SYELPDGQVITIGNER.F 285 - 291 453.2414 904.4682 904.4436 0.0246 1 K.CDVDIRK.D 316 - 326 581.3295 1160.6444 1160.6111 0.0334 0 K.EITALAPSTMK.I 316 - 326 589.3286 1176.6426 1176.6060 0.0366 0 K.EITALAPSTMK.I Oxidation (M) 329 - 336 462.2981 922.5816 922.5600 0.0217 1 K.IIAPPERK.Y 360 - 372 506.2490 1515.7252 1515.6954 0.0298 0 K.QEYDESGPSIVHR.K 360 - 372 506.2527 1515.7363 1515.6954 0.0409 0 K.QEYDESGPSIVHR.K
21	P07356	Annexin A2	38.6	266	8	7.55	27	**Start - End Observed Mr(expt) Mr(calc) Delta Miss Sequence** 38 - 47 537.3138 1072.6130 1072.5764 0.0366 0 R.DALNIETAVK.T 50 - 63 771.9626 1541.9106 1541.8413 0.0693 0 K.GVDEVTIVNILTNR.S 69 - 77 556.2996 1110.5846 1110.5458 0.0389 0 R.QDIAFAYQR.R 105 - 115 611.8281 1221.6416 1221.5877 0.0539 0 K.TPAQYDASELK.A 136 - 145 622.8444 1243.6742 1243.6156 0.0586 0 R.TNQELQEINR.V 158 - 168 613.3135 1224.6124 1224.5623 0.0502 0 K.DIISDTSGDFR.K 179 - 196 689.0285 2064.0637 2063.9760 0.0877 1 R.RAEDGSVIDYELIDQDAR.E 314 - 324 711.3830 1420.7514 1420.6874 0.0640 0 K.SLYYYIQQDTK.G
14	Q8BFZ3	Beta-actin-like protein 2	41.9	140	6	5.30	15	**Start - End Observed Mr(expt) Mr(calc) Delta Miss Sequence** 97 - 114 652.0298 1953.0676 1953.0571 0.0105 0 R.VAPDEHPILLTEAPLNPK.I 185 - 192 499.7590 997.5034 997.4790 0.0244 0 R.DLTDYLMK.I 240 - 255 895.9766 1789.9386 1789.8846 0.0540 0 R.SYELPDGQVITIGNER.F 240 - 255 895.9796 1789.9446 1789.8846 0.0600 0 R.SYELPDGQVITIGNER.F 286 - 292 453.2414 904.4682 904.4436 0.0246 1 K.CDVDIRK.D 330 - 337 462.2981 922.5816 922.5600 0.0217 1 K.IIAPPERK.Y
35	P18760	Cofilin-1	18.5	118	5	5.54	9	**Start - End Observed Mr(expt) Mr(calc) Delta Miss Sequence** 35 - 45 437.2444 1308.7114 1308.6748 0.0366 1 K.AVLFCLSEDKK.N 35 - 45 655.3682 1308.7218 1308.6748 0.0471 1 K.AVLFCLSEDKK.N 82 - 92 669.3351 1336.6556 1336.6187 0.0370 0 R.YALYDATYETK.E 82 - 92 669.3491 1336.6836 1336.6187 0.0650 0 R.YALYDATYETK.E 153 - 166 670.9175 1339.8204 1339.7711 0.0493 0 K.LGGSAVISLEGKPL.-
9	P26041	Moesin	67.7	63	3	6.22	5	**Start - End Observed Mr(expt) Mr(calc) Delta Miss Sequence** 238 - 246 552.7748 1103.5350 1103.5764 -0.0413 0 K.IGFPWSEIR.N 264 - 273 591.7788 1181.5430 1181.5869 -0.0439 0 K.APDFVFYAPR.L 439 - 448 617.2702 1232.5258 1232.5673 -0.0415 0 K.ESEAVEWQQK.A
3	Q8VDD5	Myosin-9	226.2	326	15	5.54	7	**Start - End Observed Mr(expt) Mr(calc) Delta Miss Sequence** 342 - 355 729.9309 1457.8472 1457.8606 -0.0133 0 R.VISGVLQLGNIAFK.K 663 - 670 481.2328 960.4510 960.4777 -0.0267 0 R.NTNPNFVR.C 694 - 702 509.2484 1016.4822 1016.5073 -0.0251 0 R.CNGVLEGIR.I 712 - 718 462.7362 923.4578 923.4865 -0.0287 0 R.VVFQEFR.Q

```
719 - 731   520.2798 1557.8176 1557.8515  -0.0339  1 R.QRYEILTPNSIPK.G
746 - 755   597.2985 1192.5824 1192.6088  -0.0263  0 K.ALELDSNLYR.I
765 - 775   408.5372 1222.5898 1222.6306  -0.0408  0 R.AGVLAHLEEER.D
843 - 850   477.7383 953.4620  953.4818   -0.0197  0 R.HEDELLAK.E
859 - 867   534.2698 1066.5250 1066.5519  -0.0269  1 R.EKHLAAENR.L
1393 - 1400 459.2284 916.4422  916.4614   -0.0191  0 K.DLEGLSQR.L
1418 - 1433 650.6564 1948.9474 1948.9854  -0.0380  0 R.LQQELDDLLVDLDHQR.Q
1434 - 1441 452.7284 903.4422  903.4661   -0.0239  0 R.QSVSNLEK.K
1445 - 1454 610.8188 1219.6230 1219.6448  -0.0218  1 K.KFDQLLAEEK.T
1878 - 1888 666.2962 1330.5778 1330.6000  -0.0222  0 R.QLEEAEEEAQR.A
1923 - 1932 580.3208 1158.6270 1158.6510  -0.0239  1 R.RGDLPFVVTR.R
```

33 Q9WVA4 Transgelin-2 22.3 122 4 8.39 21

```
Start - End   Observed  Mr(expt)  Mr(calc)   Delta   Miss Sequence
80 - 88    499.7946 997.5746 997.4902  0.0844  0 K.IQASSMAFK.Q
128 - 139  616.3934 1230.7722 1230.6754 0.0968  0 R.TLMNLGGLAVAR.D
161 - 171  640.3479 1278.6812 1278.5840 0.0972  0 R.NFSDNQLQEGK.N
172 - 182  609.8646 1217.7146 1217.6187 0.0960  0 K.NVIGLQMGTNR.G
```

12 P68369 Tubulin alpha-1A 50.1 223 9 4.94 28

```
Start - End   Observed  Mr(expt)  Mr(calc)   Delta   Miss Sequence
41 - 60    1004.4802 2006.9458 2006.8858 0.0600  0 K.TIGGGDDSFNTFFSETGAGK.H
65 - 79    851.4842 1700.9538 1700.8985 0.0553  0 R.AVFVDLEPTVIDEVR.T
85 - 96    470.9381 1409.7925 1409.7667 0.0258  0 R.QLFHPEQLITGK.E
113 - 121  543.3328 1084.6510 1084.6128 0.0382  0 K.EIIDLVLDR.I
216 - 229  573.6496 1717.9270 1717.8747 0.0523  0 R.NLDIERPTYTNLNR.L
265 - 280  586.3396 1755.9970 1755.9559 0.0410  0 R.IHFPLATYAPVISAEK.A
327 - 336  508.3051 1014.5956 1014.5709 0.0247  0 K.DVNAAIATIK.T
340 - 352  799.9094 1597.8042 1597.7599 0.0443  0 R.TIQFVDWCPTGFK.V
353 - 370  913.0294 1824.0442 1823.9782 0.0661  0 K.VGINYQPPTVVPGGDLAK.V
```

13 P99024 Tubulin beta-5 chain 49.6 193 9 4.78 19

```
Start - End   Observed  Mr(expt)  Mr(calc)   Delta   Miss Sequence
47 - 58    651.3401 1300.6656 1300.6299 0.0357  0 R.ISVYYNEATGGK.Y
104 - 121  653.6868 1958.0386 1957.9745 0.0640  0 K.GHYTEGAELVDSVLDVVR.K
242 - 251  565.8151 1129.6156 1129.5880 0.0277  0 R.FPGQLNADLR.K
242 - 251  565.8196 1129.6246 1129.5880 0.0367  0 R.FPGQLNADLR.K
283 - 297  830.4736 1658.9326 1658.8879 0.0447  0 R.ALTVPELTQQVFDAK.N
283 - 297  830.4849 1658.9552 1658.8879 0.0673  0 R.ALTVPELTQQVFDAK.N
310 - 318  520.3129 1038.6112 1038.5862 0.0250  0 R.YLTVAAVFR.G
337 - 350  848.9507 1695.8868 1695.8257 0.0612  0 K.NSSYFVEWIPNNVK.T
351 - 359  514.7861 1027.5576 1027.5121 0.0456  0 K.TAVCDIPPR.G
```

12 P20152 Vimentin 53.6 260 11 5.06 21

```
Start - End   Observed  Mr(expt)  Mr(calc)   Delta   Miss Sequence
37 - 50    499.2907 1494.8503 1494.7790 0.0712  0 R.TYSLGSALRPSTSR.S
51 - 64    722.8833 1443.7520 1443.6994 0.0526  0 R.SLYSSSPGGAYVTR.S
130 - 139  585.3790 1168.7434 1168.7067 0.0368  0 K.ILLAELEQLK.G
130 - 139  585.3790 1168.7434 1168.7067 0.0368  0 K.ILLAELEQLK.G
130 - 143  513.9963 1538.9671 1538.9032 0.0639  1 K.ILLAELEQLKGQGK.S
160 - 168  530.8004 1059.5862 1059.5197 0.0666  0 R.QVDQLTNDK.A
208 - 217  544.7923 1087.5700 1087.5258 0.0443  0 R.QDVDNASLAR.L
274 - 282  512.2780 1022.5414 1022.5032 0.0382  0 R.QQYESVAAK.N
283 - 292  655.3319 1308.6492 1308.5986 0.0507  0 K.NLQEAEEWYK.S
295 - 304  547.2800 1092.5454 1092.5200 0.0255  0 K.FADLSEAANR.N
403 - 410  466.7512 931.4878  931.4610  0.0268  0 K.LLEGEESR.I
```

Cell communication : Signal transduction

27 P62259 14-3-3 protein epsilon 29.1 95 3 4.63 14

```
Start - End   Observed  Mr(expt)  Mr(calc)   Delta  Miss Sequence
30 - 42    732.3979 1462.7812 1462.6974 0.0839  0 K.VAGMDVELTVEER.N  Oxidation (M)
107 - 118  619.3565 1236.6984 1236.6462 0.0522  0 K.HLIPAANTGESK.V
131 - 141  628.8278 1255.6410 1255.5833 0.0578  0 R.YLAEFATGNDR.K
```

27 P63101 14-3-3 protein zeta/delta 27.7 162 4 4.73 20

```
Start - End   Observed  Mr(expt)  Mr(calc)   Delta  Miss Sequence
42 - 49    454.2814 906.5482  906.5174  0.0308  0 R.NLLSVAYK.N
104 - 115  665.8851 1329.7556 1329.6928 0.0628  0 K.FLIPNASQPESK.V
128 - 139  640.3543 1278.6940 1278.6456 0.0485  1 R.YLAEVAAGDDKK.G
140 - 157  1021.0496 2040.0846 2039.9800 0.1047 0 K.GIVDQSQQAYQEAFEISK.K
```

24 P14206 Laminin receptor 1 32.8 163 3 4.80 13

```
Start - End   Observed  Mr(expt)  Mr(calc)   Delta  Miss Sequence
90 - 102   602.3539 1202.6932 1202.6408 0.0525  0 K.FAAATGATPIAGR.F
103 - 117  849.9825 1697.9504 1697.8526 0.0979  0 R.FTPGTFTNQIQAAFR.E
156 - 166  653.8563 1305.6980 1305.6387 0.0593  0 R.YVDIAIPCNNK.G
```

15 P63038 60 kDa heat shock protein 60.9 123 5 5.91 10

```
Start - End   Observed  Mr(expt)  Mr(calc)   Delta  Miss Sequence
61 - 72    672.8917 1343.7688 1343.7085 0.0603  0 R.TVIIEQSWGSPK.V
406 - 417  617.3263 1232.6380 1232.5885 0.0496  0 K.VGGTSDVEVNEK.K
421 - 429  480.7774 959.5402  959.5036  0.0366  0 R.VTDALNATR.A
```

| 430 - 446 | 842.9941 | 1683.9736 | 1683.8978 | 0.0759 | 0 | R.AAVEEGIVLGGGCALLRC |
| 482 - 493 | 608.3602 | 1214.7058 | 1214.6507 | 0.0552 | 0 | K.NAGVEGSLIVEK.I |

| 34 | P84078 | ADP-ribosylation factor 1 | 20.6 | 57 | 3 | 6.32 | 10 | | | | | | | |

Start - End	Observed	Mr(expt)	Mr(calc)	Delta	Miss	Sequence
20 - 30	544.3536	1086.6926	1086.6107	0.0819	0	R.ILMVGLDAAGK.T
20 - 30	552.3506	1102.6866	1102.6056	0.0810	0	R.ILMVGLDAAGK.T
110 - 117	496.7753	991.5360	991.4644	0.0716	0	R.MLAEDELR.D

| 21 | P10107 | Annexin A1 | 38.7 | 254 | 11 | 6.97 | 26 | | | | | | | |

Start - End	Observed	Mr(expt)	Mr(calc)	Delta	Miss	Sequence
30 - 53	782.0945	2343.2617	2343.1495	0.1121	0	K.GGPGSAVSPYPSFNVSSDVAALHK.A
114 - 124	631.8317	1261.6488	1261.5939	0.0550	0	K.TPAQFDADELR.G
167 - 178	447.8936	1340.6590	1340.6208	0.0381	1	K.DITSDTSGDFRK.A
167 - 178	671.3505	1340.6864	1340.6208	0.0656	1	K.DITSDTSGDFRK.A
205 - 212	454.7408	907.4670	907.4399	0.0271	0	R.ALYEAGER.R
205 - 212	454.7446	907.4746	907.4399	0.0347	0	R.ALYEAGER.R
214 - 228	551.3235	1650.9487	1650.8941	0.0546	1	R.KGTDVNVFTTILTSR.S
215 - 228	762.4437	1522.8728	1522.7991	0.0737	0	K.GTDVNVFTTILTSR.S
235 - 242	506.2924	1010.5702	1010.5298	0.0405	1	R.RVFQNYGK.Y
236 - 242	428.2355	854.4564	854.4286	0.0278	0	R.VFQNYGK.Y
270 - 281	665.3440	1328.6734	1328.6071	0.0664	0	K.CATSTPAFFAEK.L

| 22 | P48036 | Annexin A5 | 35.9 | 201 | 7 | 4.83 | 22 | | | | | | | |

Start - End	Observed	Mr(expt)	Mr(calc)	Delta	Miss	Sequence
5 - 16	634.8223	1267.6300	1267.5834	0.0467	0	R.GTVTDFPGFDGR.A
28 - 43	852.4765	1702.9384	1702.8737	0.0647	0	K.GLGTDEDSILNLLTSR.S
49 - 56	496.7637	991.5128	991.4974	0.0154	0	R.QEIAQEFK.T
107 - 115	501.3151	1000.6156	1000.5917	0.0240	0	K.VLTEIIASR.T
150 - 159	578.8582	1155.7018	1155.6798	0.0221	0	R.MLVVLLQANR.D
192 - 199	477.7874	953.5602	953.5335	0.0268	0	K.FITIFGTR.S)
275 - 283	553.8145	1105.6144	1105.5768	0.0377	0	R.SEIDLFNIR.K

| 11 | Q60864 | Stress-induced-phosphoprotein 1 | 62.5 | 253 | 6 | 6.40 | 13 | | | | | | | |

Start - End	Observed	Mr(expt)	Mr(calc)	Delta	Miss	Sequence
14 - 32	1020.0450	2038.0754	2037.9677	0.107	0	K.ALSAGNIDDALQCYSEAIK.L)
110 - 118	532.2665	1062.5184	1062.4764	0.0421	0	K.EGLQNMEAR.L
124 - 136	821.4442	1640.8738	1640.8021	0.0718	0	K.FMNPFNLPNLYQK.L
145 - 153	526.2937	1050.5728	1050.5346	0.0383	0	R.SLLSDPTYR.E
352 - 364	744.9295	1487.8444	1487.7871	0.0573	0	R.LAYINPDLALEEK.N
534 - 543	558.8463	1115.6780	1115.6373	0.0408	0	K.LMDVGLIAIR.-

| 32 | P51150 | Ras-related protein Rab-7a | 23.4 | 93 | 3 | 6.40 | 16 | | | | | | | |

Start - End	Observed	Mr(expt)	Mr(calc)	Delta	Miss	Sequence
11 - 21	529.3070	1056.5994	1056.6179	-0.0185	0	K.VIILGDSGVGK.T
39 - 48	518.7822	1035.5498	1035.5601	-0.0102	0	K.ATIGADFLTK.E
158 - 171	795.4207	1588.8268	1588.8209	0.0060	0	K.EAINVEQAFQTIAR.N

| 8 | P08113 | Endoplasmin | 92.4 | 322 | 13 | 4.74 | 14 | | | | | | | |

Start - End	Observed	Mr(expt)	Mr(calc)	Delta	Miss	Sequence
88 - 95	482.3147	962.6148	962.5800	0.0348	0	K.LIINSLYK.N
96 - 102	460.2888	918.5630	918.5287	0.0344	1	K.NKEIFLR.E
103 - 114	638.3587	1274.7028	1274.6354	0.0675	0	R.ELISNASDALDK.I
103 - 116	515.6331	1543.8775	1543.8205	0.0569	1	R.ELISNASDALDKIR.L
143 - 156	510.6133	1528.8181	1528.7668	0.0513	0	K.NLLHVTDTGVGMTR.E
385 - 395	594.3685	1186.7224	1186.6710	0.0514	0	K.SILFVPTSAPR.G
396 - 405	572.3105	1142.6064	1142.5608	0.0457	1	R.GLFDEYGSKK.S
435 - 448	743.4206	1484.8266	1484.7471	0.0795	0	K.GVVDSDDLPLNVSR.E
494 - 503	570.3190	1138.6234	1138.5731	0.0504	0	K.LGVIEDHSNR.T
672 - 682	645.3359	1288.6572	1288.5935	0.0637	0	K.DISTNYYASQK.K
683 - 690	502.7988	1003.5830	1003.5451	0.0380	1	K.KTFEINPR.H
684 - 690	438.7529	875.4912	875.4501	0.0411	0	K.TFEINPR.H
725 - 733	497.2874	992.5602	992.5179	0.0424	0	R.SGYLLPDTK.A

Metabolism: Energy pathways

| 16 | P17182 | Alpha-enolase | 47.1 | 288 | 6 | 6.37 | 16 | | | | | | | |

Start - End	Observed	Mr(expt)	Mr(calc)	Delta	Miss	Sequence
33 - 50	903.0068	1803.9990	1803.9366	0.0624	0	R.AAVPSGASTGIYEALELR.D
72 - 80	450.2883	898.5620	898.5488	0.0133	0	K.TIAPALVSK.K
81 - 89	536.8183	1071.6220	1071.5924	0.0296	1	K.KVNVVEQEK.I
270 - 281	720.3997	1438.7848	1438.7344	0.0505	0	R.YITPDQLADLYK.S
344 - 358	817.4485	1632.8824	1632.8141	0.0683	0	K.VNQIGSVTESLQACK.L
413 - 420	452.7413	903.4680	903.4549	0.0132	0	R.IEEELGSK.A

| 16 | P05202 | Aspartate aminotransferase, mitochondrial | 47.3 | 220 | 7 | 9.13 | 15 | | | | | | | |

Start - End	Observed	Mr(expt)	Mr(calc)	Delta	Miss	Sequence
108 - 122	779.4446	1556.8746	1556.8046	0.0701	0	K.ASAELALGENNEVLK.S
126 - 139	725.4400	1448.8654	1448.7988	0.0667	0	R.FVTVQTISGTGALR.V
140 - 147	439.2592	876.5038	876.4818	0.0221	0	R.VGASFLQR.F
288 - 296	490.7846	979.5546	979.5161	0.0385	0	R.VGAFTVVCK.D
326 - 337	635.8948	1269.7750	1269.7292	0.0458	0	R.IAATILTSPDLR.K
326 - 338	466.9622	1397.8648	1397.8242	0.0406	1	R.IAATILTSPDLRK.Q

							Start - End	Observed	Mr(expt)	Mr(calc)	Delta	Miss	Sequence
							356 - 364	515.8410	1029.6674	1029.6182	0.0492	1	R.TQLVSNLKK.E
17	P05064	Fructose-bisphosphate aldolase A	39.3	160	6	8.31	11	**Start - End**	**Observed**	**Mr(expt)**	**Mr(calc)**	**Delta**	**Miss Sequence**
							15 - 22	470.7626	939.5106	939.4774	0.0333	0	K.ELSDIAHR.I
							29 - 42	666.8856	1331.7566	1331.6932	0.0634	0	K.GILAADESTGSIAK.R
							323 - 330	476.2620	950.5094	950.4709	0.0386	0	K.AAQEEYIK.R
							323 - 331	554.3136	1106.6126	1106.5720	0.0407	1	K.AAQEEYIKR.A
							323 - 331	554.3142	1106.6138	1106.5720	0.0419	1	K.AAQEEYIKR.A
							332 - 342	566.8150	1131.6154	1131.5706	0.0448	0	R.ALANSLACQGK.Y
18	P16858	GAPDH	35.7	387	10	8.44	32	Start - End	Observed	Mr(expt)	Mr(calc)	Delta	Miss Sequence
							65 - 78	543.3352	1626.9838	1626.9457	0.0381	0	K.LVINGKPITIFQER.D
							117 - 137	749.0670	2244.1792	2244.0919	0.0873	0	R.VIISAPSADAPMFVMGVNHEK.Y
							144 - 160	910.4822	1818.9498	1818.8968	0.0531	0	K.IVSNASCTTNCLAPLAK.V
							199 - 213	685.3871	1368.7596	1368.7361	0.0235	0	R.GAAQNIIPASTGAAK.A
							218 - 225	435.2640	868.5134	868.5018	0.0116	0	K.VIPELNGK.L
							226 - 232	406.2172	810.4198	810.4058	0.0140	0	K.LTGMAFR.V
							233 - 246	778.9298	1555.8450	1555.8029	0.0422	0	R.VPTPNVSVVDLTCR.L
							322 - 332	630.3224	1258.6302	1258.5937	0.0365	0	R.VVDLMAYMASK.E
							322 - 332	630.3232	1258.6318	1258.5937	0.0381	0	R.VVDLMAYMASK.E
							322 - 333	694.8505	1387.6864	1387.6363	0.0501	1	R.VVDLMAYMASKE.-
26	O09131	Glutathione S-transferase omega-1	27.4	69	5	6.92	20	**Start - End**	**Observed**	**Mr(expt)**	**Mr(calc)**	**Delta**	**Miss Sequence**
							12 - 25	681.3976	1360.7806	1360.7099	0.0707	0	K.GSAPPGPVPEGQIR.V
							31 - 37	463.2351	924.4556	924.4276	0.0280	0	R.FCPFAQR.T Carbamidomethyl (C)
							49 - 57	540.3301	1078.6456	1078.6135	0.0322	0	R.HEVININLK.N
							123 - 132	549.8549	1097.6952	1097.6597	0.0355	0	K.VPPLIASFVR.S
							144 - 152	554.3092	1106.6038	1106.5607	0.0431	1	R.EALENEFKK.L
33	P35700	Peroxiredoxin-1	22.1	182	7	8.26	30	**Start - End**	**Observed**	**Mr(expt)**	**Mr(calc)**	**Delta**	**Miss Sequence**
							8 - 16	503.7939	1005.5732	1005.5284	0.0449	0	K.IGYPAPNFK.A
							111 - 120	554.3272	1106.6398	1106.5972	0.0427	0	R.TIAQDYGVLK.A
							111 - 128	661.7098	1982.1076	1982.0109	0.0967	1	R.TIAQDYGVLKADEGISFR.G
							129 - 136	460.7717	919.5288	919.5015	0.0274	0	R.GLFIIDDK.G
							129 - 140	453.9479	1358.8219	1358.7922	0.0297	1	R.GLFIIDDKGILR.Q
							141 - 151	613.3715	1224.7284	1224.6826	0.0458	0	R.QITINDLPVGR.S
							159 - 168	598.8400	1195.6654	1195.6237	0.0417	0	R.LVQAFQFTDK.H

Protein metabolism

							Start - End	Observed	Mr(expt)	Mr(calc)	Delta	Miss	Sequence
6	P58252	Elongation factor 2	95.2	124	5	6.41	5	**Start - End**	**Observed**	**Mr(expt)**	**Mr(calc)**	**Delta**	**Miss Sequence**
							2 - 10	546.3216	1090.6286	1090.5771	0.0515	0	M.VNFTVDQIR.A
							240 - 249	509.2732	1016.5318	1016.4887	0.0432	0	K.GEGQLSAAER.A
							265 - 272	456.2335	910.4524	910.4185	0.0340	0	R.YFDPANGK.F
							416 - 426	547.3389	1092.6632	1092.6179	0.0453	0	R.VFSGVVSTGLK.V
							573 - 580	461.7394	921.4642	921.4556	0.0087	0	K.SDPVVSYR.E
10	P63017	Heat shock cognate 71 kDa protein	70.8	236	13	5.37	18	**Start - End**	**Observed**	**Mr(expt)**	**Mr(calc)**	**Delta**	**Miss Sequence**
							26 - 36	614.7968	1227.5790	1227.6207	-0.0417	0	K.VEIIANDQGNR.T
							160 - 171	600.3202	1198.6258	1198.6670	-0.0411	0	K.DAGTIAGLNVLR.I
							221 - 236	564.5534	1690.6384	1690.7183	-0.0800	0	K.STAGDTHLGGEDFDNR.M
							237 - 246	618.2911	1234.5676	1234.6169	-0.0492	0	R.MVNHFIAEFK.R
							300 - 311	494.2325	1479.6757	1479.7470	-0.0713	1	R.ARFEELNADLFR.G
							302 - 311	627.2891	1252.5636	1252.6088	-0.0451	0	R.FEELNADLFR.G
							312 - 319	429.7122	857.4098	857.4494	- 0.0396	0	R.GTLDPVEK.A
							349 - 357	541.2634	1080.5122	1080.5604	-0.0481	0	K.LLQDFFNGK.E
							416 - 423	465.7547	929.4948	929.5294	-0.0346	1	K.RNTTIPTK.Q
							501 - 509	509.2637	1016.5128	1016.5614	-0.0486	1	K.ITITNDKGR.L
							510 - 517	495.2458	988.4770	988.5189	-0.0418	1	R.LSKEDIER.M
							540 - 550	660.2779	1318.5412	1318.5863	-0.0451	0	K.NSLESYAFNMK.A
							574 - 583	639.2913	1276.5680	1276.6122	-0.0441	0	K.CNEIISWLDK.N
							602 - 609	472.7433	943.4720	943.5161	- 0.0440	0	K.VCNPIITK.L
12	P09103	Protein disulfide-isomerase	57.1	133	7	4.79	14	**Start - End**	**Observed**	**Mr(expt)**	**Mr(calc)**	**Delta**	**Miss Sequence**
							60 - 67	431.7491	861.4836	861.4596	0.0241	0	K.ALAPEYAK.R
							72 - 80	501.7995	1001.5844	1001.5505	0.0339	1	K.LKAEGSEIR.L
							84 - 99	890.9596	1779.9046	1779.8275	0.0771	0	K.VDATEESDLAQQYGVR.G
							329 - 340	470.5771	1408.7095	1408.6722	0.0373	0	K.YKPESDELTAEK.I
							341 - 347	481.7499	961.4852	961.4440	0.0413	0	K.ITEFCHR.F
							427 - 438	655.3291	1308.6436	1308.5867	0.0569	0	K.MDSTANEVEAVK.V
							455 - 463	533.7825	1065.5504	1065.5091	0.0414	0	R.TVIDYNGER.T
12	P27773	Protein disulfide-isomerase A3	56.6	113	5	5.88	10	**Start - End**	**Observed**	**Mr(expt)**	**Mr(calc)**	**Delta**	**Miss Sequence**
							63 - 73	596.3225	1190.6304	1190.5931	0.0373	0	R.LAPEYEAAATR.L
							131 - 140	498.3008	994.5870	994.5560	0.0311	0	K.QAGPASVPLR.T

								259 - 271	804.4152 1606.8158 1606.7403 0.0756 0 K.DLLTAYYDVDYEK.N
								297 - 304	439.2591 876.5036 876.4817 0.0219 0 K.LNFAVASR.K
								367 - 379	691.8729 1381.7312 1381.6725 0.0587 0 K.SEPIPESNEGPVK.V
16	P19324	Serpin H1 (47 kDa heat shock protein)	46.5	120	3	8.90	9	**Start - End**	**Observed Mr(expt) Mr(calc) Delta Miss Sequence**
								101 - 115	579.6795 1736.0167 1735.9217 0.0950 1 K.LRDEEVHTGLGELLR.S
								308 - 318	612.8617 1223.7088 1223.6510 0.0578 0 K.GVVEVTHDLQK.H
								393 - 404	653.8762 1305.7378 1305.6677 0.0701 0 R.DNQSGSLLFIGR.L
10	P38647	Stress-70 protein, mitochondrial	73.4	397	9	5.91	13	**Start - End**	**Observed Mr(expt) Mr(calc) Delta Miss Sequence**
								77 - 85	479.7308 957.4470 957.4879 -0.0409 0 K.VLENAEGAR.T
								160 - 173	777.4011 1552.7876 1552.8323 -0.0447 0 K.LYSPSQIGAFVLMK.M
								207 - 218	621.8179 1241.6212 1241.6728 -0.0515 0 K.DAGQISGLNVLR.V
								349 - 360	667.3468 1332.6790 1332.7289 -0.0499 0 R.AQFEGIVTDLIK.R
								349 - 361	497.2584 1488.7534 1488.8300 -0.0766 1 R.AQFEGIVTDLIKR.T
								378 - 391	723.8605 1445.7064 1445.7548 -0.0484 0 K.SDIGEVILVGGMTR.M
								395 - 405	645.8167 1289.6188 1289.6728 -0.0540 0 K.VQQTVQDLFGR.A
								626 - 634	510.7139 1019.4132 1019.4520 -0.0387 0 K.DSETGENIR.Q
								635 - 646	616.3114 1230.6082 1230.6568 -0.0485 0 R.QAASSLQQASLK.L

Regulation of nucleic acid metabolism

18	Q9EQU5	Protein SET	33.3	180	5	4.22	19	**Start - End**	**Observed Mr(expt) Mr(calc) Delta Miss Sequence**
								57 - 67	637.3608 1272.7070 1272.6561 0.0510 0 R.LNEQASEEILK.V
								83 - 89	408.7590 815.5034 815.4865 0.0170 1 K.RSELIAK.I
								122 - 131	604.8239 1207.6332 1207.5972 0.0360 0 R.VEVTEFEDIK.S
								136 - 149	920.9449 1839.8752 1839.7992 0.0761 0 R.IDFYFDENPYFENK.V)
								154 - 166	482.9012 1445.6818 1445.6423 0.0395 0 K.EFHLNESGDPSSK.S

Protein folding

33	Q99LP6	GrpE protein homolog 1, mitochondrial	24.4	161	8	8.58	26	**Start - End**	**Observed Mr(expt) Mr(calc) Delta Miss Sequence**
								65 - 72	493.8080 985.6014 985.5556 0.0458 1 K.AKLEEQLR.E
								81 - 89	501.7849 1001.5552 1001.5141 0.0411 0 R.ALADTENLR.Q
								81 - 89	501.7869 1001.5592 1001.5141 0.0451 0 R.ALADTENLR.Q
								101 - 109	543.2985 1084.5824 1084.5376 0.0449 0 K.LYGIQGFCK.D
								110 - 120	629.3781 1256.7416 1256.6864 0.0553 0 K.DLLEVADILEK.A
								110 - 120	629.4009 1256.7872 1256.6864 0.1009 0 K.DLLEVADILEK.A
								128 - 138	647.8497 1293.6848 1293.6313 0.0536 0 K.EEISNNNPHLK.S
								187 - 196	500.8031 999.5916 999.5601 0.0316 0 K.EPGTVALVSK.V
36	P17742	Peptidyl-prolyl cis-trans isomerase A	17.9	185	7	7.74	20	**Start - End**	**Observed Mr(expt) Mr(calc) Delta Miss Sequence**
								20 - 28	528.3051 1054.5956 1054.5335 0.0621 0 R.VSFELFADK.V
								20 - 31	460.6164 1378.8274 1378.7496 0.0777 1 R.VSFELFADKVPK.T
								20 - 31	690.4260 1378.8374 1378.7496 0.0878 1 R.VSFELFADKVPK.T
								83 - 91	577.8199 1153.6252 1153.5655 0.0597 0 K.FEDENFILK.H
								132 - 144	513.2833 1536.8281 1536.7276 0.1005 1 K.VKEGMNIVEAMER.F 2
								132 - 144	769.4380 1536.8614 1536.7276 0.1339 1 K.VKEGMNIVEAMER.F 2
								134 - 144	655.8383 1309.6620 1309.5642 0.0978 0 K.EGMNIVEAMER.F 2

Cell cycle

14	P10126	Elongation factor 1-alpha 1	50	177	7	9.10	16	**Start - End**	**Observed Mr(expt) Mr(calc) Delta Miss Sequence**
								21 - 30	560.8203 1119.6260 1119.5924 0.0336 0 K.STTTGHLIYK.C
								85 - 96	468.9226 1403.7460 1403.7197 0.0262 0 K.YYVTIIDAPGHR.D
								135 - 146	438.9270 1313.7592 1313.7343 0.0249 0 R.EHALLAYTLGVK.Q
								135 - 146	657.8920 1313.7694 1313.7343 0.0351 0 R.EHALLAYTLGVK.Q
								166 - 172	468.7705 935.5264 935.5076 0.0188 1 K.RYEEIVK.E
								248 - 255	488.2897 974.5648 974.5437 0.0212 0 R.LPLQDVYK.I
								256 - 266	513.3220 1024.6294 1024.6030 0.0265 0 K.IGGIGTVPVGR.V

Lipopolysaccharide binding; ATP binding

10	P20029	78 kDa glucose-regulated protein (Bip)	72.3	166	5	5.07	9	**Start - End**	**Observed Mr(expt) Mr(calc) Delta Miss Sequence**
								51 - 61	614.8412 1227.6678 1227.6207 0.0471 0 R.VEIIANDQGNR.I
								166 - 182	630.0302 1887.0688 1886.9639 0.1049 0 K.VTHAVVTVPAYFNDAQR.Q
								199 - 214	830.4892 1658.9638 1658.8879 0.0760 0 R.IINEPTAAAIAYGLDK.R
								525 - 533	537.8023 1073.5900 1073.5465 0.0435 0 K.ITITNDQNR.L
								534 - 541	493.7830 985.5514 985.5080 0.0435 0 R.LTPEEIER.M

		Oxidoreductase, Stress response					

13	Q61753	D-3-phosphoglycerate dehydrogenase	56.5	252	8	6.12	16

Start - End	Observed	Mr(expt)	Mr(calc)	Delta	Miss	Sequence
9 - 20	717.8679	1433.7212	1433.6643	0.0570	0	K.VLISDSLDPCCR.K 2
22 - 33	649.8920	1297.7694	1297.7242	0.0453	0	K.ILQDGGLQVVEK.Q
59 - 69	565.8239	1129.6332	1129.5979	0.0354	0	K.VTADVINAAEK.L
147 - 155	450.2976	898.5806	898.5600	0.0207	0	K.TLGILGLGR.I
237 - 247	550.3247	1098.6348	1098.6033	0.0315	0	R.GGIVDEGALLR.A
352 - 364	666.4022	1330.7898	1330.7457	0.0442	0	K.GTIQVVTQGTSLK.N
385 - 394	536.3125	1070.6104	1070.5720	0.0384	0	K.QADVNLVNAK.L
462 - 469	465.2950	928.5754	928.5494	0.0260	0	R.GQPLLVFR.A

9	P07901	Heat shock protein HSP 90-alpha	84.7	325	13	4.93	15

Start - End	Observed	Mr(expt)	Mr(calc)	Delta	Miss	Sequence
88 - 100	675.3440	1348.6734	1348.7272	-0.0538	0	R.TLTIVDTGIGMTK.A
88 - 100	683.3395	1364.6644	1364.7221	-0.0577	0	R.TLTIVDTGIGMTK.A
174 - 182	482.1929	962.3712	962.4127	- 0.0415	0	R.TDTGEPMGR.G
186 - 201	672.3232	2013.9478	2014.0371	-0.0893	1	K.VILHLKEDQTEYLEER.R
210 - 224	593.6246	1777.8520	1777.9403	-0.0883	0	K.HSQFIGYPITLFVEK.E
285 - 293	576.2495	1150.4844	1150.5506	-0.0661	0	K.YIDQEELNK.T
285 - 293	576.2576	1150.5006	1150.5506	-0.0499	0	K.YIDQEELNK.T
294 - 300	451.2433	900.4720	900.5181	-0.0461	0	K.TKPIWTR.N
340 - 346	408.2396	814.4646	814.5065	-0.0419	0	R.ALLFVPR.R
347 - 356	632.8005	1263.5864	1263.6360	-0.0496	1	R.RAPFDLFENR.K
348 - 356	554.7521	1107.4896	1107.5349	-0.0452	0	R.APFDLFENR.K
388 - 401	757.3570	1512.6994	1512.7784	-0.0789	0	R.GVVDSEDLPLNISR.E
501 - 511	618.2714	1234.5282	1234.5942	-0.0660	0	K.DQVANSAFVER.L

9	P11499	Heat shock protein HSP 90-beta	83.2	488	18	4.97	23

Start - End	Observed	Mr(expt)	Mr(calc)	Delta	Miss	Sequence
42 - 55	515.5862	1543.7368	1543.8205	-0.0838	1	R.ELISNASDALDKIR.Y
73 - 82	597.8010	1193.5874	1193.6404	-0.0530	0	K.IDILPNPQER.T
83 - 95	675.3440	1348.6734	1348.7272	-0.0538	0	R.TLTLVDTGIGMTK.A
83 - 95	683.3395	1364.6644	1364.7221	-0.0577	0	R.TLTLVDTGIGMTK.A
169 - 177	476.2175	950.4204	950.4570	-0.0365	0	R.ADHGEPIGR.G
181 - 196	672.3232	2013.9478	2014.0371	-0.0893	1	K.VILHLKEDQTEYLEER.R
205 - 219	603.6295	1807.8667	1807.9509	-0.0842	0	K.HSQFIGYPITLYLEK.E
276 - 284	576.2495	1150.4844	1150.5506	-0.0661	0	K.YIDQEELNK.T
276 - 284	576.2576	1150.5006	1150.5506	-0.0499	0	K.YIDQEELNK.T
285 - 291	451.2433	900.4720	900.5181	-0.0461	0	K.TKPIWTR.N
292 - 306	924.3608	1846.7070	1846.7897	-0.0827	0	R.NPDDITQEEYGEFYK.S
338 - 347	618.7966	1235.5786	1235.6299	-0.0512	1	R.RAPFDLFENK.K
339 - 347	540.7463	1079.4780	1079.5287	-0.0507	0	R.APFDLFENK.K
379 - 392	757.3570	1512.6994	1512.7784	-0.0789	0	R.GVVDSEDLPLNISR.E
429 - 435	446.1936	890.3726	890.4174	-0.0448	0	K.FYEAFSK.N
439 - 448	571.2600	1140.5054	1140.5523	-0.0469	0	K.LGIHEDSTNR.R
482 - 491	580.7706	1159.5266	1159.5761	-0.0494	0	K.SIYYITGESK.E
558 - 565	505.2378	1008.4610	1008.5062	-0.0452	1	K.AKFENLCK.L

20	P06151	L-lactate dehydrogenase A chain	36,4	161	7	7.62	18

Start - End	Observed	Mr(expt)	Mr(calc)	Delta	Miss	Sequence
82 - 90	529.2570	1056.4994	1056.4546	0.0448	0	K.DYCVTANSK.L
91 - 99	457.3066	912.5986	912.5756	0.0230	0	K.LVIITAGAR.Q
158 - 169	624.8273	1247.6400	1247.5928	0.0472	0	R.VIGSGCNLDSAR.F
233 - 243	625.8594	1249.7042	1249.6554	0.0488	0	K.QVVDSAYEVIK.L
269 - 278	399.8977	1196.6713	1196.6700	0.0013	1	R.RVHPISTMIK.G
270 - 278	521.3130	1040.6114	1040.5688	0.0426	0	R.VHPISTMIK.G
306 - 315	572.8169	1143.6192	1143.5771	0.0421	0	K.VTLTPEEEAR.L

20	P08249	Malate dehydrogenase, mitochondrial	35.5	136	5	8.93	15

Start - End	Observed	Mr(expt)	Mr(calc)	Delta	Miss	Sequence
92 - 104	669.8904	1337.7662	1337.7126	0.0537	0	K.GCDVVVIPAGVPR.K
166 - 176	617.3821	1232.7496	1232.7129	0.0368	0	K.IFGVTTLDIVR.A
177 - 185	496.7875	991.5604	991.5338	0.0266	0	R.ANTFVAELK.G
230 - 239	537.3062	1072.5978	1072.5764	0.0214	0	R.IQEAGTEVVK.A
315 - 324	565.8287	1129.6428	1129.6053	0.0376	0	K.MIAEAIPELK.A

31	P17751	Triosephosphate isomerase	26.6	121	5	6.90	20

Start - End	Observed	Mr(expt)	Mr(calc)	Delta	Miss	Sequence
60 - 69	569.3124	1136.6102	1136.5648	0.0454	0	K.IAVAAQNCYK.V
161 - 175	801.9860	1601.9574	1601.8817	0.0757	0	K.VVLAYEPVWAIGTGK.T
161 - 175	801.9883	1601.9620	1601.8817	0.0803	0	K.VVLAYEPVWAIGTGK.T
176 - 188	489.6029	1465.7869	1465.7161	0.0708	0	K.TATPQQAQEVHEK.L
195 - 206	624.3315	1246.6484	1246.5902	0.0583	0	K.SNVNDGVAQSTR.I

7. References

Aguzzi A. Molecular pathology of prion diseases. Vox Sang 2000; 78 Suppl 2: 25.

Aguzzi A, O'Connor T. Protein aggregation diseases: pathogenicity and therapeutic perspectives. Nat Rev Drug Discov 2010; 9: 237-248.

Anantharam V, Kanthasamy A, Choi CJ *et al.* Opposing roles of prion protein in oxidative stress- and ER stress-induced apoptotic signaling. Free Radic Biol Med 2008; 45: 1530-1541.

Asif A, Yevzlin AS. Arterial stent placement in arteriovenous dialysis access by interventional nephrologists. Semin Dial 2009; 22: 557-560.

Asif AR, Armstrong VW, Voland A, Wieland E, Oellerich M, Shipkova M. Proteins identified as targets of the acyl glucuronide metabolite of mycophenolic acid in kidney tissue from mycophenolate mofetil treated rats. Biochimie 2007; 89: 393-402.

Bananis E, Murray JW, Stockert RJ, Satir P, Wolkoff AW. Microtubule and motor-dependent endocytic vesicle sorting in vitro. J Cell Biol 2000; 151: 179-186.

Bananis E, Nath S, Gordon K *et al.* Microtubule-dependent movement of late endocytic vesicles in vitro: requirements for Dynein and Kinesin. Mol Biol Cell 2004; 15: 3688-3697.

Barenco MG, Valori CF, Roncoroni C, Loewer J, Montrasio F, Rossi D. Deletion of the amino-terminal domain of the prion protein does not impair prion protein-dependent neuronal differentiation and neuritogenesis. J Neurosci Res 2009; 87: 806-819.

Ben-Zvi AP, Goloubinoff P. Review: mechanisms of disaggregation and refolding of stable protein aggregates by molecular chaperones. J Struct Biol 2001; 135: 84-93.

Benaud C, Gentil BJ, Assard N *et al.* AHNAK interaction with the annexin 2/S100A10 complex regulates cell membrane cytoarchitecture. J Cell Biol 2004; 164: 133-144.

Beringue V, Mallinson G, Kaisar M *et al.* Regional heterogeneity of cellular prion protein isoforms in the mouse brain. Brain 2003; 126: 2065-2073.

Borchelt DR, Taraboulos A, Prusiner SB. Evidence for synthesis of scrapie prion proteins in the endocytic pathway. J Biol Chem 1992; 267: 16188-16199.

Brandenburg LO, Lucius R, Tameh AA *et al.* Internalization and signal transduction of PrP(106-126) in neuronal cells. Ann Anat 2009; 191: 459-468.

Brandner S, Isenmann S, Raeber A *et al.* Normal host prion protein necessary for scrapie-induced neurotoxicity. Nature 1996; 379: 339-343.

Brown DR, Clive C, Haswell SJ. Antioxidant activity related to copper binding of native prion protein. J Neurochem 2001; 76: 69-76.

Brown DR, Qin K, Herms JW *et al.* The cellular prion protein binds copper in vivo. Nature 1997a; 390: 684-687.

Brown DR, Schulz-Schaeffer WJ, Schmidt B, Kretzschmar HA. Prion protein-deficient cells show altered response to oxidative stress due to decreased SOD-1 activity. Exp Neurol 1997b; 146: 104-112.

Brown DR, Wong BS, Hafiz F, Clive C, Haswell SJ, Jones IM. Normal prion protein has an activity like that of superoxide dismutase. Biochem J 1999; 344 Pt 1: 1-5.

Brown HA, Gutowski S, Moomaw CR, Slaughter C, Sternweis PC. ADP-ribosylation factor, a small GTP-dependent regulatory protein, stimulates phospholipase D activity. Cell 1993; 75: 1137-1144.

Bucci C, Thomsen P, Nicoziani P, McCarthy J, van DB. Rab7: a key to lysosome biogenesis. Mol Biol Cell 2000; 11: 467-480.

Bueler H, Aguzzi A, Sailer A et al. Mice devoid of PrP are resistant to scrapie. Cell 1993; 73: 1339-1347.

Capellari S, Zaidi SI, Urig CB, Perry G, Smith MA, Petersen RB. Prion protein glycosylation is sensitive to redox change. J Biol Chem 1999; 274: 34846-34850.

Caughey B. In vitro expression and biosynthesis of prion protein. Curr Top Microbiol Immunol 1991; 172: 93-107.

Caughey B, Baron GS. Prions and their partners in crime. Nature 2006; 443: 803-810.

Caughey B, Race R, Chesebro B. Comparative sequence analysis, in vitro expression and biosynthesis of mouse PrP. Prog Clin Biol Res 1989; 317: 619-636.

Caughey B, Raymond GJ. The scrapie-associated form of PrP is made from a cell surface precursor that is both protease- and phospholipase-sensitive. J Biol Chem 1991; 266: 18217-18223.

Clarke AR, Jackson GS, Collinge J. The molecular biology of prion propagation. Philos Trans R Soc Lond B Biol Sci 2001; 356: 185-195.

Cockcroft S, Thomas GM, Fensome A et al. Phospholipase D: a downstream effector of ARF in granulocytes. Science 1994; 263: 523-526.

Collinge J, Whittington MA, Sidle KC et al. Prion protein is necessary for normal synaptic function. Nature 1994; 370: 295-297.

Cooper I, Malina KC, Cagnotto A, Bazzoni G, Salmona M, Teichberg VI. Interactions of the prion peptide (PrP 106-126) with brain capillary endothelial cells: coordinated cell killing and remodeling of intercellular junctions. J Neurochem 2010.

Cory AH, Owen TC, Barltrop JA, Cory JG. Use of an aqueous soluble tetrazolium/formazan assay for cell growth assays in culture. Cancer Commun 1991; 3: 207-212.

Daniel B, DeCoster MA. Quantification of sPLA2-induced early and late apoptosis changes in neuronal cell cultures using combined TUNEL and DAPI staining. Brain Res Brain Res Protoc 2004; 13: 144-150.

DeArmond SJ, Kristensson K, Bowler RP. PrPSc causes nerve cell death and stimulates astrocyte proliferation: a paradox. Prog Brain Res 1992; 94: 437-446.

DeArmond SJ, Qiu Y, Sanchez H *et al*. PrPc glycoform heterogeneity as a function of brain region: implications for selective targeting of neurons by prion strains. J Neuropathol Exp Neurol 1999; 58: 1000-1009.

Donaldson JG. Arfs, phosphoinositides and membrane traffic. Biochem Soc Trans 2005; 33: 1276-1278.

Donaldson JG. Phospholipase D in endocytosis and endosomal recycling pathways. Biochim Biophys Acta 2009; 1791: 845-849.

Dong CF, Shi S, Wang XF *et al*. The N-terminus of PrP is responsible for interacting with tubulin and fCJD related PrP mutants possess stronger inhibitive effect on microtubule assembly in vitro. Arch Biochem Biophys 2008; 470: 83-92.

Edenhofer F, Rieger R, Famulok M, Wendler W, Weiss S, Winnacker EL. Prion protein PrPc interacts with molecular chaperones of the Hsp60 family. J Virol 1996; 70: 4724-4728.

Fensome-Green A, Cockcroft S. Reconstitution system based on cytosol-depleted cells to study the regulation of phospholipase D. Methods Mol Biol 2006; 332: 299-310.

Ferrer I. Synaptic pathology and cell death in the cerebellum in Creutzfeldt-Jakob disease. Cerebellum 2002; 1: 213-222.

Fletcher DA, Mullins RD. Cell mechanics and the cytoskeleton. Nature 2010; 463: 485-492.

Fournier JG. Cellular prion protein electron microscopy: attempts/limits and clues to a synaptic trait. Implications in neurodegeneration process. Cell Tissue Res 2008; 332: 1-11.

Fournier JG, Escaig-Haye F, Billette d, V, Robain O. Ultrastructural localization of cellular prion protein (PrPc) in synaptic boutons of normal hamster hippocampus. C R Acad Sci III 1995; 318: 339-344.

Gauczynski S, Peyrin JM, Haik S *et al*. The 37-kDa/67-kDa laminin receptor acts as the cell-surface receptor for the cellular prion protein. EMBO J 2001; 20: 5863-5875.

Gilch S, Bach C, Lutzny G, Vorberg I, Schatzl HM. Inhibition of cholesterol recycling impairs cellular PrP(Sc) propagation. Cell Mol Life Sci 2009; 66: 3979-3991.

Giorgi A, Di FL, Principe S *et al*. Proteomic profiling of PrP27-30-enriched preparations extracted from the brain of hamsters with experimental scrapie. Proteomics 2009; 9: 3802-3814.

Goldmann W. PrP gene and its association with spongiform encephalopathies. Br Med Bull 1993; 49: 839-859.

Gorodinsky A, Harris DA. Glycolipid-anchored proteins in neuroblastoma cells form detergent-resistant complexes without caveolin. J Cell Biol 1995; 129: 619-627.

Gorvel JP, Chavrier P, Zerial M, Gruenberg J. rab5 controls early endosome fusion in vitro. Cell 1991; 64: 915-925.

Graner E, Mercadante AF, Zanata SM *et al.* Cellular prion protein binds laminin and mediates neuritogenesis. Brain Res Mol Brain Res 2000; 76: 85-92.

Grant SG, O'Dell TJ, Karl KA, Stein PL, Soriano P, Kandel ER. Impaired long-term potentiation, spatial learning, and hippocampal development in fyn mutant mice. Science 1992; 258: 1903-1910.

Hachiya NS, Watanabe K, Sakasegawa Y, Kaneko K. Microtubules-associated intracellular localization of the NH2-terminal cellular prion protein fragment. Biochem Biophys Res Commun 2004a; 313: 818-823.

Hachiya NS, Watanabe K, Yamada M, Sakasegawa Y, Kaneko K. Anterograde and retrograde intracellular trafficking of fluorescent cellular prion protein. Biochem Biophys Res Commun 2004b; 315: 802-807.

Hajj GN, Lopes MH, Mercadante AF *et al.* Cellular prion protein interaction with vitronectin supports axonal growth and is compensated by integrins. J Cell Sci 2007; 120: 1915-1926.

Haraguchi T, Fisher S, Olofsson S *et al.* Asparagine-linked glycosylation of the scrapie and cellular prion proteins. Arch Biochem Biophys 1989; 274: 1-13.

Harris DA. Cell biological studies of the prion protein. Curr Issues Mol Biol 1999; 1: 65-75.

Harris DA. Trafficking, turnover and membrane topology of PrP. Br Med Bull 2003; 66: 71-85.

Hehnly H, Xu W, Chen JL, Stamnes M. Cdc42 regulates microtubule-dependent Golgi positioning. Traffic 2010; 11: 1067-1078.

Henle KJ, Jethmalani SM, Nagle WA. Stress proteins and glycoproteins (Review). Int J Mol Med 1998; 1: 25-32.

Herms J, Tings T, Gall S *et al.* Evidence of presynaptic location and function of the prion protein. J Neurosci 1999; 19: 8866-8875.

Honda A, Nogami M, Yokozeki T *et al.* Phosphatidylinositol 4-phosphate 5-kinase alpha is a downstream effector of the small G protein ARF6 in membrane ruffle formation. Cell 1999; 99: 521-532.

Hsich G, Kenney K, Gibbs CJ, Lee KH, Harrington MG. The 14-3-3 brain protein in cerebrospinal fluid as a marker for transmissible spongiform encephalopathies. N Engl J Med 1996; 335: 924-930.

Jang B, Kim E, Choi JK *et al*. Accumulation of citrullinated proteins by up-regulated peptidylarginine deiminase 2 in brains of scrapie-infected mice: a possible role in pathogenesis. Am J Pathol 2008; 173: 1129-1142.

Jeffrey M, Goodsir CM, Fowler N, Hope J, Bruce ME, McBride PA. Ultrastructural immuno-localization of synthetic prion protein peptide antibodies in 87V murine scrapie. Neurodegeneration 1996; 5: 101-109.

Jeffrey M, Halliday WG, Bell J *et al*. Synapse loss associated with abnormal PrP precedes neuronal degeneration in the scrapie-infected murine hippocampus. Neuropathol Appl Neurobiol 2000; 26: 41-54.

Jin T, Gu Y, Zanusso G *et al*. The chaperone protein BiP binds to a mutant prion protein and mediates its degradation by the proteasome. J Biol Chem 2000; 275: 38699-38704.

Johnston AR, Black C, Fraser J, MacLeod N. Scrapie infection alters the membrane and synaptic properties of mouse hippocampal CA1 pyramidal neurones. J Physiol 1997; 500 (Pt 1): 1-15.

Junttila MR, Saarinen S, Schmidt T, Kast J, Westermarck J. Single-step Strep-tag purification for the isolation and identification of protein complexes from mammalian cells. Proteomics 2005; 5: 1199-1203.

Kaiser C, Ferro-Novick S. Transport from the endoplasmic reticulum to the Golgi. Curr Opin Cell Biol 1998; 10: 477-482.

Kanaani J, Prusiner SB, Diacovo J, Baekkeskov S, Legname G. Recombinant prion protein induces rapid polarization and development of synapses in embryonic rat hippocampal neurons in vitro. J Neurochem 2005; 95: 1373-1386.

Keshava Prasad TS, Goel R, Kandasamy K *et al*. Human Protein Reference Database--2009 update. Nucleic Acids Res 2009; 37: D767-D772.

Knight RS, Will RG. Prion diseases. J Neurol Neurosurg Psychiatry 2004; 75 Suppl 1: i36-i42.

Korte S, Vassallo N, Kramer ML, Kretzschmar HA, Herms J. Modulation of L-type voltage-gated calcium channels by recombinant prion protein. J Neurochem 2003; 87: 1037-1042.

Kosako H, Goto H, Yanagida M *et al*. Specific accumulation of Rho-associated kinase at the cleavage furrow during cytokinesis: cleavage furrow-specific phosphorylation of intermediate filaments. Oncogene 1999; 18: 2783-2788.

Kretzschmar HA, Tings T, Madlung A, Giese A, Herms J. Function of PrP(C) as a copper-binding protein at the synapse. Arch Virol Suppl 2000; 239-249.

Kurschner C, Morgan JI. The cellular prion protein (PrP) selectively binds to Bcl-2 in the yeast two-hybrid system. Brain Res Mol Brain Res 1995; 30: 165-168.

Kurschner C, Morgan JI. Analysis of interaction sites in homo- and heteromeric complexes containing Bcl-2 family members and the cellular prion protein. Brain Res Mol Brain Res 1996; 37: 249-258.

Lasmezas CI. Putative functions of PrP(C). Br Med Bull 2003; 66: 61-70.

Lawson VA, Collins SJ, Masters CL, Hill AF. Prion protein glycosylation. J Neurochem 2005; 93: 793-801.

Lee S, Antony L, Hartmann R *et al.* Conformational diversity in prion protein variants influences intermolecular beta-sheet formation. EMBO J 2010; 29: 251-262.

Legname G, Baskakov IV, Nguyen HO *et al.* Synthetic mammalian prions. Science 2004; 305: 673-676.

Lima FR, Arantes CP, Muras AG, Nomizo R, Brentani RR, Martins VR. Cellular prion protein expression in astrocytes modulates neuronal survival and differentiation. J Neurochem 2007; 103: 2164-2176.

Linden R, Martins VR, Prado MA, Cammarota M, Izquierdo I, Brentani RR. Physiology of the prion protein. Physiol Rev 2008; 88: 673-728.

Liu GP, Wei W, Zhou X *et al.* I(2)(PP2A) regulates p53 and Akt correlatively and leads the neurons to abort apoptosis. Neurobiol Aging 2010.

Lodish HF. Molecular cell biology. 2004; 5th ed.

Lopez CD, Yost CS, Prusiner SB, Myers RM, Lingappa VR. Unusual topogenic sequence directs prion protein biogenesis. Science 1990; 248: 226-229.

Ma J, Lindquist S. Wild-type PrP and a mutant associated with prion disease are subject to retrograde transport and proteasome degradation. Proc Natl Acad Sci U S A 2001; 98: 14955-14960.

Magalhaes AC, Silva JA, Lee KS *et al.* Endocytic intermediates involved with the intracellular trafficking of a fluorescent cellular prion protein. J Biol Chem 2002; 277: 33311-33318.

Malaga-Trillo E, Solis GP, Schrock Y *et al.* Regulation of embryonic cell adhesion by the prion protein. PLoS Biol 2009; 7: e55.

Mallik S, Yang W, Norstrom EM, Mastrianni JA. Live cell fluorescence resonance energy transfer predicts an altered molecular association of heterologous PrPSc with PrPC. J Biol Chem 2010; 285: 8967-8975.

Markgraf DF, Peplowska K, Ungermann C. Rab cascades and tethering factors in the endomembrane system. FEBS Lett 2007; 581: 2125-2130.

Matteoni R, Kreis TE. Translocation and clustering of endosomes and lysosomes depends on microtubules. J Cell Biol 1987; 105: 1253-1265.

McKinley MP, Bolton DC, Prusiner SB. A protease-resistant protein is a structural component of the scrapie prion. Cell 1983; 35: 57-62.

McMurray CT. Neurodegeneration: diseases of the cytoskeleton? Cell Death Differ 2000; 7: 861-865.

Mei GY, Li Y, Wang GR *et al*. [Molecular interaction between PrP protein and the signal protein 14-3-3 beta]. Bing Du Xue Bao 2009; 25: 208-212.

Morel E, Fouquet S, Strup-Perrot C *et al*. The cellular prion protein PrP(c) is involved in the proliferation of epithelial cells and in the distribution of junction-associated proteins. PLoS One 2008; 3: e3000.

Morot-Gaudry-Talarmain Y, Rezaei H, Guermonprez L, Treguer E, Grosclaude J. Selective prion protein binding to synaptic components is modulated by oxidative and nitrosative changes induced by copper(II) and peroxynitrite in cholinergic synaptosomes, unveiling a role for calcineurin B and thioredoxin. J Neurochem 2003; 87: 1456-1470.

Morrison HA, Dionne H, Rusten TE *et al*. Regulation of early endosomal entry by the Drosophila tumor suppressors Rabenosyn and Vps45. Mol Biol Cell 2008; 19: 4167-4176.

Mouillet-Richard S, Ermonval M, Chebassier C *et al*. Signal transduction through prion protein. Science 2000; 289: 1925-1928.

Mouillet-Richard S, Laurendeau I, Vidaud M, Kellermann O, Laplanche JL. Prion protein and neuronal differentiation: quantitative analysis of prnp gene expression in a murine inducible neuroectodermal progenitor. Microbes Infect 1999; 1: 969-976.

Muslin AJ. Road Rage: Cardiac Rab1 and ER-to-Golgi Traffic. Circ Res 2001; 89: 1087-1088.

Naslavsky N, Stein R, Yanai A, Friedlander G, Taraboulos A. Characterization of detergent-insoluble complexes containing the cellular prion protein and its scrapie isoform. J Biol Chem 1997; 272: 6324-6331.

Nielsen E, Cheung AY, Ueda T. The regulatory RAB and ARF GTPases for vesicular trafficking. Plant Physiol 2008; 147: 1516-1526.

Nielsen E, Severin F, Backer JM, Hyman AA, Zerial M. Rab5 regulates motility of early endosomes on microtubules. Nat Cell Biol 1999; 1: 376-382.

Nielsen E, Severin F, Hyman AA, Zerial M. In vitro reconstitution of endosome motility along microtubules. Methods Mol Biol 2001; 164: 133-146.

Nieznanski K. Interactions of Prion Protein With Intracellular Proteins: So Many Partners and no Consequences? Cell Mol Neurobiol 2009.

Nieznanski K, Nieznanska H, Skowronek KJ, Osiecka KM, Stepkowski D. Direct interaction between prion protein and tubulin. Biochem Biophys Res Commun 2005; 334: 403-411.

Oakley AJ. Glutathione transferases: new functions. Curr Opin Struct Biol 2005; 15: 716-723.

Oesch B, Teplow DB, Stahl N, Serban D, Hood LE, Prusiner SB. Identification of cellular proteins binding to the scrapie prion protein. Biochemistry 1990; 29: 5848-5855.

Pan T, Wong BS, Liu T, Li R, Petersen RB, Sy MS. Cell-surface prion protein interacts with glycosaminoglycans. Biochem J 2002; 368: 81-90.

Paruch S, El-Benna J, Djerdjouri B, Marullo S, Perianin A. A role of p44/42 mitogen-activated protein kinases in formyl-peptide receptor-mediated phospholipase D activity and oxidant production. FASEB J 2006; 20: 142-144.

Priola SA, Caughey B. Inhibition of scrapie-associated PrP accumulation. Probing the role of glycosaminoglycans in amyloidogenesis. Mol Neurobiol 1994; 8: 113-120.

Prusiner SB. Prions. Proc Natl Acad Sci U S A 1998a; 95: 13363-13383.

Prusiner SB. The prion diseases. Brain Pathol 1998b; 8: 499-513.

Puxeddu E, Uhart M, Li CC *et al*. Interaction of phosphodiesterase 3A with brefeldin A-inhibited guanine nucleotide-exchange proteins BIG1 and BIG2 and effect on ARF1 activity. Proc Natl Acad Sci U S A 2009; 106: 6158-6163.

Rachidi W, Mange A, Senator A *et al*. Prion infection impairs copper binding of cultured cells. J Biol Chem 2003; 278: 14595-14598.

Ramljak S, Asif AR, Armstrong VW *et al*. Physiological role of the cellular prion protein (PrPc): protein profiling study in two cell culture systems. J Proteome Res 2008; 7: 2681-2695.

Re L, Rossini F, Re F *et al*. Prion protein potentiates acetylcholine release at the neuromuscular junction. Pharmacol Res 2006; 53: 62-68.

Rieger R, Edenhofer F, Lasmezas CI, Weiss S. The human 37-kDa laminin receptor precursor interacts with the prion protein in eukaryotic cells. Nat Med 1997; 3: 1383-1388.

Riek R, Hornemann S, Wider G, Glockshuber R, Wuthrich K. NMR characterization of the full-length recombinant murine prion protein, mPrP(23-231). FEBS Lett 1997; 413: 282-288.

Rothman JE. The protein machinery of vesicle budding and fusion. Protein Sci 1996; 5: 185-194.

Roucou X, LeBlanc AC. Cellular prion protein neuroprotective function: implications in prion diseases. J Mol Med 2005; 83: 3-11.

Rudd PM, Endo T, Colominas C *et al.* Glycosylation differences between the normal and pathogenic prion protein isoforms. Proc Natl Acad Sci U S A 1999; 96: 13044-13049.

Rudd PM, Merry AH, Wormald MR, Dwek RA. Glycosylation and prion protein. Curr Opin Struct Biol 2002; 12: 578-586.

Russell MR, Nickerson DP, Odorizzi G. Molecular mechanisms of late endosome morphology, identity and sorting. Curr Opin Cell Biol 2006; 18: 422-428.

Sakudo A, Ikuta K. Fundamentals of prion diseases and their involvement in the loss of function of cellular prion protein. Protein Pept Lett 2009; 16: 217-229.

Sakudo A, Lee DC, Nishimura T *et al.* Octapeptide repeat region and N-terminal half of hydrophobic region of prion protein (PrP) mediate PrP-dependent activation of superoxide dismutase. Biochem Biophys Res Commun 2005; 326: 600-606.

Santuccione A, Sytnyk V, Leshchyns'ka I, Schachner M. Prion protein recruits its neuronal receptor NCAM to lipid rafts to activate p59fyn and to enhance neurite outgrowth. J Cell Biol 2005; 169: 341-354.

Satoh H, Yamato O, Asano T *et al.* Cerebrospinal fluid biomarkers showing neurodegeneration in dogs with GM1 gangliosidosis: possible use for assessment of a therapeutic regimen. Brain Res 2007; 1133: 200-208.

Satoh J, Onoue H, Arima K, Yamamura T. The 14-3-3 protein forms a molecular complex with heat shock protein Hsp60 and cellular prion protein. J Neuropathol Exp Neurol 2005; 64: 858-868.

Schmidt H, Otto M, Niedmann P *et al.* CSF lactate dehydrogenase activity in patients with Creutzfeldt-Jakob disease exceeds that in other dementias. Dement Geriatr Cogn Disord 2004; 17: 204-206.

Schimmoller F, Simon I, Pfeffer SR. Rab GTPases, directors of vesicle docking. J Biol Chem 1998; 273: 22161-22164.

Schmoranzer J, Simon SM. Role of microtubules in fusion of post-Golgi vesicles to the plasma membrane. Mol Biol Cell 2003; 14: 1558-1569.

Schmitt-Ulms G, Legname G, Baldwin MA *et al.* Binding of neural cell adhesion molecules (N-CAMs) to the cellular prion protein. J Mol Biol 2001; 314: 1209-1225.

Shyng SL, Huber MT, Harris DA. A prion protein cycles between the cell surface and an endocytic compartment in cultured neuroblastoma cells. J Biol Chem 1993; 268: 15922-15928.

Sideri TC, Stojanovski K, Tuite MF, Grant CM. Ribosome-associated peroxiredoxins suppress oxidative stress-induced de novo formation of the [PSI+] prion in yeast. Proc Natl Acad Sci U S A 2010; 107: 6394-6399.

Spielhaupter C, Schatzl HM. PrPC directly interacts with proteins involved in signaling pathways. J Biol Chem 2001; 276: 44604-44612.

Spisni E, Valerii MC, Manerba M *et al*. Effect of copper on extracellular levels of key pro-inflammatory molecules in hypothalamic GN11 and primary neurons. Neurotoxicology 2009; 30: 605-612.

Stahl N, Borchelt DR, Hsiao K, Prusiner SB. Scrapie prion protein contains a phosphatidylinositol glycolipid. Cell 1987; 51: 229-240.

Steele AD, Emsley JG, Ozdinler PH, Lindquist S, Macklis JD. Prion protein (PrPc) positively regulates neural precursor proliferation during developmental and adult mammalian neurogenesis. Proc Natl Acad Sci U S A 2006; 103: 3416-3421.

Toni M, Massimino ML, Griffoni C, Salvato B, Tomasi V, Spisni E. Extracellular copper ions regulate cellular prion protein (PrPC) expression and metabolism in neuronal cells. FEBS Lett 2005; 579: 741-744.

Turk E, Teplow DB, Hood LE, Prusiner SB. Purification and properties of the cellular and scrapie hamster prion proteins. Eur J Biochem 1988; 176: 21-30.

Turu M, Slevin M, Ethirajan P *et al*. The normal cellular prion protein and its possible role in angiogenesis. Front Biosci 2008; 13: 6491-6500.

Vanlandingham PA, Ceresa BP. Rab7 Regulates Late Endocytic Trafficking Downstream of Multivesicular Body Biogenesis and Cargo Sequestration. Journal of Biological Chemistry 2009; 284: 12110-12124.

Varela-Nallar L, Toledo EM, Chacon MA, Inestrosa NC. The functional links between prion protein and copper. Biol Res 2006; 39: 39-44.

Volpicelli-Daley LA, Li Y, Zhang CJ, Kahn RA. Isoform-selective effects of the depletion of ADP-ribosylation factors 1-5 on membrane traffic. Mol Biol Cell 2005; 16: 4495-4508.

Vonderheit A, Helenius A. Rab7 associates with early endosomes to mediate sorting and transport of Semliki forest virus to late endosomes. PLoS Biol 2005; 3: e233.

Watts JC, Huo H, Bai Y *et al*. Interactome analyses identify ties of PrP and its mammalian paralogs to oligomannosidic N-glycans and endoplasmic reticulum-derived chaperones. PLoS Pathog 2009; 5: e1000608.

Weis WI, Scheller RH. Membrane fusion. SNARE the rod, coil the complex. Nature 1998; 395: 328-329.

Wessel D, Flugge UI. A method for the quantitative recovery of protein in dilute solution in the presence of detergents and lipids. Anal Biochem 1984; 138: 141-143.

Westergard L, Christensen HM, Harris DA. The cellular prion protein (PrP(C)): its physiological function and role in disease. Biochim Biophys Acta 2007; 1772: 629-644.

Wu G, Nakajima K, Takeyama N *et al*. Species-specific anti-apoptotic activity of cellular prion protein in a mouse PrP-deficient neuronal cell line transfected with mouse, hamster, and bovine Prnp. Neurosci Lett 2008; 446: 11-15.

Wunderlich W, Fialka I, Teis D *et al*. A novel 14-kilodalton protein interacts with the mitogen-activated protein kinase scaffold mp1 on a late endosomal/lysosomal compartment. J Cell Biol 2001; 152: 765-776.

Yedidia Y, Horonchik L, Tzaban S, Yanai A, Taraboulos A. Proteasomes and ubiquitin are involved in the turnover of the wild-type prion protein. EMBO J 2001; 20: 5383-5391.

Yoo BC, Krapfenbauer K, Cairns N, Belay G, Bajo M, Lubec G. Overexpressed protein disulfide isomerase in brains of patients with sporadic Creutzfeldt-Jakob disease. Neurosci Lett 2002; 334: 196-200.

Zanata SM, Lopes MH, Mercadante AF *et al*. Stress-inducible protein 1 is a cell surface ligand for cellular prion that triggers neuroprotection. EMBO J 2002; 21: 3307-3316.

Zerial M, McBride H. Rab proteins as membrane organizers. Nat Rev Mol Cell Biol 2001; 2: 107-117.

Publications

Zafar, S., von, A. N., Oellerich, M., Zerr, I., Schulz-Schaeffer, W. J., Armstrong, V. W., and Asif, A. R. (2011) Proteomics Approach to Identify the Interacting Partners of Cellular Prion Protein and Characterization of Rab7a Interaction in Neuronal Cells. *J. Proteome. Res.*

Abstracts/Posters Published

<u>**Zafar S**</u>**,** Asif AR., Armstrong VW, Oellerich M, One-C-Terminus One-STrEP-tagged human prion protein expression, purification, localization and identification of interacting proteins in mammalian cell line, Clinical Chemistry and Laboratory Medicine, 2008; 46(9):A175.

<u>**Zafar S**</u>**,** Asif AR., Armstrong VW, Oellerich M, Human cellular prion protein (PrP^C): Distribution and co-localization with early endosome in a neuronal cell line, Clinical Chemistry and Laboratory Medicine, 2009; 47(9):A63.

<u>**Zafar S**</u>, Asif AR., Armstrong VW, Oellerich M, Molecular interaction of human Prion protein and cytoskeleton associated proteins. International conference of 'Prion' Thessaloniki-Chalkidiki, Greece, 2009.

<u>**Zafar S**</u>, Ahsen NV, Oellerich M, Schulz-Schaeffer WJ, Armstrong VW, Asif AR, Human cellular prion protein (PrP^C): Human Cellular Prion Protein (PrP^C): Identification of Novel Interacting Partners & Characterization in association with endosome and microtubules. 2010.

Acknowledgements

I bow my head in gratitude to "**Almighty Allah**", whose blessings and exaltation flourished my thoughts, which enabled me to accomplish this task. Countless thanks to Allah, the Beneficent and the Merciful, from the depth of my heart. He is the One Who always takes troubles away from me and blessed me with courage and strength. Blessings and salutation on "**Hazrat Muhammad (PBUH)",** who is forever a torch of knowledge and tower of guidance for me.

My special gratitude to the Late Prof. Dr. Victor W. Armstrong for an interesting project, constant encouragement, affection, care and support until the last moment of his life (May his soul rest in peace amen). I owe very special thanks to Prof. M. Oellerich, director of the department of Clinical Chemistry, UMG, for his cooperation and for providing me privileges in this department. I would like to thank Dr. A. R. Asif and Prof. Nicolas von Ahsen who facilitated my work.

My very special thanks to Prof. Philip D. Walson (Visiting Professor, Dept of Laboratory Medicine, UMG) for his time and his critical review of my thesis.

I express my particular gratitude to my scientific supervisors, Prof. Dr. Uwe Groβ and Prof. Dr. Nils Brose, for their outstanding supervision, support and contribution to my success. Their constructive criticism and suggestions are highly appreciated.

My sincere thanks to Dr. Nadeem Sheikh for his care, valuable guidance, skilled advice and moral support over the last 10 years and I wish to continue to have this eternally.

My special thanks to Dr. Ihtzaz Ahmed Malik who picked me up from the Frankfurt airport and dropped me off in Goettingen to start my new life as a Doctoral student. He helped, bore and supported me from the very first day in Germany until today to make me fly in colors. Thanks for being there when I needed you the most. I also would like to say thanks to Dr. Ahmed Shariq for his encouragement during my PhD work.

I am thankful to Dr. Hassen Dihazi and Dr. Matthius Schmitz for providing me antibodies. I am also thankful to Dr. Inga Zerr, Joanna Gawinecka, Dr. Christina Behrman and Dr. Sanja Ramaljak for their time discussing prion protein.

For technical support and an enjoyable working atmosphere, I wish to thank both past and present members from the institute: Christa, Christina, Darinka, Frank, Hazir, Misbah, Qasim, Reiner, Sandra and Suzana. I would also like to thank all of my friends back in Pakistan and here who shared the ups and downs during my stay in Germany. I am craving to say thanks to Naila, Sadia and Sadaf to be with me to accomplish my brainless adventures.

Finally, I would like to thank my family back home, my sisters Shaista and Huma, my brother Najam and Amma Aba, for their undaunting perseverance and support all this time that I have been away from them in the pursuit of my goal.
Thanks.   **Saima**

Curriculum vitae

Family Name   Zafar

First name   Saima

Date of birth   16.12.1982

Place of birth   Lahore, Pakistan

Citizenship   Pakistani

Education

2007- 2010   **PhD in biology**

                     Department of Clinical Chemistry,

                     University Medical Center,

                     Georg-August University, Goettingen

                     Title: "Cellular Prion Protein: Identification and
                     Characterization of Novel Interacting Partners".

2005-2007   **Master of Philosophy (M.Phil.) in Molecular Biology**

                     Center of Excellence in Molecular Biology,

                     University of the Punjab, Lahore, Pakistan

                     Title: "Effect of Small Interfering RNA against the p7 Gene of
                     Hepatitis C Virus Genotype 1a".

2003 – 2005   **Master of Science in Zoology**

                     Gold Medal, Role of Honor

                     University of the Punjab, Lahore, Pakistan

2000 – 2003   **Bachelors of Science (Hons.) in Zoology**

                     Gold Medal, Role of Honor

                     University of the Punjab, Lahore, Pakistan

1998 – 2000   **College Education**

                     Multan, Pakistan.